Parametric Influence on Surface Integrity of Ti6Al4V alloy in Ultrasonic Vibration Assisted Turning

Submitted in partial fulfillment of the requirements
for the award of degree of

DOCTOR OF PHILOSOPHY
in
Mechanical Engineering

by

D. VENKATA SIVAREDDY

(Roll. No. 716124)

under the supervision of

Dr. A. Venu Gopal
Professor
Department of Mechanical Engineering
&
Dr. P. Vamsi Krishna
Associate Professor
Department of Mechanical Engineering

DEPARTMENT OF MECHANICAL ENGINEERING
NATIONAL INSTITUTE OF TECHNOLOGY WARANGAL
WARANGAL - 506 004, TELANGANA, INDIA.
SEPTEMBER-2021

Parametric Influence on Surface Integrity of Ti6Al4V alloy in Ultrasonic Vibration Assisted Turning

Submitted inpartial fulfillment of the requirements
for the award of degree of

DOCTOR OF PHILOSOPHY
in
Mechanical Engineering

by

D. VENKATA SIVAREDDY

(Roll. No. 716124)

under the supervision of

Dr. A. Venu Gopal	**Dr. P.Vamsi Krishna**
Professor	Associate Professor
Dept. of Mechanical Engineering	Dept. of Mechanical Engineering

DEPARTMENT OF MECHANICAL ENGINEERING
NATIONAL INSTITUTE OF TECHNOLOGY WARANGAL
WARANGAL-506 004, TELANGANA, INDIA.
SEPTEMBER -2021

CERTIFICATE

This is to certify that the work presented in the thesis entitled **"Parametric Influence on Surface Integrity of Ti6Al4V alloy in Ultrasonic Vibration Assisted Turning "** which is being submitted by **Mr. D. Venkata Sivareddy (Roll No. 716124),** is a bonafide work submitted to Department of Mechanical Engineering, National Institute of Technology Warangal in partial fulfillment of the requirement for the award of the degree of **Doctor of Philosophy in Mechanical Engineering.**

To the best of our knowledge, the work incorporated in the thesis has not been submitted to any other university or institute for the award of any other degree or diploma.

Dr. A. Venu Gopal   Dr. P. Vamsi Krishna
Professor   Associate Professor
Supervisor   Co-Supervisor
Department of Mechanical Engineering   Department of Mechanical Engineering
National Institute of Technology Warangal   National Institute of Technology Warangal
Warangal-506 004, Telangana, India.   Warangal-506 004, Telangana, India.

Prof. A. Kumar
Chairman-DSC
Head of the Department
Department of Mechanical Engineering
National Institute of Technology Warangal
Warangal-506 004, Telangana, India.

Declaration

This is to certify that the work presented in the thesis entitled **"Parametric Influence on Surface Integrity of Ti6Al4V alloy in Ultrasonic Vibration Assisted Turning"** is a bonafide work done by me under the supervision of **Dr.A.Venu Gopal**, Professor, Department of Mechanical Engineering, NIT Warangal, India and **Dr. P. Vamsi Krishna**, Associate Professor, Department of Mechanical Engineering, NIT Warangal, India was not submitted elsewhere for the award of any degree.

I declare that this written submission represents my ideas in my own words and where others' ideas or words have been included, i have adequately cited and referenced the original sources. I also declare that i have not misrepresented or fabricated or falsified any idea / data / fact / source in my submission. I understand that any violation of the above will be a cause for disciplinary action by the Institute and can also evoke penal action from the sources which have thus not been properly cited or from whom proper permission has not been taken when needed.

....
(Signature)

....
(Name of the student)

....
(Roll No.)

Date: ....

Dedicated

To

My Family

ABSTRACT

Ti6Al4V alloys have outstanding mechanical properties such as high strength-to-weight ratio, high hardness, excellent fatigue properties and high corrosion resistance. However, the low thermal conductivity, high chemical affinity to tool materials and high strength at elevated temperature impairs severely the machinability of TI6Al4V alloy with conventional machining. The chips formed during machining of these alloys do not carry away enough heat which leads to increased heat in the tool and subsequently damage. All these factors bring major challenges in machining of titanium alloys for aerospace manufacturing. The high cutting forces and cutting temperatures produced during machining causes plastic deformation of the workpiece and generates the residual stresses which influence the fatigue life and functionality of the component.

Ultrasonic Vibration Assisted Turning (UVAT) is an advanced machining technique to machine difficult to cut materials, in which high frequency and low energy vibro impacts are superimposed on the movement of the cutting tool. UVAT is an intermittent cutting operation in which the cutting tool is separated from workpiece repeatedly at periodical intervals by inducing ultrasonic vibrations. The momentary separation between the cutting tool and the workpiece causes a multi-fold decrease in the level of cutting forces and cutting temperatures with a concomitant improvement in surface finish. Though some investigations are carried out on the effectiveness of UVAT process, the surface integrity improvement and its effect on fatigue life of components is not much explored. Therefore, it is necessary to investigate the affect of surface properties on fatigue life of the Ti6Al4V alloy components machined in UVAT process.

The present study evaluates the surface integrity of Ti6Al4V alloy components produced from UVAT process using both Finite Element (FE) simulation and experimental results. The deformation behavior of material in FE simulations depends on Johnson-Cook parameters used in constitutive material model. In the present work, Machining based Approach (MA) by considering the strain along the chip-tool contact is developed to determine the JC parameters for Ti6Al4V alloy. Orthogonal cutting experiments are conducted to develop regression model for cutting force (F_c), feed force (F_f) and chip thickness (t_c). Oxley chip formation theory is used to evaluate physical quantities like strain, strain rate, temperature and equivalent stress at primary deformation zone at predefined

cutting conditions. The objective function which defines the difference between predicted and measured flow stress is optimized for minimum error to obtain the JC parameters. It is found that the JC parameters obtained from the current method predict more accurate values of flow stresses as compared to those reported in the literature.

In the first phase, the fundamentals of UVAT process are studied to know the influence of machining parameters in UVAT process. From this study, it is observed that ultrasonic frequency, ultrasonic amplitude and cutting speed are three important machining parameters which affect the performance of UVAT process. It is established that tool work contact ratio (TWCR) plays a key role in UVAT process. Increase in both vibrating parameters and decrease in cutting speed reduce the TWCR which in turn improve the performance of UVAT process. Experiments are conducted on Ti6Al4V alloy at various machining conditions to evaluate the performance of UVAT in terms of TWCR. It is observed that, the cutting force, cutting temperature and surface roughness are decreased with reduction in TWCR. Similarly, the variation of cutting force, cutting temperature and surface roughness at various machining conditions are evaluated and compared with CT process. It is observed that, the decrease in TWCR with increase in intensity of ultrasonic power improves the performance of UVAT compared to CT for all machining conditions. In order to evaluate the growth of flank wear of the cutting tool in machining of Ti6Al4V alloy, two important wear parameters i.e. average flank wear (V_B) and maximum flank wear (V_M) are considered for both CT and UVAT. Scanning Electron Microscope (SEM) is used to evaluate flank wear at various cutting speeds and ultrasonic powers. The fracture in cutting edge of the cutting tool is observed in CT process due to high compressive stresses with high cutting temperature whereas smooth wear is observed in UVAT due to low cutting temperature.

In the second phase, the machining induced residual stresses are evaluated at various machining conditions using both numerical and experimental techniques. The JC parameters determined from MA are used to evaluate both Circumferential Residual Stress (CRS) and Axial Residual Stress (ARS) on surface as well as along the depth of the machined component inUVAT process. X-Ray diffraction technique has been used to evaluate the surface residual stresses to validate the developed FE model. Experiments are conducted on Ti6Al4V alloy at various machining conditions to evaluate the thermo-mechanical phenomenon in UVAT process. Reduction in the cutting force and the cutting temperature are observed with increase in intensity of ultrasonic power whereas increase in the cutting

temperature and moderate decrease in the cutting force is observed with increase in the cutting speed for given cutting conditions. However, there is an increase in cutting force and cutting temperature with increase in feed and depth of cut. Similarly, residual stress distribution in terms of compressive and tensile layer thickness is analyzed at same cutting conditions to evaluate the thermo-mechanical loading in UVAT process. The increase in ultrasonic power leads to change the surface CRS from tensile to compressive whereas the surface ARS changes from low compressive to higher compressive state. It is also found that the tensile layer thickness is decreased and compressive layer thickness of CRS and ARS are increased with increase in ultrasonic power. Rise in thermal load with increase in cutting speed decreases the compressive layer thickness and increases the level of superficial CRS and ARS. The variation of CRS and ARS at different feed rates and depth of cuts also evaluated with respect to thermo-mechanical phenomenon.

In the last phase, fatigue strength of Ti6Al4V alloy samples prepared from CT and UVAT process is evaluated. In this regard, three machining conditions known as CT, UVAT and UVAT$_{opt}$ are considered to evaluate the effect of surface properties like surface roughness and surface residual stresses on fatigue life of Ti6Al4V alloy component. The fatigue test is conducted at frequency of 20 Hz and cyclic ratio of -1 with uniaxial tension compression loading on servo hydraulic machine. The fatigue strength for both CT and UVAT samples are evaluated using step by step method. The initial stress amplitude for fatigue test is considered based on yield strength of material. The fatigue tests are conducted at 80%, 75%, 70%, and 60% yield strength of material for both CT and UVAT process samples. The improved surface and induced compressive surface residual stresses requires more number of cycles to fail for all stress amplitude in UVAT compared to CT process. Finally, it is observed that there is significant improvement in fatigue strength of Ti6Al4V alloy with UVAT compared to CT process.

ACKNOWLEDGEMENTS

List of Contents

xi

LIST of TABLES

LIST OF ABBREVIATIONS AND SYMBOLS

Symbol		*Description*
ε	:	Equivalent strain
ε^{pl}	:	Equivalent plastic strain
$\acute{\varepsilon}$	:	Equivalent strain rate
$\varepsilon°/\varepsilon°_o$	:	Reference strain rate
σ	:	Plastic flow stress
σ_n	:	Stress amplitude at n number of cycles
ω	:	Angular frequency
μ	:	Coefficient of friction
$\emptyset$	:	Shear angle
α	:	Rake angle
β	:	Heat factor
ρ	:	Density
τ	:	Frictional stress value
τ_{th}	:	Threshold value for the Coulomb friction stress
a	:	amplitude
f	:	Frequency
f_r	:	Feed rate
h	:	Thickness of primary deformation zone
m	:	Thermal softening coefficient
n	:	Hardening coefficient
n_{eq}	:	Equivalent strain hardening coefficient
p	:	Normal pressure
t	:	Time
t_c	:	Chip thickness
t_u	:	Uuncut chip thickness
$v_{t,max}$	:	Maximum velocity of the tool
w	:	Width of cut

x(t)	:	Instantaneous position
x'(t)	:	Instantaneous velocity
1-D	:	One dimensional
2-D	:	Two dimensional
3-D	:	Three dimensional
A	:	Initial yield stress
ALE	:	Arbitrary Lagrangian-Eulerian
ARS	:	Axial Residual Stress
ANOVA	:	Analysis of variance
B	:	Hardening modulus
BUE	:	Built up edge
C	:	Strain rate sensitivity coefficient
C_p	:	Specific heat
CT	:	Conventional Turning
CCD	:	Central Composite Design
CRS	:	Circumferential Residual Stress
D	:	Damage parameter
D	:	Diameter
DOC	:	Depth of Cut
F_c	:	Cutting force
F_f	:	Feed force of thrust force
HCF	:	high cycle fatigue
J-C	:	Johnson-Cook
FEM	:	Finite Element Modelling
MA	:	Machining approach
N	:	Rotational speed
N_{limit}	:	Number of cycles for fatigue limit
$N_{failure}$	:	Number of cycles for failure
PDZ	:	Primary Deformation Zone
PSO	:	Particle Swam Optimization
P_u	:	Ultrasonic power intensity

R_a	:	Surface roughness
RSM	:	Response Surface Methodology
SDZ	:	Secondary Deformation Zone
SEM	:	Scanning Electron Microscopy
SHPB	:	Split-Hopkinson Pressure Bar
T	:	Temperature
T_c	:	Cutting temperature
T_{melt}	:	Melting temperature
T_{room}	:	Room temperature
T_p	:	Time period
TWCR	:	Tool work contact ratio
UVAT	:	Ultrasonic Vibration Assisted Turning
$UVAT_{opt}$	:	Optimum condition for UVAT
UVAM	:	Ultrasonic Vibration Assisted Machining
V	:	Cutting speed
V_B	:	Average flank wear
V_M	:	Maximum flank wear
V_t	:	Speed of the tool
V_c	:	Critical speed
XRD	:	X Ray Diffraction

Chapter 1

Introduction

1.1   Introduction

Nowadays, high quality machining of advanced materials like titanium and nickel alloys is an important concern for the manufacturing industries. The main characteristics that encourage broad introduction of titanium alloys i.e. Ti6Al4V into aerospace, biomedical, chemical and petroleum industries are their high strength-to-weight ratio and superior corrosion resistance[1]. However, there are some difficulties in machining of Ti6Al4V alloys due to its low thermal conductivity and chemical affinity towards cutting tool materials. This leads to rapid tool wear due to diffusion and concentration of large amount of heat on cutting edge which results in poor machinability of titanium alloys with conventional machining processes. Moreover, the properties of titanium alloys at high temperature lead to form thin chips during machining which results in reduced contact area with cutting tool. The reduction in contact area increases the distribution of temperature and pressures on cutting tool. Hence, it is very important to minimize the problems encountered in machining of titanium alloys with alternative machining techniques.

1.2   Need of machining

Turning is one of the fundamental machining operation can be performed on lathe machine to generate part geometry and surface texture. It is widely used for many applications in manufacturing industry to produce large number of simple to complex components. In turning, a single-point cutting tool is used to obtained desired shape of components in which

tool is fed against a rotating workpiece either in parallel or perpendicular to the axis of rotation. In turning, rotation of workpiece is termed as primary motion whereas feed motion is known as secondary motion.

Machining of Ti6Al4V alloy with conventional turning (CT) generates high cutting force (F_c) and high cutting temperature (T_c) in primary deformation zone due to its properties [2]. To make matters worse, the desired shape of many aerospace components are produced with machining process. However, production of these components with CT is not economical due to use of low cutting speeds and low feed rates. In order to improve the productivity of machined titanium components, cutting fluid for cooling and lubrication are recommended to reduce the friction between tool-workpiece and also dissipate heat generated due to plastic deformation of material at cutting zone [3]. However, in recent years, due to raising demand of replacing traditional cooling lubrication methods to avoid environmental problems and increasing cost burdens, advanced machining techniques are on raise. The cost of cutting fluid in machining process is 16% of the total production costs, may reach 20%-30% in machining of difficult to cut materials life Ti6Al4V alloy, while tooling cost is 4% of total product cost [4,5]. Cutting fluid related cost in machining process is mainly due to environmental concerns which include handling and disposal of cutting fluids must obey stringent rules of environmental protection. The cost factor along with health and environmental issues associated with the use of cutting fluids are the main reasons for reducing their use. Hence, advanced machining process that signifies cost saving and concurrently improves the performance of machining process, is assisted dry machining. Furthermore, as the technology in machining progressed, newly developed machining processes were introduced to improve the machinability of Ti6Al4V alloys.

1.3   Ultrasonic Vibration Assisted Turning (UVAT)

Ultrasonic Vibration Assisted Turning (UVAT) is a newly developed machining process for difficult to cut materials in which high frequency vibration, 20 KHz with low amplitude vibro-impacts are superimposed on a movement of cutting tool. UVAT process has been found to be effective for machining of modern alloys over CT process. The reduction in cutting force and cutting temperature with improved surface and enhanced tool life is observed in UVAT compared to CT process [6–10]. The fundamental feature of this new machining technique is that, the cutting tool undergoes a cyclic displacement in either of

independent x, y and z directions with very small amplitude. This new class of machining was introduced during 1960s in which hydraulic vibrator was used to apply vibrations onto cutting tool with a frequency range of 0-125 Hz. In UVAT, direction of vibration can be either in tangential direction or in radial direction or in axial direction as shown in figure 1.1.
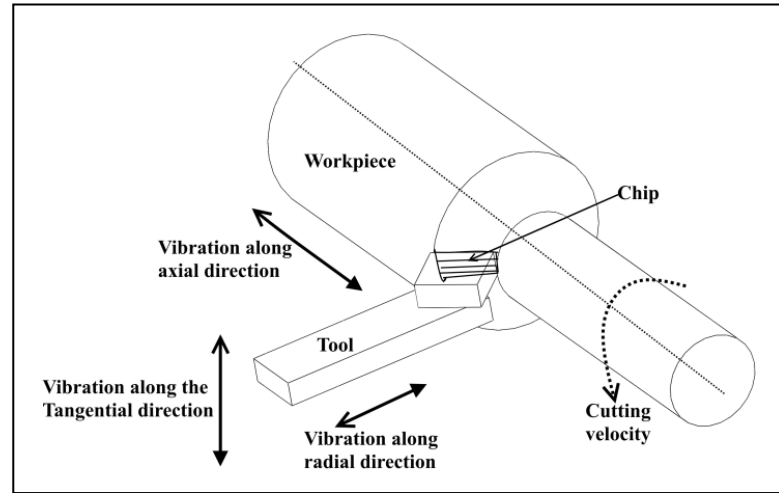
Figure 1.1: Different types of cutting vibrations in UVAT[7]

Initially, magnetostrictive effect or joule's effect was used to generate ultrasonic vibration in 1842. This method was completely obsolete due to loss of energy in generation of ultrasonic vibration. Later, piezoelectric effect was used to generate vibration to minimize the energy loss during conversion from electrical energy to mechanical displacement. The piezoelectric transducer with ceramic plates uses piezoelectric effect to converts an electrical energy of 20 KHz frequency to mechanical vibration with very small amplitude. The amplitude available at the end of piezoelectric transducer may not enough to produce discontinuous cutting between tool and workpiece. Hence, boosters and acoustic horns are connected between the transducer and the cutting tool to enhance the amplitude. The ultrasonic vibration system used for machining consists of an ultrasonic generator, piezoelectric transducer, concentrator or booster, and acoustic horn. The amplification of amplitude at the end of horn depends on its shape and size. For this amplification, various horn profiles such as cylindrical, stepped, conical, Bezier and exponential are used[11, 12].

1.4   Kinematics of Ultrasonic Vibration Assisted Machining

Ultrasonic Vibration Assisted Machining (UVAM) system can be classified into one dimensional (1-D) and two dimensional (2-D) UVAM systems according to their relative movement between cutting tool and workpiece. The coordinate system used to classify the

UVAT system is shown in figure 1.2. The X, Y and Z axis represents the primary cutting direction i.e upfeed direction, normal to nominal uncut surface of the workpiece i.e depth of cut (DOC) direction, and cross feed direction i.e feed direction respectively.
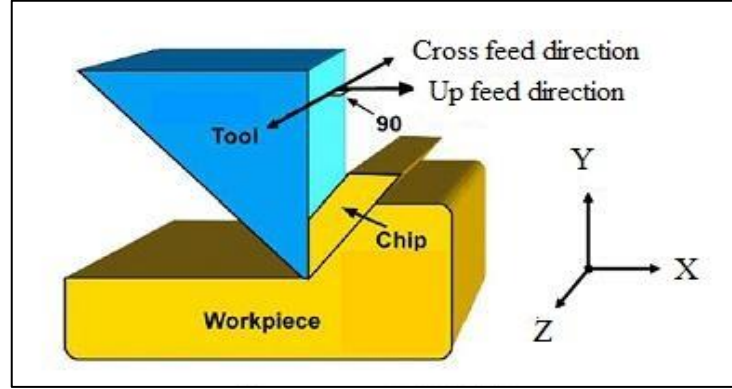
Figure 1.2: Coordinate system for UVAT system[13]

1.4.1 1-D UVAM

In 1-D UVAM process, cutting tool moves in a linear path with simple harmonic motion, which is superimposed on the movement of the workpiece. The cutting tool is continuously disengages with workpiece per each cycle of vibration. Hence, intermittent cutting is possible in UVAM process. However, there exists a critical velocity below which cutting tool breaks the contact with workpiece periodically [14].
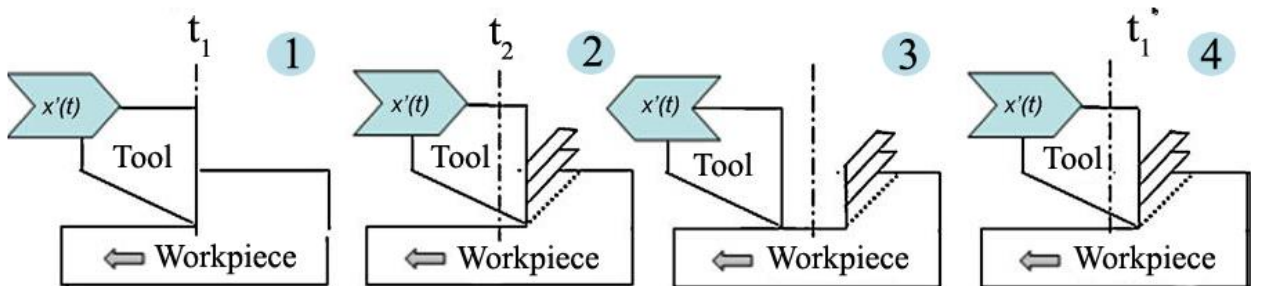
Figure 1.3: Machining in 1-D vibration assisted machining[13]

In UVAM system, the relative position and velocity of the cutting tool with respect to workpiece are given by

$$x(t) = a \sin(\omega t) + Vt \qquad (1.1)$$

$$x'(t) = a\omega \cos(\omega t) + V \qquad (1.2)$$

where ' $x(t)$' and ' $x'(t)$' are instantaneous position and velocity of the tool at a time t,

'ω' is angular frequency and

'V' is the workpiece cutting speed.

4

For a given oscillatory motion of the tool, the speed of tool (V_t) must always greater than the speed of workpiece (V). Hence, the condition for separation between tool and workpiece is V_t > V. If V_t < V, the continuous contact between tool and workpiece occurs even though tool vibrates with harmonic motion. Then critical velocity in UVAM process can be defined with instantaneous velocity of the cutting tool and it is give by

$$V_c = 2\pi fa \quad\quad\quad\quad\quad\quad (1.3)$$
$$V = \pi DN \quad\quad\quad\quad\quad\quad (1.4)$$

where 'f' is frequency and 'a' is amplitude of oscillation,

'D' is the diameter of the workpiece and

'N' is the rotational speed of workpiece.

The relative position of the tool and workpiece for one oscillating cycle of UVAM is shown in figure 1.3. At time t_1, i.e staring of the cut, the rake face of the tool is in contact with workpiece and it is about to start a cut. Then at time t_2, the tool completes the forward motion of the linear vibrating cycle and velocity become zero at this position. In position 3, tool starts its backward motion and its withdrawn from the rake face of the tool and in position 4, tool commences another cycle of cutting and moving forward to contact with the workpiece.. The total duration of cycle is 'T_p' and is equal to '1/f'. The total cutting time in one cycle of motion is 't_2-t_1' [13]. The duty cycle of 1-D UVAM is defined based on the portion of cutting action takes place between tool and workpiece. The duty cycle in other words known as Tool work contact ratio (TWCR).

Tool work contact ratio   or   Duty cycle = (t_2-t_1) / T_p \quad\quad (1.5)

The larger the value of TWCR, the larger the portion of each cycle that the tool is cutting. The value of TWCR always lies between 0 to 1 where 1 indicates the continuous cutting action between tool and workpiece.

1.4.2 2-D UVAM

The cutting action in 2-D UVAM for each cycle of vibration is shown in figure 1.4. In this cutting technique, the tool tip vibrates elliptically with the help of ultrasonic vibrator. At first instant t_1, cutting tool is free of cutting and it is located at the rightward end as shown in figure 1.4. When cutting starts at t_2, the cutting force becomes positive. After cutting the workpiece for certain time in this cutting period, the tool vibration speed in thrust direction

exceeds the chip flow speed and then cutting force becomes negative due to negative friction between tool rake face and chip. Moreover, the vibrating tool helps to pull out the chip away from the workpiece. Finally, the cutting ends when tool and workpiece are again in the same direction and then tool disengages from workpiece [15].
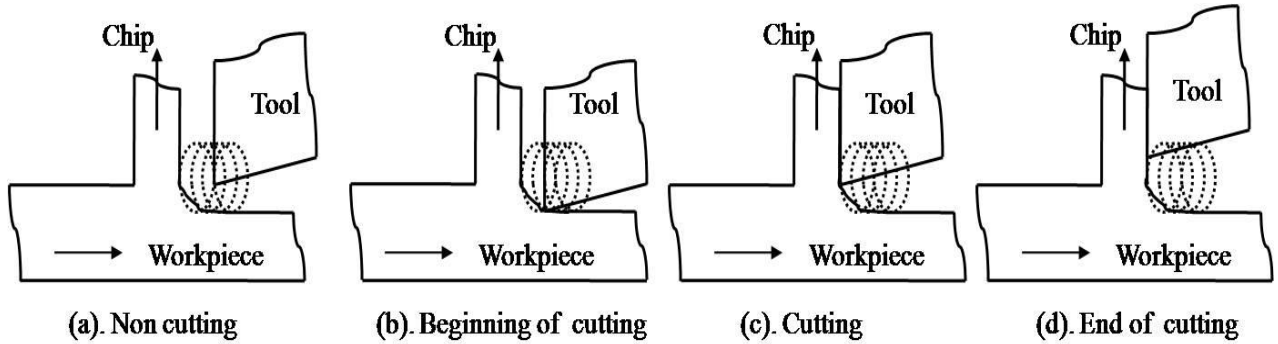
Figure 1.4: Machining stages in 2-D vibration assisted machining

1.5 Tool wear

In machining of Ti6Al4V alloy, there is a possibility of generation of localized adiabatic zones due to its low thermal conductivity. The raise in cutting temperature with increase in cutting velocity promotes the use of lower cutting speeds for machining [16]. The use of higher cutting velocities reduces tool life due to rapid wear of the tool cutting edge. The segmented chips formed during cutting causes the rapid growth of tool wear due to action of dynamic forces on cutting edge of the tool. Moreover, the concentration of localized temperature regions adjacent to cutting edge also increases the rapid tool wear [17, 18]. It is thus obvious that high cutting force and temperature developed in cutting of Ti-alloy increases the wear of the tool.

1.6   Residual stresses

Surface integrity is the most influential parameter for quality and performance of the machined components. Surface integrity of components depends on thermo-mechanical loading induced during machining process. The most significant factors used for evaluating surface integrity are residual stress, surface roughness, hardness and microstructure. Particularly, machining residual stresses have considerable effect on life of components by influencing its corrosion resistance and fatigue strength. Furthermore, residual stresses induced during machining have detrimental effect on product geometry and dimensional stability. Thus, it is important to analyze the residual stress distribution in machined

6

component based on material behavior and cutting conditions. Residual stresses can be either tensile (positive) or compressive (negative). The positive residual stresses deteriorate the life of components by initiating crack propagation whereas the compressive residual stresses improve its mechanical properties. The state of residual stress induced during machining process not only depends on cutting conditions but also on the material used. The thermo-mechanical phenomenon occurred during cutting process is the main source for the generation of residual stresses during machining process. The increase in thermal load due to increase in temperature is the source for generation of positive (tensile) residual stresses. Whereas, severe plastic deformation occurred during cutting process is responsible for negative residual stresses. In addition, the volumetric change of material due to phase transformation arising from difference of temperature during cutting process generates either tensile or compressive nature of residual stresses. But, it is difficult to estimate the importance of each of these factors in generation of residual stresses. The combined effect of thermo-mechanical loading and phase transformation decides the state of residual stress in components. Hence the final stress state of material not only depends on mechanical and physical properties of material, but also on the machining parameters used in machining process [19]. The mechanism of generation of residual stresses in machined components is shown in figure 1.5.

Phase transformation: High cutting temperature generated in machining and the cooling rate causes phase transformation on newly generated surface which results change in grain structure. The non-uniform change between surface layers and bulk material induce residual stresses. If the grain size is more, the surface layer tends to expand and bulk material around the surface layer constraints its expansion. This leads to generation of compressive residual stresses. In contrast, decrease in grain size due to phase transformation induces tensile residual stresses.

Plastic deformation due to thermal loads: In general, thermal gradients occur due to variation of temperature in cutting process. The heat generated in cutting causes the superficial layer to expand more than its subsurface layers. Since, thermal expansion prevented by subsurface layers compressive stresses is generated on surface layers. After cooling, surface layer tends to return to original position due to elastic recovery which in turn tensile residual stresses produced.

Plastic deformation due to mechanical loads: Machining forces causes compressive plastic deformation on machined surface layer. The contracted surface layer tends to comeback to

original position after removing machining process. However bulk material beneath the surface prevents the expansion of surface which in turn compressive residual stress formed.

The effect of phase transformation on residual stress generally occurs when there is more cutting temperature. However, the effect of thermo-mechanical loading on residual stress occurs simultaneously in most machining operations.
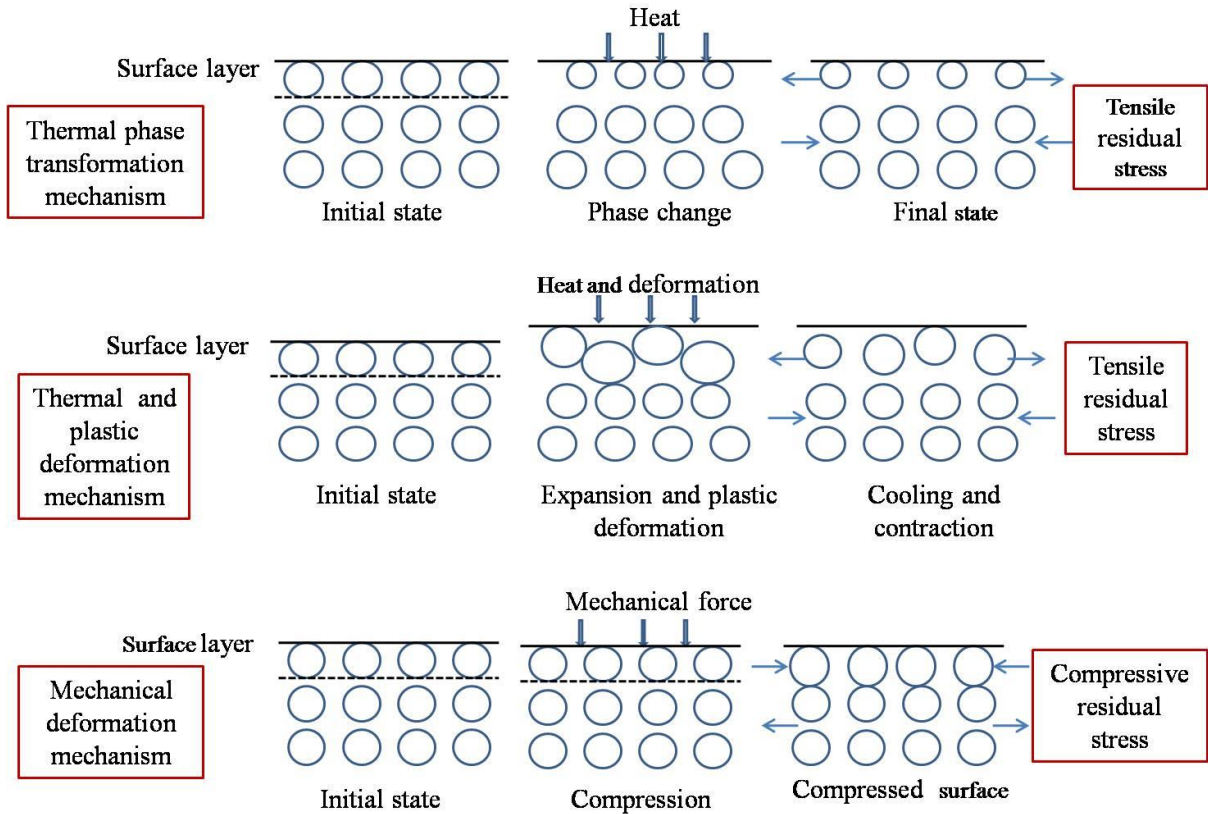
Figure 1.5: Thermo-mechanical loading during formation of residual stresses

1.7 Fatigue life

Fatigue failure is an important concern for the parts subjected to cyclic loading. Fatigue failure generally depends on surface integrity of machined components. Fatigue crack initiates from the free surface of the component which implies that product performance depends on the surface properties. In fact, component surface experiences severe mechanical and thermal loads, crack initiation and propagation depends on surface conditions after machining [20, 21]. Several researchers observed that the endurance limit strongly depends on the machining process and its impact the fatigue strength also[22, 23]. Previous research suggested that the roughness produced on the surface is not enough to estimate the fatigue

strength, highlight the importance of surface integrity. The geometrical irregularities and metallurgical changes after machining on the surface affect the surface integrity. Surface integrity extremely influences the surface and subsurface of machined component when it is subjected to dynamic loads. Surface integrity indicates surface characteristics like surface hardness, surface roughness and residual stresses. Among these characteristics residual stress plays a significant role. The residual stresses generated in the machining depend on the material properties and machining parameters used. Residual stresses induced during machining process due to thermo-mechanical loading significantly affect the fatigue life of machine component. The residual stresses induced during machining have significant effect on dimensional stability and life of machined surface. The type of residual stresses induced during machining has significant affect on the fatigue strength of machined component [24]. The increased heat energy with increase in cutting temperature promotes tensile residual stresses which reduce the fatigue life of component by initiating and propagating crack growth. However, mechanical loading is responsible for compressive a residual stress which improves the life of the component when it is subjected to cyclic loading. The compressive residual stresses and high hardness induced during machining process improves the fatigue life.

1.8   Finite Element Modeling and Simulation

Finite element modeling (FEM) is an important tool for better understanding of chip formation process during machining. FEM allows to deal with deformation characteristics like strain, strain rate, tool-chip contact, frictional characteristics like coefficient of friction, local heating and temperature effect, loading characteristics like boundary and loading conditions, and other phenomena occurred in machining problems.

The input parameters required for FEM machining simulation are shown in figure 1.6. The accuracy of any FE simulation of machining depends on selection of accurate constitutive material model which represents the behavior of the material at the extreme conditions that exist in shear zones. There are several constitutive material models with varying degree of accuracy to reproduce the thermo-mechanical loading occurred in metal cutting. Among these constitutive laws, Johnson-Cook (J-C) flow stress model is widely used material model for machining simulations since material behavior is expressed adopted for as a function of strain

(ε), strain rate ($\dot{\varepsilon}$) and temperature (T). Moreover, J-C constitutive law used in many FE codes successfully predicts the flow stress similar to machining conditions.
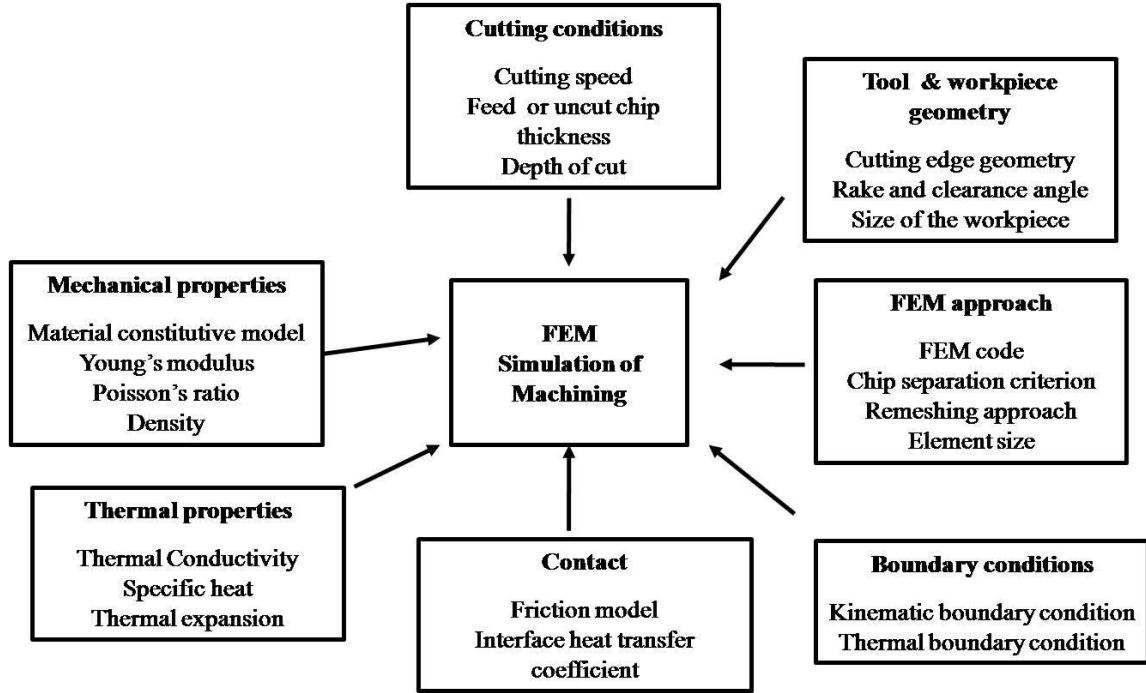
Figure 1.6: Important input parameters for FEM machining simulation

1.8.1 Johnson-cook material model

Johnson–Cook constitutive law is widely used for the analysis of flow stress of the materials which are highly influenced by thermo-mechanical loading [25]. The effect of thermo-mechanical loading i.e strain, strain rate and temperature on the flow stress is defined by three distinctive terms

$$\sigma = [A + B(\varepsilon)^n]\left[1 + C\,ln\left(\frac{\varepsilon^o}{\varepsilon_0^o}\right)\right]\left[1 - \left(\frac{T - T_{room}}{T_{melt} - T_{room}}\right)^m\right]$$

where σ is the equivalent plastic flow stress

ε is an equivalent plastic strain

$\dot{\varepsilon}/\varepsilon^o_o$ is the reference strain rate

T_{room} is the room temperature

T_{melt} is the melting temperature

The material parameters or constants are as follows

A is the initial yield stress

B is the hardening modulus

C is the strain rate sensitivity coefficient

10

n   is the hardening coefficient

and   m   is the thermal softening coefficient

This J-C material model has been used for simulations to predict the dynamic behavior of materials. The advantage of the J-C model is that the strain, strain rate and temperature are considered at the same time and proportional to flow stress of the material. The selection of suitable J-C parameters plays an important role in accuracy of FE simulation of machining as many J-C parameter sets are available in literature for the same material. The variation of J-C parameters for same materials could be attributed to different approaches used for finding material constants. The quasi-static tests and dynamic tests are commonly used experimental techniques to identify the J-C material constants. The tension and compression tests come under static test which are performed under different temperatures whereas Taylor and Split-Hopkinson Pressure Bar (SHPB) techniques are dynamic tests in which experiments are performed at different strain rates. In machining of Ti6Al4V alloy, the strains and strain rates observed in chip formation process are high due to severe material deformation. The strain rates observed in static test are low, when compared to strain rates obtained in machining process. Hence, flow stress data obtained from static test cannot predict the machining simulation results accurately[26]. SHPB is often commonly used dynamic technique in which experiments were conducted at higher strain rates in the range of 10^3 to 10^4 s^{-1}. The experimental configuration of SHPB technique is so complex and expensive, needs a lot of experimental data to obtain higher fitting to obtain material parameters [27]. Although, higher strain rates upto 10^5 s^{-1} were used to identify J-C parameters for material constitutive equations, lower strains were observed during Taylor test which are often less than strains induced during machining process [28].

1.9 Thesis outline

Chapter 1 described the problems associated with the machining of difficult to cut materials like Ti6Al4V alloy with conventional machining. Then, brief introduction of UVAT process is discussed along with its kinematics. Introduction of tool wear, residual stresses generation and fatigue life of machined components in machining of Ti6Al4V alloy is also presented. Finally, the importance of J-C parameters in FE modeling is described.

Chapter 2 reviews the previous research work done in machining of Ti6Al4V alloy, with CT and UVAT process. This chapter also discussed the tool geometry, tool work combination

while machining Ti6Al4V alloy. The effect of machining parameters in performance improvement of both CT and UVAT methods are discussed. The methods available to determine the J-C parameters are also presented.

Chapter 3 discussed the various steps involved in FE modeling of machining process and also presented the procedure for FE modeling used for UVAT process.

Chapter 4 described the experimental procedures in CT and UVAT. Various equipments, tools, measuring devices used and their specifications are presented in this chapter.

Chapter 5 discussed the machining approach to determine the J-C parameters for Ti6Al4V alloy to improve the accuracy of FE modeling of machining process. This methodology used modified Oxley chip formation theory to evaluate the physical quantities required for J-C material model at required rake angle.

Chapter 6 discussed the important machining parameters which effects the TWCR in UVAT method. Then, experiments are conducted to evaluate the performance of UVAT in terms of TWCR. The performance of UVAT is also compared with CT at various machining conditions. This chapter also discussed the effect of ultrasonic vibrations on the flank wear of the tool and compares with CT.

Chapter 7 discussed the machining induced residual stresses in UVAT at various machining parameters using FE modeling and simulations. The residual stress depth profiles are also evaluated with respect to thermo-mechanical loading at various machining conditions. Then, the effect of surface properties on fatigue life of Ti6Al4V alloy components are evaluated in UVAT and compared with CT machined components.

Chapter 8 concludes the summary of the current and also suggest the direction of future work.

Chapter 2

Literature Review

2.1 Introduction

Surface integrity plays an important role in improving the fatigue life of any machined component. The surface properties of Ti6Al4V alloy affects life of component when it subjected to dynamic loading. Ultrasonic Vibration Assisted Machining is a promising cutting technique for all variety of materials like ductile, hard, brittle, plastic and composite materials to improve their machinability. The discontinuous contact between tool and workpiece reduce the cutting force, cutting temperature and surface roughness. However, experimental and theoretical investigations are still needed to know the effect of thermo-mechanical loading on UVAT of Ti6Al4V alloy. Moreover, deeper understanding of intermittent cutting action in UVAT is necessary to know the fatigue strength of machined component with respect to surface integrity.

2.2 Machinability of Titanium alloys

Machinability is an indication of the ease with which material can be machined with low cost. The machinability of Titanium alloys is difficult due to their properties like low thermal conductivity and high chemical reactivity with tool materials. The machinability of material can be assessed by tool material, cutting parameters, tool geometry, cutting forces, and tool temperature [29–31]. This section explains observed effects from literature on these issues.

2.2.1 Cutting tool

The machinability of titanium alloys is improved with paramount qualities of cutting tools. The cutting tools should posses the high hardness and toughness, high thermal conductivity and good chemical inertness to withstand the high stresses and chip segmentation process, to diminish thermal gradient and to slowdown the reaction process [32]. The degree to which each of these properties required depends on properties of workpiece material.

. Machining of titanium alloys at higher cutting speeds tend to generate high temperatures and stresses at tool nose region which further causes plastic deformation and subsequent tool failure [33]. Titanium alloys are very reactive with cutting tool materials at and above the interfacial temperature of 500 ºC . Tungsten carbide (WC-Co) cutting tools are used to machine titanium alloys at cutting speed of 45 m/min [34]. At high temperature, Tungsten carbide cutting tools used for machining of titanium alloys form titanium carbide (TiC) which resist the deformation at higher temperature. Titanium alloys are usually machined with uncoated Tungsten carbide (WC-Co) tools at and above cutting speed of 45 m/min and coated carbide tools for higher cutting speeds [34]. The coating on the tool acts as a thermal barrier which further reduces the cutting forces by reducing the coefficient of friction. Furthermore, the composition of WC-Co tool improves the crater wear resistance in machining of titanium alloys by forming protective layer at higher cutting speeds.

2.2.2 Cutting parameters and tool geometry

Experimentally it is found that cutting speed is the important cutting parameter influence the tool life. It is also suggested that the cutting speeds of 30 m/min and 60 m/min are economical for machining of titanium with High Speed Steel (HSS) and carbide cutting tools respectively [32]. However, the tool life is not changed much with feed rate (f_r), but feed rate is very sensitive in machining of titanium alloys. Machining at high feed rates is desirable to increase productivity. Similarly, the tool geometry also has a considerable influence on the tool life in machining of titanium alloys. Cutting tools used in machining have finite sharpness. The contact between flank surface and machined surface induce ploughing force.

2.2.3 Cutting forces

Cutting forces are considered as an important process parameter for characterizing machining processes and selecting suitable cutting tool [35, 36]. The ploughing force is significantly used in mechanism of chip formation, stress calculation and tool wear monitoring. Frictional force generated during machining has a significant role in estimation of machinability of materials. In general, frictional force is proportional to the normal force between mating surfaces and is independent of the contact area. Frictional force in machining is developed as newly generated surfaces contact with the cutting tool.

2.2.4 Cutting tool temperature

The importance of measuring temperatures during machining and evaluating their effects on both the cutting edge of the tool and the workpiece has long been appreciated [37]. The limitation of cutting speed in machining of workpiece materials depends on the tool wear. The prediction of temperature in machining is complex due to its asymptotic increase with cutting speed. Moreover, the measurement of temperature close to the cutting edge of the tool is also a challenging task in metal cutting process [38]. The cutting temperature has a significant role in the tool wear. It is also evident that temperature dependent mechanisms are responsible for progression of tool wear [39]. However, maximum temperature is used to determine the tool life. Apart from the tool life, the temperature gradient on machine surface also affects subsurface deformation characteristics and residual stresses in the finished part [37] .

Thermal stresses are generated in cutting tool during machining of titanium alloys due to its lower conductivity. The heat generated during machining of titanium alloys flow into the tool than the chip. This causes frequent failure of tool due to thermal stresses and fracture failure [40].

There are various techniques of tool temperature measurement. In addition to thermocouples, the infrared (IR) radiation techniques are widely used method for temperature measurement.

2.3 Ultrasonic Vibration Assisted Turning

Ultrasonic vibration assisted turning (UVAT) is an intermittent cutting technique in which high frequency (f) and low-amplitude (a) vibrations are added to the movement of the cutting tool. This action results in separation of the cutting tool from the workpiece at regular intervals of time that further enhances the surface finish and tool life by reducing cutting force and cutting temperature in UVAT compared with CT process. UVAT has been found effective in machining of hard materials as per the requirement for industries, as it to overcome high heat generation and consequent rapid wear of cutting tool edges that occur during CT. UVAT is preferred by many researchers in analysing the mechanics and advantages resulted from vibration assistance. A critical review of Vibration assistance in turning process and its performance evaluation by various means done by researchers are reported in table 2.1.

Table 2.1: Historical background of cutting parameters used in UVAT method

References	Workpiece material	Parameters				
		Vibrating Parameters		Cutting parameters		
		Frequency KHz	Amplitude μm	Cutting speed m/min	Depth of cut mm	Feed rate mm/rev
Balamuth, 1966[41]	Ti6Al4V, tool steel	20	25			
Skelton. R.C,1968 [42]	Mild steel	12.4	2.54	137-166	0.762	0.13
Weber *et al*,1984 [43]	Steel-C60,Glass, Ceramics,XSCrNiMo18	20	a = 8-12 b = 8-12	0-420	0.1	
Kumabe and Hachisuka,1984[44]	SS, Hard Steel	19.8	24	6	0.01	0.015, 0.03
Kumabe et al., 1989[45]	Ceramics, glass	19.6	16	0.2		
Moriwaki *et al,* 1991 [46]	Stainless steel-SUS303Se	40	3	1.4-4.2	0.0023	
Kim *et al,*1993 [47]	CFRP	19.5	15	19-165	0.05-0.3	
Shamoto *et al,* 1994 [48]	Copper	0-0.006	a=5 b=5	0.26	0.01	
Moriwaka, *et al,* 1995 [49]	Oxygen free-Copper	20	a = 0-8 b = 11-16	5	0.005	
Kim and choi, *et al,*1997 [50]	CR-39	20	26.4	0-89.4	0.1	
Shamoto *et al,* 1999[51]	Steel-SUS-42OJ2	20	a = 4.5 b = 4.5	3.4	0.01	
Liu, *et al,*2002 [52]	Particle reinforced metal matrix	20	15	4.24-12.72	0.1-0.5	

	composite SiCp/Al					
Xiao *et al*,2002 [53]	S45C steel	20	15	58	0.05	
Gao, *et al*,2002 [54]		19.46	15	5.4-44	0.1	
Suzuki *et al*,2003 [55]	JIS: SUS420J2	19.6	3-6	0.25-0.7	0.001-0.005	
Babitsky, *et al* , 2004 [56]	Inconel-718	20	15	17	0.8	
Mitrofinov *et al*, 2004[8]	Inconel 718	20	15	18.6	0.4	
Ma *et al*, 2004[15]	Al-52S	18.76	a = 4 b = 4	15.75	0.05	
Mitrofinov *et al*, 2005 [15]	Inconel 718	20	13	18.6	1	
Mitrofinov*et al*, 2005 [57]	Inconel 718	20	7.5	18.6	0.4	0.1
Ma, *et al*, 2005[58]	Al-52S	18.66	a = 3.5 b = 3.5	3.94-18.93	0.05	
Zhong, *et al*, 2005[59]	Aluminium-based metal matrix composites	20	23	1.5-3	1-3	
Ahmed *et al*,2006 [60]	Inconel 718	20	30	38	0.1	
Ahmed, *et al*,2007[61]	Inconel 718	20	15	18.6	0.4	
Ahmed *et al*,2007 [6]	Inconel 718	20	15	0.1	0.4	
Nath et al, 2007[62]	DF2 (Low alloy steel)	19	15	50-90	0.2	0.1-0.2
Nategh *et al,* 2012 [63]		20	6-16	31.8-126	1-2	
Razavi *et al*,2012[64]	Aluminium 6061	20	6-16	31.8-126	1-2	

2.3.1 Machinability and cutting stability of UVAT method

The reduction in thermo-mechanical loading, high cutting stability and lower tool wear in UVAT improves the surface integrity of machined component compared to compared to CT process. Previous studies reported that the large reduction in cutting force (12%-80%) is observed in UVAT process under the same cutting conditions; however, the reasons for this lower cutting force are explained with various mechanisms in these studies. Few researchers stated that the multifold decrease in cutting force is mainly due to low friction between the tool and workpiece interface. On the other hand, reduction of cutting force in UVAT depends on tool-workpiece contact time for each cycle of vibration [44]. Hence, it is inevitable to review the causes for the lower coefficient of friction at different cutting conditions in UVAT method.

Skelton [42] investigated the performance of UVAT system by applying ultrasonic vibration using magnetostrictive transducer in both vertical and horizontal directions on carbide tip cutting tool. The decrease in friction between chip and cutting tool due to reversal of chip and pulsating action of cutting tool per cycle of vibration in UVAT process were responsible for low cutting force and cutting temperature.

Weber et al. [43] superimposed high frequency and low amplitude ultrasonic vibrations on the cutting tool to investigate the efficiency of UVAT method. A significant improvement in tool life was observed in machining of glass ceramic due to large reduction in cutting force and removal of heat from the cutting tool. The ultrasonic vibrations induced during machining caused the formation of powdered chips which further improves the tool life. Moreover, reduction in built up edge formation in machining of C60 steel and XSCrNiMo18 with UVAT method was responsible for the improved surface finish of machined workpiece.

Most of the work on UVAT was performed with wide range of transducers developed with piezo-ceramic rings in Kobe University, Japan in the 1990s [46,48]. A significant reduction in the cutting force and improved surface was observed with diamond tools with the introduction of vibrations on the cutting tool. However, their experimental results were not validated with any other method results. Moreover, built up edge (BUE) formation only considered for their surface roughness analysis without any validation. Similarly, Kim and Choi [50] have used UVAT for machining of ferrite, glass and optical plastics and it has

shown mirror surface finish compared to CT. Furthermore, ultrasonic vibrations in machining of low carbon steel has shown significant improvement in tool chatter suppression when compared to CT [53]. Liu et al. [52] observed significant reduction in cutting forces and improvement in surface finish in machining of SiCp/Al composites material with ultrasonic vibrations.

Numerical analysis is one of the powerful technique to evaluate machining process effectively. Mitrofanov et al. [8, 10, 57, 65] used simulation studies to know the effect of machining parameters on cutting force, cutting temperature and chip formation in UVAT. A decrease in the feed rate reduced a considerable amount of cutting force and cutting temperature in the machining zone. It was also found that the interaction between tool and workpiece is about 40% of vibration period. This helps to reduce the frictional heating, to have lower stresses and strains and to produce thinner chips. It was also observed that considerable reduction in average cutting force and equivalent strains observed when frequency increased from 10 to 30 KHz. This indicates that decrease in time of contact between tool and workpiece has significant effect on performance of UVAT process. Similarly, Babitsky et al. [7] compared the performance of UVAT with CT in machining of C263, Inconel-718 and Mild steel through experimentation in terms of the surface roughness and roundness machined surfaces. There was a substantial improvement in roundness of machined workpiece in UVAT compared to CT process. Moreover, the surface finish improvement in machining of Inconel-718 and C263 with cutting speed of 10–25 m/min range was 40–50% and 20-25% respectively when compared to CT process. In another study [56], FEM simulation with frictional less contact mode was used to optimize the machining parameters with respect to cutting force and improved surface profiles was observed with experimental results

Ahmed et al. [61], investigated the performance of UVAT of Inconel using FE simulation and validated through experimentation with respect to chip shape and distribution of equivalent plastic strains and stress, friction, cutting force and temperature. The cutting force was reduced by 20-25% due to absence of friction force at tool chip interface.

The surface produced in UVAT was compared with CT with studies of nano indentation, light microscopy and scanning electron microscopy (SEM) [57]. The width of hardened layer is greater than that of affected surface layer in UVAT compared to CT. A three dimensional thermo-mechanically couple FE model is developed for both CT and UVAT

process and identified that the equivalent plastic strain was reduced by 5-7 % and average cutting force reduced by 47% in UVAT. The microstructure of machined surface was not affected due to reduction in cutting temperature in UVAT. In a numerical study of UVAT of aged Inconel, cutting temperature, stress and strain distribution in cutting region was evaluated. The equivalent plastic strains of machined surface were reduced by 20 % in UVAT compared to CT [10]. The mean level of stresses and cutting forces were considerably lower in UVAT.

In another study[66], the performance and cutting stability of ultrasonic machining were evaluated in terms of TWCR. The performance of ultrasonic vibration cutting was improved by lowering TWCR by increasing amplitude and frequency at lower cutting speeds. Nath and Rahman [67] studied the effect of tool vibration frequency, tool vibration amplitude and workpiece cutting speed on mechanism of ultrasonic vibration cutting. They also studied the significance of TWCR with respect to both vibration and cutting parameters in ultrasonic vibration cutting. Increase in both the frequency and amplitude and the decrease in the cutting speed reduce the TWCR, which in turn reduces both cutting force, tool wear and improves surface quality. Experimentally, it was observed that ultrasonic vibration cutting promises better tool life compared to CT at lower cutting speeds in machining of Inconel 718.

Riaz Muhammad et al. [68] developed a 3-D FE model to evaluate the performance of UVAT of Ti-15333 in terms of cutting force and cutting temperature at various cutting conditions. The advantage of reduced cutting force in UVAT process is decreased with increase in cutting speed and decayed beyond 60 m/min. Further, it is also observed that machinability of material with UVAT process was improved with low vibro-impacts. The small impacts due to vibration at the tool workpiece interface improved the machinability with generation of shorter chips and reduced cutting forces. In an another study, Maurotto et al. [69] developed an improved UVAT setup and conducted experiments on β-titanium alloy (Ti-15-3-3-3). The substantial reduction in cutting force was observed in UVAT compared to CT process due to improved in surface topography and sub surface layer in machining of β-titanium alloy.

Sandip patil et al.[70] Investigated the effect of UVAT in machining of Ti6Al4V alloy in terms of cutting forces, cutting temperature; effective stresses, surface quality, chip morphology and microstructure and validated the results with experimental results. The variation of equivalent stresses in UVAT process was explained with four stages and

concluded that there was a significant reduction in stress level on cutting tool and workpiece and maximum occurs only at loading of the tool on workpiece. The significant reduction in cutting force and cutting temperature was observed in UVAT along with improved surface finish compared to CT process. Moreover, the thickness of chips produced in UVAT process was thin and continuous whereas thick and uneven chips were produced in CT process at same cutting conditions.

In another study, Silberschmidt et al.[71] evaluated the performance of UVAT process through both experimentation and simulation in machining of Inconel 718. FE model developed for both UVAT and CT were used to evaluate cutting force, the stress and strain state. The surface of workpiece was improved with less influence on the workpiece material microstructure in UVAT compared to CT. It is also reported that chips produced during UVAT process contact the cutting tool about 40% of cutting time. Hence, the mean stress levels in UVAT process are low with considerable reduction in cutting force.

In UVAT, the direction of vibration also plays a major role in performance of machining process. The vibratory motion can be applied either in tangential or transverse direction to workpiece. Hence, there is a need to review the advantage of direction of vibration in UVAT. Ahmed Syed Adnan and Sathyan Subbiah [72] investigated the effect of transverse vibrations in UVAT process. In this orthogonal cutting, transverse vibrations at frequency of 40 KHz were applied to the carbide cutting tool in machining of Al-2024 tubes. The grooves were formed on work surface in transverse direction with vibrations whereas groves were formed along cutting velocity direction with no vibrations. This concluded that applying vibrations in transverse vibration has some advantages over CT but not more than that UVAT along cutting direction. Celaya et al. [73] investigated the effect of tool vibration on surface quality of mild steel at various cutting speeds, feed rates and depth of cuts. From spectral analysis, they reported that vibration in cutting speed direction reduces the crests produced by the tool and reduced the waviness of generated geometry. It was reported that the vibration applied in cutting direction improved more surface finish (40%) than vibration applied in feed direction (6 %).

The frictional behavior at tool workpiece interface plays a significant role in generation of cutting temperature in machining operation. The effect of friction between chip tool interfaces in UVAT process is evaluated by analytical modeling [74]. The experiments were conducted on Al 6061 using carbide cutting tool to validate the analytical modeling for

UVAT process. From experiments, its observed that the coefficient of friction encountered in UVAT is relatively high compared with CT process. The stress distribution and coefficient of friction at chip tool contact length are evaluated at different cutting speeds and amplitudes. They concluded that the normal and frictional forces were increased with increase in cutting speed and decreased with increase in amplitude and frequency in UVAT.

Zhang and Wang [75] studied the effect of tangential vibration to cutting tool in UVAT of Ti6Al4V alloy with numerical analysis. The large reduction in cutting force, cutting temperature and equivalent stress was observed in UVAT compared to CT. Sofuoglu et al.[76] conducted numerical analysis to understand the performance of Hot Ultrasonic Assisted Turning (HUAT) of titanium and Hastelloy-X alloys. They observed that the significant reduction in cutting force and effective stress was observed in HUAT compared to CT and UVAT. Lofti and Amini [77] developed a finite element model for CT, UVAT and elliptical vibration assisted turning to investigate the machinability factors on Inconel 718. The large reduction in cutting force was observed with elliptical ultrasonic vibration cutting due to reduced contact between chip and rake face in sticky zone.

The stability of cutting system plays a crucial role in its performance evaluation. The instability of cutting systems leads to higher cutting forces, BUE formation and chipping of cutting tool which results in lower tool life. The force and chatter cutting models were used to verify and compare the dynamic cutting stability of UVAT with CT system [54, 66, 77, 78]. From this analysis, it was observed that the cutting force in UVAT was low compared to CT due to its high cutting stability. The tool geometry especially tool nose radius plays an important role in stability of cutting system. Moreover, it was also found that the cutting system stability was improved with high rake angle and lower clearance angles [66]. The increased stability with UVAT method may increase the tool life compared to CT.

2.3.2 Surface profiles in UVAT

UVAT is a promising machining technique for hard materials to produce better surface finish on complex machined products due to its high cutting stability. The quality of machined surface depends on acceleration of tool wear with continuous machining operation. The nano-finished surfaces were produced with ultrasonic vibration cutting by reducing abrasive tool wear at lower feed rates[62]. The improvement in surface and geometrical properties were better in UVAT compared to CT. Previous studies reported that there was

large improvement in surface finish along with lower roundness and waviness errors in UVAT method compared to CT [42, 50]. Gao et al. [54] reported that the reduction in surface roughness with UVAT was in the range of 32-56% for all conditions due to the effective depression of the influence of friction cracks and surface plastic deformation. It was also found that the surface roughness and roundness were improved in the range of 25-50% and 25-60%, respectively, in machining of hard materials with UVAT than CT[7]. Zhang et al. [75] also confirmed the precise surface finish of Ti-alloy with diamond turning in UVAT. Similarly, the geometrical error, i.e surface roundness was reduced with the inclined ultrasonic cutting compared to CT of SCM435 (40HRC).

2.3.3 Tool work contact ratio in UVAT

In UVAT, the reduction in cutting force and cutting temperature depends on the time of separation of tool from workpiece. The contact ratio between cutting tool and workpiece is expressed in terms of TWCR which defines the time available for contact of tool with workpiece per one cycle of vibration in UVAT process. Hence, it is important to evaluate the performance of UVAT in terms of TWCR for better understanding. In one of the study, the performance and cutting stability of ultrasonic machining were evaluated in terms of TWCR [53]. The performance of ultrasonic vibration cutting was improved by lowering TWCR by increasing amplitude and frequency at lower cutting speeds. The machinability of Ti6Al4V alloy in UVAT was improved by controlling TWCR. Hence, it is important to identify both vibrating and cutting parameters which influence TWCR to enhance the performance of UVAT process. Nath and Rahman [67] studied the influence of machining parameters on TWCR by varying cutting speed and feed rate(f_r).

2.3.4 Effect of Parameters in UVAT

The performance of UVAT method depends on the machining parameters, tool geometry and the properties of tool-workpiece materials. The two important vibration parameters: frequency and amplitude help to improve performance of UVAT process by lowering cutting force and cutting temperature with improved surface. Several researchers have studied the influence of vibrations in UVAT of difficult to cut materials. The decrease in friction between chip and cutting tool due to reversal of chip and pulsating action of cutting tool per cycle of vibration in UVAT process were responsible for low cutting force and cutting temperature [65]. Some authors compared the performance of UVAT and CT for

certain range of machining parameters. The performance of UVAT process was improved by considering lower cutting speeds at higher frequency and amplitude in machining of Inconel 718 material [8, 58] found that the surface finish and dimensional accuracy with UVAT of Inconel-718 was higher at lower cutting speeds compared to CT. In another study, it was found that higher values of amplitude and frequency caused larger reduction in cutting force in UVAT process [60]. However, the cutting force was doubled when feed rate increased from 0.1 to 0.2 mm/rev due to resistance offered by the cutting tool in the direction of feed. Maurotto et al. [69] found significant reduction in cutting force and improved surface finish in machining of both Ti and Ni alloys with ultrasonic vibration. Muhammad et al. [69] observed a significant reduction in cutting force with increase in cutting speed and depth of cut. Maximum temperature developed in the cutting region in machining of Ti alloy with UVAT process was more compared to CT. Iorio et al. [80] developed a new vibration cutting system to improve the surface texture of AZ31 magnesium alloys. From this study, it was observed that frequency, cutting speed and feed rate were the critical parameters to vary the surface texture on machined component. Puga et al. [81] applied ultrasonic vibrations to cutting tool to conduct experiments on cast and wrought aluminium alloys to test the effect of intermittent cutting. The large reduction in surface roughness and maximum peak height of surface was observed with an increase in feed rate. Xu et al.[82]studied the effect of process parameters on chip morphology of 304 austenitic stainless steel in UVAT and CT. It was identified that the ideal shape of chip and chip breaking was obtained with vibration. Moreover, it was identified that distortion of chip was minimum at lower cutting conditions. In another study, Lotfi et al.[83] studied the effect of ultrasonic vibration on tool wear and surface roughness in machining of AISI 4140 steel. The reduction in contact time between tool and workpiece in UVAT resulted in lower heat conduction from deformed chip to rake face of the cutting tool which improves the tool life. In order to evaluate the effect of vibration assistance, Maroju et al. [84] studied the effect of low frequency in UVAT process. It was identified that reduction in cutting force and tool wear were not so effective at low frequency vibrations. It was also shown that compressive residual stresses were dominant due to added vibration.

To sum up the above discussion, tangential direction of vibration provides better results than other direction of vibration in UVAT process. Moreover, the cutting stability of UVAT system also improved with tangential direction of vibration. The previous studies indicated that the performance of UVAT process is improved with lower cutting conditions. Few studies indicated that the intermittent cutting action between tool and workpiece is

responsible for reduction in cutting force and cutting temperature, and improvement in surface compared to CT process. Therefore, there is a need to investigate machining parameters effect on tool workpiece contact ratio and selection of parameters based on lower pulsating action between tool and workpiece in UVAT process.

2.4 Machining induced residual stresses

Residual stresses are commonly induced by thermo-mechanical loading occurred due to non-uniform plastic deformation and phase transformation. The mechanical loading raised in the machining zone is found to be responsible for larger compressive residual stresses whereas thermal loading raised in the primary and secondary zone of machining is responsible for generation of tensile residual stress. The metallurgical changes occurred due to raise of temperature to critical level results in either tensile or compressive residual stress. However, the complexity involved in generation of residual stresses due to thermo-mechanical loading, no clear cut conclusions can be drawn. From previous works, it is observed that several researchers contradict each other. The presence of thermo-mechanical loading on machined surface during machining process is shown in figure 2.1.
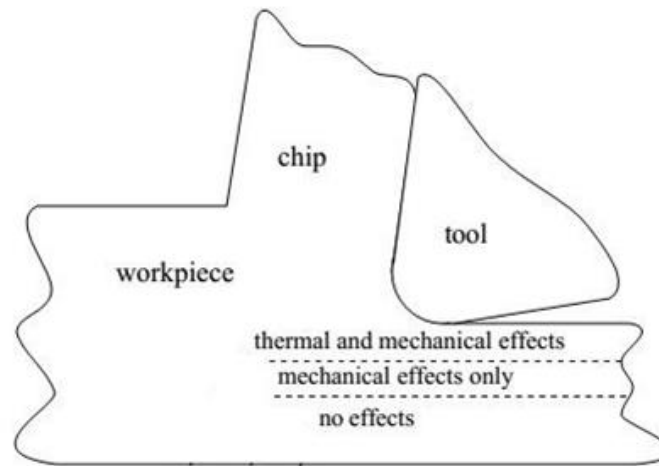
Figure 2.1: Development of residual stress along subsurface due to various loads [85]

The nature of residual stress is tensile or compressive depending upon the conditions of loading. They are not uniform throughout the deformed material and the nature of residual stress effect the product performance and life. Tensile residual stresses helps to initiate the crack propagation when subjected to cyclic loading and thus results in short fatigue life where as compressive residual stresses enhance the component performance and product life. Generally tensile residual stresses pertain near the machined surface due to predominant

thermal loads compared to mechanical loads. Friction play an important role in case of tensile residual stress as it generates high temperatures and eventually develops predominant thermal loads at surface. Further the machined surface cools at faster rate compared to that of subsurface layers leads to decrease in grain sizes, this indicate that surface contracts more and is subjected to compressive loading. When the strains drop to zero the resulting residual stress will be tensile in nature. The subsurface is allowed to expand leading to shear bands, indicate it is subjected to tensile loading and when the strains drop to zero it will result in compressive residual stress. Because, compressive residual stress increases the ability to withstand the tensile working loads that occur during working of the product and prevent crack initiation. In contrast, tensile residual stresses decrease the amount of working stresses that the component can sustain, which lead to premature failure of components.

2.4.1 Experimental efforts in Residual stresses

Liu and Barash [86] evaluated the effect of parameters on the generation of residual stresses. They observed that the residual stresses profiles on the machined surface depend on shear plane, flank wear of the tool and cutting edge. The shape of cutting edge has major effect on residual stress pattern near the machined surface and depth of cut has no effect on subsurface stress profiles.

Sadat and Bailey [87] conducted orthogonal experiments on AISI 4340 to determine the effects of cutting parameters on residual stresses. In this study, deflection etching technique was used to measure the residual stresses. They reported that the subsurface residual stresses were increased with an all cutting parameters. However, maximum residual stresses at low speeds were tensile and became compressive with increase in cutting speed. Similarly, Jang [88] used X-ray diffraction (XRD) technique to determine the effect of machining parameters on machining induced residual stresses on AISI 304 stainless steel. They reported that principal surface residual stresses were very close to hoop and axial direction of workpiece and also confirmed that tool sharpness has significant influence on the surface residual stress.

Matsumoto [89] conducted hard turning experiments to determine residual stress profiles. From experiments, it was identified that feed rate and depth of cut has no influence on subsurface residual stresses. It was also found that fatigue life of hard turned components

was increased due to high subsurface compressive stresses. However, the subsurface residual stress profiles were significantly affected with cutting edge of tool.

Jacobson [90] performed turning experiments on hardened M50 steel with different cutting tool at various depth of cuts. The compressive residual stresses were observed on the surface of machined component. The compressive residual stresses were observed with higher negative rake angle and smaller nose radius. However, depth of cut has no significant in generation of residual stresses. In another study by Thiele and Melkote [91], the effect of hardness and hone edged tools on residual stresses was evaluated by conducting hard turning experiments on AISI 52100. They reported that large edge hone tools produce measurable sub-surface plastic flow with large compressive residual stress.

Outeiro et al. [19] analyze the effect of thermo-mechanical phenomenon on residual stress distribution in machining of Inconel 718 and stated that these stresses were mainly due to the heterogeneous plastic deformation caused by the cutting forces and the effect of thermal load was negligible. It is commonly admitted that severe plastic deformation and large heat generation during machining process develops compressive and tensile nature of residual stresses profiles respectively. Copello [92] observed that tool tip radius and feed rate have significant effect on distribution of residual stress whereas rake angle and cutting speed have negligible effect. Arrazola et al.[93] analyzed the effect of cutting parameters on residual stress distribution in machining of Inconel 718 using 3D FE model. They reported that tensile residual stresses were increased with increase in heat generation. Xin et al.[94] attested from their experimental study that subsurface layers of machined component were also affected during machining of titanium alloy. They also reported that compressive surface residual stresses were increased with increase in feed rate and DOC and decreased with increase in cutting speed.

2.4.2 FE modeling of machining induced residual stresses

FEM is an important tool for predicting residual stresses in metal cutting. Mishra and Prasad, [95] developed an analytical model using FEM to determine residual stress profiles based on moving heat source. This model analyzed the effect of thermo-mechanical loading on residual stresses in grinding process. In this study, thermo-mechanical loading was considered in terms of magnitude of mechanical force, the rate of heat input, and the speed of movement of the workpiece. Lin [96] developed a FE model to analyze the strain filed in

workpiece. Moreover, the developed strain filed was used to determine stresses filed using concept of particle flow. In similar research aimed at determine the effect of thermal and mechanical loading, Wiesner [97] developed a FE model to evaluate the generation of residual stresses in orthogonal cutting of AISI 304. The finite difference method was used to find the workpiece temperature. The developed model was validated using experimental residual stresses measured by X-ray diffraction technique. They concluded that thermo-mechanical loading caused the generation of tensile residual stresses. Shih [98] developed a FE simulation using plane-strain condition for orthogonal machining. The material model used in developed simulation considers the effects of strain, strain rate and temperature. Though the simulation results were comparable with experimental results, model was mot discussed the mechanism caused residual stresses. Hua [99], developed a FE model using DEFORM 2D with Lagrangian approach to simulate orthogonal cutting of AISI 52100. The simulation results were validated with experimental results. In this study the effect of feed rate, workpiece hardness, and cutting edge on the subsurface residual stress generation was analyzed. In another study by Liu and Guo [100], Abaqus/Explicit was used to investigate the effect of sequential cuts and frictional force on generation of residual stresses in machining of AISI 304 stainless steel. The residual stress of affected layer changes its magnitude and nature from one cut to other sequential cut. Moreover, the frictional condition of tool chip interface is sensitive to residual stress generation machining. Although, the results from FE models are informative to analyze the residual stresses profiles in metal cutting, the mechanisms responsible for residual stresses are not clarified clearly. Hence, advance FEM are required to analyze the mechanism involved in the residual stresses.

From above literature it is identified thermo mechanical loading occurred during cutting process is the reason for formation of residual stresses. Hence, it is important to identify the parameter which affects heat generation and mechanical loading which eventually affect the residual stresses.

2.4.3 Residual stresses in UVAT

There are so many techniques to reduce the heat and mechanical force in cutting process. Ultrasonic vibration assisted turning is an important manufacturing process in which cutting tool is continuously excited with high ultrasonic frequency and low amplitude. The

intermittent cutting action between tool and workpiece in UVAT process reduce the generation of heat and mechanical load which results in improved state of residual stress[9].

The mechanism of residual stress distribution in UVAT was studied by few authors. Nestler and Schubert [102] studied the residual tress distribution in UVAT process by imparting vibration in cutting, radial and feed direction. It was identified that negative residual stresses were observed on surface of the workpiece when vibrations imparted in cutting and radial direction. Naresh and Vamsi[85] conducted numerical analysis to understand the dynamic changes in residual stress distribution in various stages of UVAT during Ti6Al4V alloy machining and results were compared with CT. The effect of intermittent cutting on residual stress was analyzed in UVAT using both FE simulation and experimentation. A three dimensional (3-D) FE model was developed for UVAT process and model was validated with experimental results in terms of cutting force, cutting temperature and residual stresses. The axial and hoop residual stresses were analyzed experimentally using X-ray diffraction technique. They observed that the nature of residual stresses is predominantly compressive in UVAT compared to CT, due to the reduced the cutting forces, effective stresses, and temperature. Sharma et al.[103] developed an optimization model to evaluate the significance of cutting and vibrating parameters on minimization of surface residual stresses. In this study authors used X-ray diffraction technique to measure the surface residual stresses at various cutting conditions. They reported that ultrasonic power intensity (P_u) plays a major role in minimization of surface residual stresses. From above literature, it is observed that the studies on thermo mechanical phenomenon on residual stress distribution in UVAT are not fully understood. Furthermore, there is an ambiguity among researcher on distribution of residual stresses with machining parameters in UVAT process.

2.4.4 Tool wear in UVAT

The use of higher cutting velocities in machining of Ti6Al4V alloy reduces tool life due to rapid wear of the tool cutting edge. The segmented chips formed during cutting of Ti-alloy causes the rapid growth of tool wear due to action of dynamic forces on cutting edge of the tool. Moreover, the concentration of localized temperature regions adjacent to cutting edge also increases the rapid tool wear. It is thus obvious that high cutting force and temperature developed in cutting of Ti-alloy increases the wear of the tool.

The significant reduction in surface roughness was observed in UVAT due to reduced deep cracks in the material when compared to CT [76]. The pulsating action of cutting tool in UVAT method is responsible for reduction of cutting force and cutting temperature and reduction in frictional resistance between tool and the flow of chip [104].

The properties of cutting tool also play a significant role in development of Fc and Tc during machining of Ti-alloy. It is proved that carbide cutting tools are preferred for machining of Ti-alloys due to its high strength at elevated temperature, toughness and cost effective [33]. The cobalt in tungsten carbide cutting tools act as a binder to hold the carbide particles together at high temperature. The abrasive action between machined surface and flank face of the tool causes the flank wear, where as the exchange of atoms between tool and the flow of chip interface causes the wear on the rake face of the tool[104, 105].

Previous studies attested that the increased Fc and Tc accelerated the wear of the tool due to thermal softening [107]. The desired machining output depends on the tool-work contact ratio(TWCR), length of cut, tool wear and cutting conditions [107–110]. The geometry of cutting tool is altered with prolonged machining time due to built-up edge (BUE) and breakage of cutting tool edge, and this causes Fc is increased with wear of the tool. Hence, tool life can be predicted with relation between Fc and flank wear[111–114].

Nath et al. [62] examined the effect of ultrasonic vibration on flank wear of the tool at wide range of cutting conditions for low alloy steel and compared with CT also. The tool life in CT is low compared to UVAT at same conditions. The rate of flank wear is increased with prolonged machining time for both cutting process. They also observed that higher tool life is obtained for 50-90 m/min range of cutting velocity and 0.1-0.2 mm/rev range of feed rate. The effect of vibrating parameters on rate of wear is not considered for their study. The wear mechanisms responsible for various stages of flank wear for prolonged machining time in UVAT is not discussed. Moreover, the high Fc and Tc developed during machining of Ti6Al4V alloy enhances the chemical reactivity between tool and workpiece in CT process. Hence, it is important to evaluate the effect of intermittent cutting action on flank wear rate in UVAT of Ti alloy at various cutting conditions.

2.5 Fatigue life

The fatigue life of component produced from various machining processes shows different behavior. Machining induced residual stresses, surface hardness and surface quality produced in machining process are attributed to variation of fatigue strength for different machining process [115,116]. High cycle fatigue strength of Ti6Al4V alloy has considerable interest as the failure of the component is still unpredictable. The fatigue crack initiation and crack propagation in high cycle fatigue (HCF) tests are sensitive to microstructure [118]. Moreover, machined surface with higher roughness promotes beginning of fatigue crack quickly. It is observed that machined surface is work hardened severely with micro cracks. The difference in formation of micro cracks depends on process used and its machining parameters [116, 118].

2.6 Johnson Cook material model parameters

The fitted J-C models by Taylor and SHPB techniques lead to some deviations from plastic behavior of Ti6Al4V alloy. Hence, a new methodology to identify suitable J-C parameters for Ti6Al4V alloy has to develop to obtain more reliable results from FEM machining simulation. Chandrasekaran et al. [120] attested that the shear stress obtained with SHPB test parameters was high at primary deformation zone compared with experimental data due to limited range of plastic strain. Although, higher strain rates upto 10^5 s^{-1} were used to identify J-C constants for material constitutive equations, lower strains were observed during Taylor test which are often less than strains induced during machining process [28]. Hence J-C models fitted by Taylor and SHPB techniques lead to some deviations from plastic behavior of Ti6Al4V alloy. In an another attempt, Sartkulvanich et al. [121] used a computer program called OXCUT, in which the relative thickness of both primary deformation zone (PDZ) and secondary deformation zone (SDZ) were used for determination of material constants. From this analysis, it was found that the material constants showed the real behavior of material under thermo-mechanical loading in FE simulations of machining process.

The analytical models developed by researchers were used to determine J-C parameters. Ning and Liang [122] used modified Oxley's model to determine J-C material constants, in which cutting forces and temperature were taken as input. Pujana et al. [123]

used an analytical model developed by Tounsi et al.[124] to determine J-C constants based on thermo-mechanical loading by considering both PDZ and SDZ as input. Moreover, accurate measurement of physical quantities of machining process is difficult due to complex contact phenomenon. The reliability and accuracy of J-C constants obtained from analytical models depend on assumptions made and the mathematical complexity of the analytical model. In this regard sensitivity analysis evaluates the accuracy of J-C constants determined from analytical models. Ning et al.[125] investigated the accuracy of input J-C constants and cutting parameters on cutting force obtained from analytical modeling. It is concluded that predicted cutting forces are in good agreement with machining results.

Recently, a hybrid method based on machining test and FE code has been developed to determine J-C constants by minimizing error between experimental and predicted cutting forces [126]. Although the aforementioned methods have considerable importance in identifying J-C constants, the effectiveness and reliability of these methods are still questionable due to the complexity of experiments and mathematical calculations. In a study by Malakizadi et al.[127] developed an inverse approach in which Oxley' machining theory incorporating with J-C material model was used with response surface methodology (RSM) for identifying material constants for various materials. The optimum set of coefficient of friction values was determined from FE simulation, which was used to identify J-C parameters for different materials.

From previous research, it is observed that orthogonal tests were conducted to identify J-C material constants without considering the effect of tool geometry. In an another attempt, Daoud et al.[128] included the effect of rake angle to determine J-C material constants from machining based approach. In this method, Oxley's chip formation model was used to determine strain, strain rate and temperature at shear deformation zone where the effect of strain at chip-tool interface was ignored. The deformation behavior of low thermal conductivity materials like Ti6Al4V alloy is different from other material. In this context, it is important to consider the chip formation model which considers the effect of strain on chip-tool interface[129]. In another work, Ning et al.[130] determined J-C material constants for ultra-fine grained titanium by comparing experimental cutting force with cutting force determined from chip formation model. The equivalent strain hardening exponent was used in analytical model to calculate cutting force. Finally, it is concluded that the experimental cutting forces were in close agreement with predicted cutting forces obtained by using J-C

constants from machining approach. The sensitivity analysis determines the accuracy of input J-C constants on predicted simulation results.

2.7 Motivation of the work

Ultrasonic vibration assisted turning is one of the most effective machining technique to machine difficult to cut materials like Ti6Al4V alloy to avoid the problems encountered in CT. Experimental and numerical methods reveals that the significant improvement in surface finish along with reduction in cutting force and cutting temperature is obtained with UVAT method compared to CT of Ti6Al4V alloy. However, the relation between range of machining and vibrating parameters with the cutting performance in UVAT method has not been established.

The surface integrity induced by the machining process may have significant effect on fatigue life of components used in aerospace industry. The surface integrity refers to the surface characteristics (topography characteristics) and sub surface characteristics (sub layer characteristics). These characteristics may change due to variation of thermo mechanical loading during cutting process. Residual stress is one of the important characteristic affected by the variation of thermo mechanical loading during cutting process. Hence it is important to study the effect of machining parameters on residual stresses in UVAT of Ti6Al4V alloy. Numerical and experimental studies indicated that there is generation of compressive residual stresses on the surface of machined component during machining of Ti6Al4V alloy with UVAT process. However, the type and magnitude of residual stresses formed on surface and subsurface layer of machined component in UVAT of Ti6Al4V alloy has not been discussed. The relation between thermo mechanical loading and residual stresses in machining process can easily understand by finite element simulations. The reliability of any FE machining simulation depends strongly on the material model which describes actual deformation characteristics of material during metal cutting. Johnson and Cook material model is widely used in the modeling of machining processes as this describes the flow stress in terms of strain, strain rate and temperature. However, different J-C parameters are available in literature for the same material which affects the predicted results from FE simulation. Hence, there is a need to find a method to determine material parameters which gives minimum deviation between experimental and predicted values. The material parameters identified from the analytical and numerical methods do not represents the behavior of materials since

they are affected by the secondary shear zone. Hence, there is need to identify the material parameters for JC constitutive model by considering friction at tool chip interface to predict accurate results from FE simulation.

The main objectives of this research work are listed as follows

1. To determine Johnson Cook material model parameters for Ti6Al4V alloy using machining based methodology by considering equivalent strain rate coefficient.

2. To investigate the relation between machining parameters and cutting performance in UVAT of Ti6Al4V alloy.

3. To investigate the effect of thermo mechanical loading on residual stresses in UVAT of Ti6Al4V alloy.

4. To characterize the tool wear in UVAT of Ti6Al4V alloy.

5. To analyze the effect of surface integrity on fatigue life improvement of Ti6Al4V alloy components in UVAT process.

2.8. Research methodology

The methodology adopted to accomplish the objectives defined for this research work is depicted in the figure 2.2. This includes both finite element simulation and experimentation for both CT and UVAT. Initially, orthogonal experiments were conducted to determine suitable J-C parameters for Ti6Al4V alloy using machining approach. Then, the performance of UVAT process was evaluated based on tool work contact ratio in terms of cutting force, cutting temperature and surface roughness. The surface integrity of Ti6Al4V alloy was analyzed based on residual stress profiles and flank wear of the tool was compared between both CT and UVAT. Finally, the impact of surface integrity on fatigue strength was analyzed and compared for both CT and UVAT processes.
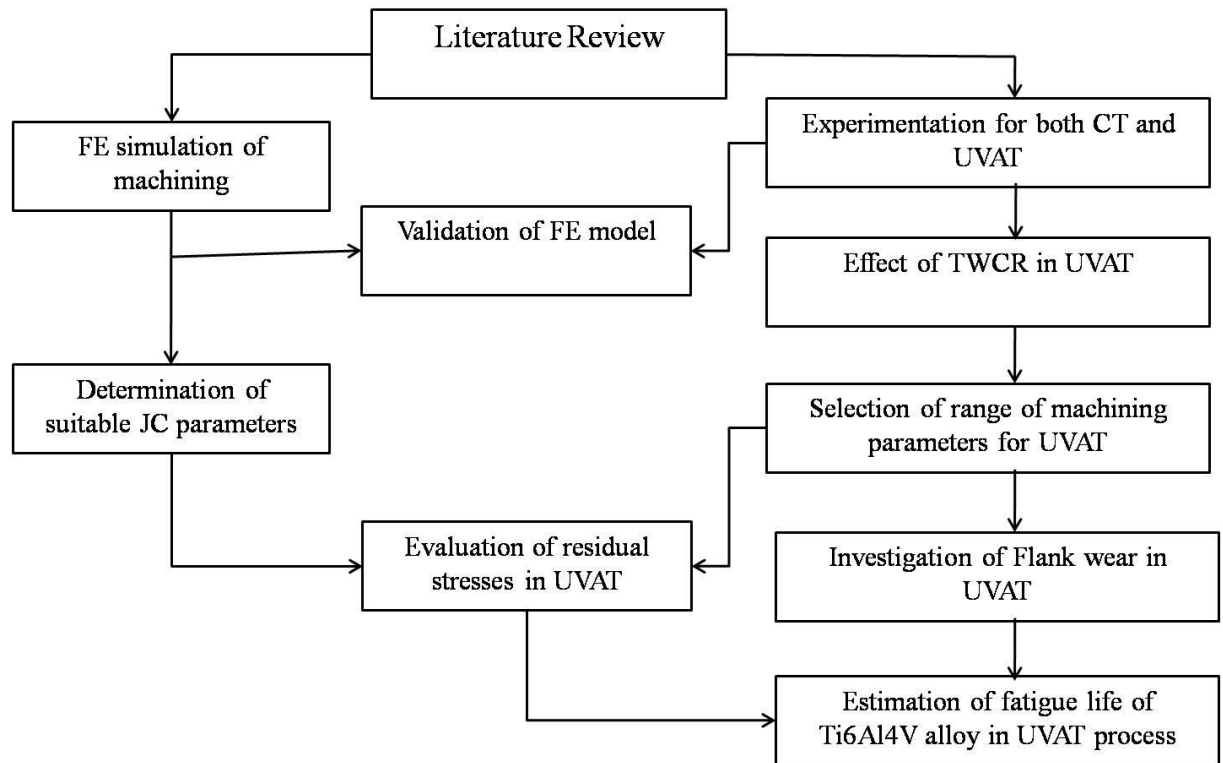
Figure 2.2: Research Methodology adopted for current work

Chapter 3

FE Modeling and Simulation of Turning process

3.1 Introduction

Analytical modeling of UVAT method is difficult due to complexity of the machining process. The analytical modeling of UVAT includes the modeling of tool and workpiece, accurate prediction of chip flow, coupling of thermo-mechanical loading, application of impact loading, perfect contact interaction and frictional interface between tool-chip. Finite Element Method (FEM) is a powerful tool for simulation of machining process. Metal cutting is a non-linear and coupled thermo-mechanical process involves complex stress field. The actual cutting process can be designed and analyzed with help of FEM for accurate prediction of material deformation and stress distribution under various loading conditions. The experimental results can be used to validate the developed FE models for further analysis.

The present work is modeled and analyzed using ABAQUS frame work [131]. ABAQUS is commonly used commercial FE package in analyzing nonlinear problems with greater user advantage compared to other, in which standard codes are already available to perform standard machining operations. The coupled temperature displacement model is used to model thermo-mechanical machining problem available from dynamic explicit library of ABAQUS. This model helps to predict effective stresses, plastic strains, cutting forces, residual stresses and also temperatures.

The basic steps involved in modeling a machining process are pre-processing, processing or analysis and post processing. The pre-processing stage involve, creating the 2-D sketch of tool and workpiece, material definition, choice of formulation and meshing, selection of element type, assignment of material properties to tool and workpiece, selection of solver and its definition, contact interaction and definition of boundary condition. Analysis part is done by ABAQUS software program based on the pre-process inputs. Post- processing helps in determination and reporting of results from the model. The detailed development of FE models for turning in ABAQUS is discussed below.

3.2 Development of FE model for orthogonal turning

A 3D FE model developed in ABAQUS with updated Lagrangian approach is used to analyze machining of Ti6Al4V alloy. The workpiece is assumed as an isotropic material and Tungsten carbide (WC) cutting tool is assumed as a rigid to reduce the total simulation time. Coupled temperature-displacement of Hex-dominated (C3D8RT) element which facilitates both thermo-mechanical loading is selected with maximum elemental growth with higher accuracy. From mesh sensitivity analysis, optimized model is observed with 22780 elements of workpiece and 6420 elements of cutting tool with rake and clearance angles. The simulations are performed with plane strain assumption as this is orthogonal machining process. The results are noted at near steady state condition. In this study, rigid tool is provided with vibrations and workpiece is assigned with cutting speed in x-direction for UVAT process.

3.2.1 Model geometry

The dimensions and details of workpiece and cutting tool used in FE simulation are shown in figure 3.1 and table 3.1. The relative movement between tool and workiece in orthogonal cutting process is shown in figure 3.1. In orthogonal cutting, the tool edge is normal to the cutting direction. In the FE simulation of Ti-alloy, a deformable workpiece with dimension of 3.5 mm in length, 0.8 mm in height and 0.4 mm width was used. In order to satisfy the orthogonal machining condition, Tungsten carbide cutting tool is assumed as rigid and modeled with dimensions of 0.6 mm in length, 0.6 mm in width and 0.6 mm in height. The workpiece is partitioned at a depth of 0.2 from the top surface for fine meshing.

Table 3.1: Details of workpiece and cutting tool

Details	Material	Dimensions
Workpiece	Ti6Al4V alloy	Cuboid: 3.5 X 0.4 X 0.8 mm (LBH) Portioned at a depth of 0. 2 mm
Cutting tool	Tungsten Carbide	Cutting tool : Wedge shape: 0.6 X 0.6 X 0.6 mm (LBH) 10˚ back rake angle and 5˚ clearance angle
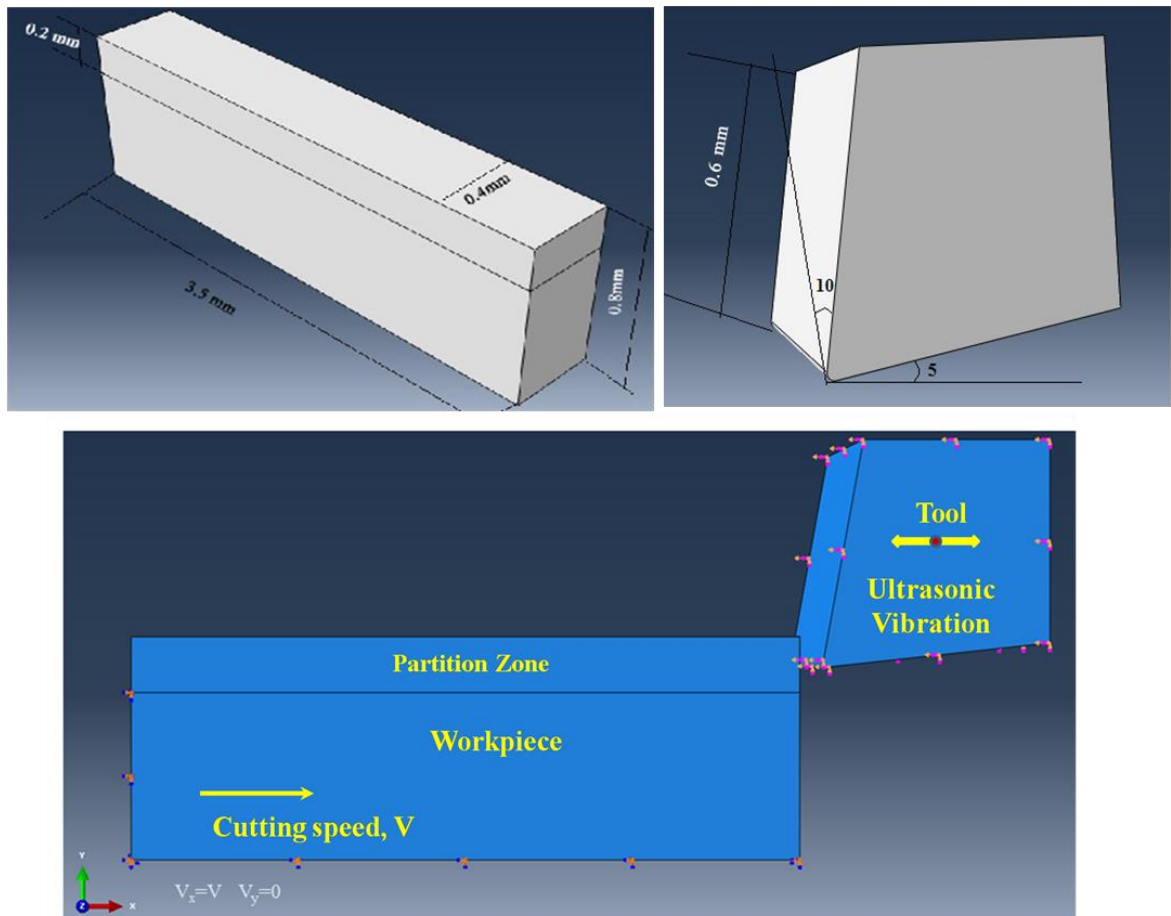
Figure 3.1: Modeling and relative movement of workpiece and cutting tool

3.2.2 Material modeling

The accurate prediction of FE simulation results depends on material model which describes material deformation in terms of flow stress. Flow stress is an instantaneous yield stress derived from product of strain, strain rate and temperature. The non-linearity of material flow stress is increases with the increase of strain and strain rate whereas it is decreases with increase in temperature. There are various material models in literature in which Oxley model,

Johnson-Cook model, Mechanical threshold stress model and Zerilli-Armstrong material model are commonly used for machining simulations.

Many researchers have compared the material modeling techniques for same materials based on process outcomes such as cutting force, cutting temperature and etc. with experimental results. They found that the deviation of process outcomes predicted by Johnson-Cook model with experimental results is low. Hence this model is well preferred by most of the researchers and also Johnson-Cook model is the most popular model and often used as the benchmark for comparison of different other models. In addition, the basic form of this model is readily acceptable to most of the computer codes and is readily available in ABAQUS.

Johnson-Cook flow stress model is a widely used material model adopted for machining simulations since material behavior is expressed as a function of strain, strain rate and temperature [132]. This material model considers effect of plastic deformation in terms of strain and strain rate and thermal softening in terms of temperature. This model can also be used effectively for the material undergone saw tooth chip formation.

3.2.2.1 Johnson cook material model

Johnson-Cook model considers the equivalent Von Mises flow stress as a function of equivalent plastic strain, strain rate and temperature. It is an empirical model which combines the effect of hardening, plastic deformation and thermal softening of material occurred during metal cutting process to evaluate instantaneous flow stress. This J-C model is given by an equation 3.1

$$\sigma = (A + B\varepsilon^n)\left[1 + Cln\left(\frac{\varepsilon^o}{\varepsilon_0^o}\right)\right]\left[1 - \left(\frac{T-T_r}{T_m-T_r}\right)^m\right] \qquad (3.1)$$

The first term of this equation represents strain hardening; second term of this equation indicates that flow stress increases with increase in strain rate and third term indicates that flow stress decreases with increasing temperature of the material. The reference strain considered in this model is normalized with strain rate. Moreover, flow stress becomes zero as the cutting temperature reaches to melting temperature of material due to thermal softening.

3.2.2.2 Separation criteria and Damage equation

The chip formation and separation from material follows a criteria used in FE simulation. There are various physical and geometrical criteria to describe the chip formation in metal cutting modeling. The physical model are defined with effective plastic stress and strain along with strain energy density whereas geometric models are defined b considering the distance between the overlapping nodes and the tool tip.

Simulations are conducted to predict chip flow and chip breaking phenomenon. Movement and control of chip along chip-tool contact length on the rake face of the tool is important. Deformation of work material, contact properties, friction, large plastic strains, strain-hardening, and thermal softening effects play a major role in chip formation mechanism. Many fracture models are available and precisely depend on type of the material used in simulation such as simple fracture model to complex Johnson's cook damage equation. All the fracture models are based on the yield strength of the material and fracture occurs when it exceeds the yield strength. Johnson's cook damage equation is commonly employed for all difficult cut materials like Ti alloys. This model is an extension of specific distortion energy criterion for fracture mechanics, which can be attributed to its reliable results [133].

The selection of fracture based model in FE modeling of chip formation should consider fracture initiation and fracture propagation. Johnson-Cook damage model is a cumulative-damage fracture model that takes into account the loading history, which is represented by the strain to fracture. The strain to fracture is expressed as a function of the strain rate, temperature, and pressure. This model is based on the value of the equivalent plastic strain at element integration points. J-C failure model is employed in these FE simulations to account for material deformation, behavior of chip separation and chip crack initiation. This model considers both stress tri-axiality and strain rate effect for accurate prediction of fracture in orthogonal cutting tests. According to JC model, damage parameter D is defined as

$$D = \sum \left(\frac{\Delta \varepsilon^{pl}}{\varepsilon^{pl}} \right) \qquad (3.2)$$

The fracture of the material occurs when D=1. Where $\Delta \varepsilon^{pl}$ is increment of the equivalent plastic strain which is updated at every analysis increment; ε_f is equivalent

strain at failure and is expressed as J-C ductile fracture model with five damage parameters is given by an equation (3.3).

$$\varepsilon_f = \left[D_1 + D_2 \exp(D_3 \frac{p}{q})\right]\left[1 + D_4 \ln\left(\frac{\varepsilon^p}{\varepsilon}\right)\right]\left[1 + D_5 T^*\right] \qquad (3.3)$$

Where $\Delta\varepsilon^{pl}$ depends on non-dimensional equivalent plastic strain rate, $\frac{\varepsilon^p}{\varepsilon}$ is the ratio of hydrostatic pressure to Von-Mises equivalent stress, $(D_1 \sim D_5)$ are the damage constants and T^* temperature term under thermal softening parameter m in JC model equation. Damage parameters D_1, D_2, and D_3 are predominant compared with the two others. To determine the damage model's constants, the strain to failure is to be established in function of the triaxial state of stresses. This step gives the constants D_1, D_2, and D_3. Subsequently, strain rate parameter, D_4, and temperature parameter D_5 can be established. The damage parameters for a particular material can determine from axi-symmetric tensile tests. At least, three tests must be conduct to build the exponential curve of the strain to fracture in function of the stress tri-axiality..The parameter D_4 can be estimated by torsion tests at different shear strain rate; hence it is named as strain rate parameter. To obtain parameter D_4, a curve of a reduced strain to failure versus the strain rate should be drawn in natural semi-log graph.

$$\text{Reduced strain to failure to determine } D_4 = \frac{\varepsilon_f - (D_1 + D_2)}{(D_1 + D_2)} \qquad (3.4)$$

The parameter D_5 is estimated by conducting the test at various temperatures close to the actual temperatures generated for the model. The shear strain to failure versus the shear strain rate curve must be generated at different temperatures. Then D_5 is estimated by plotting a reduced strain to failure versus temperature. All the data should be collected at high strain rate.

$$\text{Reduced strain to failure term to determine } D_5 = \frac{\varepsilon_f - (D_1 + D_2)\left(1 + D_4\left(\ln\frac{\varepsilon^o}{\varepsilon_0}\right)\right)}{(D_1 + D_2)\left(1 + D_4\left(\ln\frac{\varepsilon^o}{\varepsilon_0}\right)\right)} \qquad (3.5)$$

In addition to the above, properties of the materials such as density, elasticity, poisons ratio, thermal conductivity, specific heat capacity and etc. must be defined to workpiece material as well as tool material as required for the model. The properties of both workpiece and tool used in the simulation, Johnson cook and damage parameters of workpiece material are represented in the table 3.2.

Table 3.2: Material properties and parameters used in FE simulation of machining process

Material properties [70]		Workpiece	Tool
Density	kg/m^3	4420	15000
Thermal Conductivity	W/m-^{o}C	7.264	40.8
Young's modulus	GPa	114	550
Inelastic heat fraction		0.9	0.1
Specific heat	J/kg-^{o}C	526	330
Poisson ratio		0.31	0.3

J-C parameters[134]						
A (MPa)	B (MPa)	C	n	m	T$_m$(^{o}C)	Strain rate (s^{-1})
724.7	683.1	0.035	0.47	1	1650	2000

Damage parameters[135]				
D1	D2	D3	D4	D5
-0.09	0.28	0.48	0.014	3.18

3.2.3 Model formulation and element type

The developed FE model must be flexible to treat different geometries and material correctly. In transient FE models, the considered region is divided into elements by fixing elements to either workpiece or space. In the Lagrangian approach, the elements move with the material whereas the material flows through the immovable elements in Eulerian approach. In Eulerian approach, attention is focused on the field from element to element at the same time whereas in Lagragian approach, attention is focused on change in element with time. Each approach has its advantages and disadvantages[135], however, the updated Lagrangian formulation has been widely used in majority of works since mid-1980s.

3.2.3.1 Lagrangian formulation

With advancement of technology, Lagrangian approach is encouraged for machining simulation. In Lagrangian approach, it is assumed that finite element mesh is attached and follows the material deformation. This approach provides simple system for formation of chips especially for discontinuous chip formation. However, this approach has been limited to analysis of chip formation in ductile material due to element distortion. The large strain occurs in the deformation of material causes element distortion when it passes over the shear plane in simulation. Remeshing technique is used to over this problem in this approach. Most

of the simulation codes are designed based on this approach due to simple and easy to understand. Hence the default formulation of ABAQUS is Lagrangian.

In the updated Lagrangian formulation, the elements encounter large plastic deformation ahead of cutting edge as elements move with the workpiece. In updated Lagrangian formulation, initial contact of tool and workpiece also considered for cutting simulation and continued upto steady state conditions. However, large computation power and time are required to reach the steady state condition. In the Lagrangian formulation, various chip separation criteria are provided to machining simulations to describe the separation chip from material. The criteria are based the threshold value of material strain [99,135], strain energy density[136, 137]],fracture strain [133] and the critical distance from the cutting edge[138,139] Furthermore, various algorithms have been used for chip separation when condition for failure is satisfied. In unzipped condition, nodes are separated along the predefined line when tool approach the material. The location and failure stress are assumed in such unzipped approach [136].

3.2.3.2 Eulerian formulation

In the Eulerian formulation, attention is focused on a fixed point in space and observes the changes occurring there. In this approach workpiece is assumed to move through meshed volume in the cutting zone. The advantage of this approach is that element shapes are not distorted with time. In Eulerian approach, visco-plastic effects are considered in matal cutting due to large deformation. However, the chip separation criteria is a major concern in this approach due to ambiguity in drawing elements. Experimentation is required to confirm the chip shape and shear angle [141]. The major general concern in Eulerian approach is definition of material property from element to element.

3.2.3.3 Arbitrary Lagrangian-Eulerian (ALE) formulation

Arbitrary Lagrangian Eulerian approach is formed by combining the characteristics of both Lagrangian and Eulerian approaches. In this approach, FE mesh is neither attached to workpiece nor fixed in space. The problem is solved for displacement using Lagrangian approach when mesh follows the movement of material and then repositioned for solving velocities using Eulerian approach. In machining simulations, Eulerain approach is used for modeling area of cutting zone to reduce element distortion. Lagrangian approach is used for

the unconstrained material flow at boundaries. Furthermore shape of the chip occurs as a function of plastic deformation of the material. This approach is shown in figure 3.2.
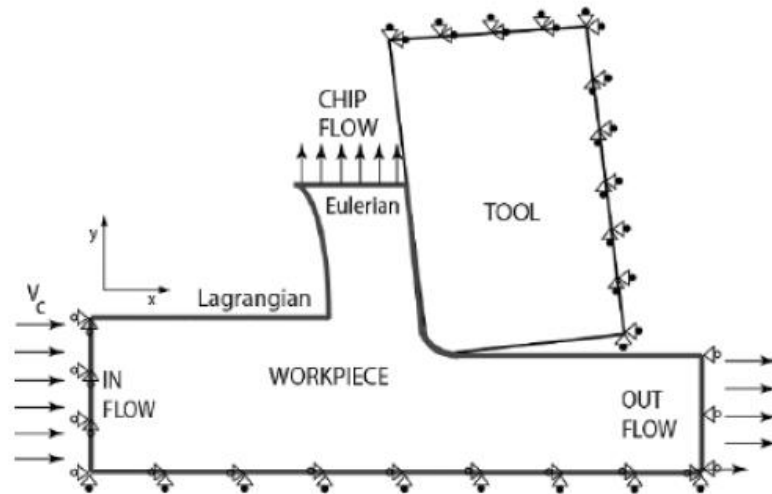
Figure 3.2: Eulerian and Lagrangian boundary conditions in ALE simulation [142]

In the current research work, element formulation is done to avoid the default Lagrangian formulation in ABAQUS framework. In this transient machining simulation, ALE formulation technique with purely Lagrangian boundary condition is used.

3.2.4 Meshing and element type

In FE simulation of machining process, meshing play a prominent role in obtaining reliable results towards the experimental results. Free meshing with quadrilateral type is default meshing technique in ABAQUS. The algorithms used for meshing, medial axis and advanced front algorithm are shown in figure 3.3. Advanced front algorithm is more advantageous over the medial axis algorithm as the mesh elements adjusts itself based on the complexity of the model. In ABAQUS/Explicit, adaptive meshing is designed to handle a large variety of problems with smoothing methods. In general, mesh smoothing is done in ALE with evolving geometry technique based on enhanced algorithm. This technique is used to diminish the distortion of the elements[131].
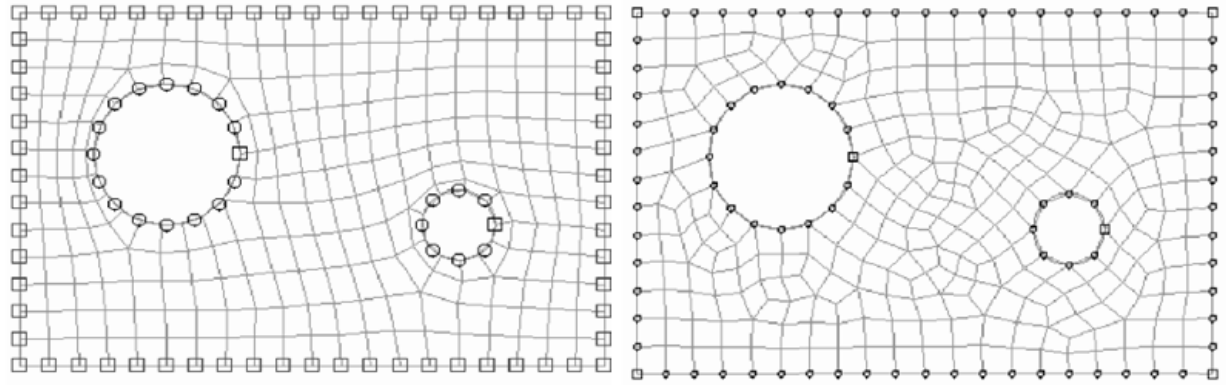
Figure 3.3: Mesh generation in medial axis and advanced front algorithms

The element type selected is C3DRT (8 node thermally coupled cuboid with tri-linear displacement and thermal effects), which is popularly known as coupled temperature displacement element. This is typically used in thermo-mechanical issues as it suits well for such problems. The geometric order is linear, because, 2nd order elements cannot be generated in HEX and WEDGE element shapes. The analysis is made assuming 3-D stressed elements with default allowable distortion as 0.1. Controlled hourglass option reduces the effect of these elements upon the equivalent stress, equivalent plastic strain and cutting forces. Element deletion is sometimes desired because it helps to delete the over strained elements in machining zone. In a transient problem like machining simulation, minimal additional input is required to invoke the adaptive meshing capability. ALE formulation technique with purely Lagrangian boundary condition is used in current model. ALE Adaptive mesh domain is used to produce adaptive mesh in the workpiece. The mesh constraints and relocating are provided in such a way that mesh follows underlying work material. The frequency of relocating considered for this study is 100, which means remeshing will be done after 100 increments. During each adaptive meshing increment, the new mesh is created by performing one or more mesh sweeps and then assigns the solution variables to the new mesh. The intensity of remeshing per increment per incremental step considered in this study is 3. During each mesh sweep, nodes in the domain are relocated, based on the current positions of neighboring nodes and elements. This reduces element distortion to a greater extent.

3.2.4.1 Sensitivity of the FE model

In the analysis process, when the considered element's size is too small, too many elements are generated. This increases computational intensity, resulting in a model that is either too time-consuming to solve, or in potential errors in the calculated values. Therefore, a reasonable element size (number of elements) is a main factor that should be considered in a

finite-element analysis. From convergence study, it is observed that the variation of cutting force is less than 5% beyond 28440 elements of workpiece. The cutting tool is meshed with 7890 elements with rake and clearance angles. This FE model is integrated with re-meshing technique for continuous chip formation process. In order to reduce the total simulation time, only the top portion of workpiece is fine meshed with 40 number of elements along its 0.2 mm of partition height and 875 elements along its 3.5 mm length as shown in figure 3.4. This FE model is integrated with re-meshing technique for continuous chip formation process. It is necessary to mention that the number of nodes in contact with the tool varied during the contact time, depending on its position. At the penetration stage of the tool, the number of nodes in contact was maximized. The number of nodes also changed during the penetration and a retraction stage of the tool movement. The contact surfaces of workpiece and tool , the desired depth of cut and direction of movement of cutting tool and workpiece are defined in assembly process of modeling.
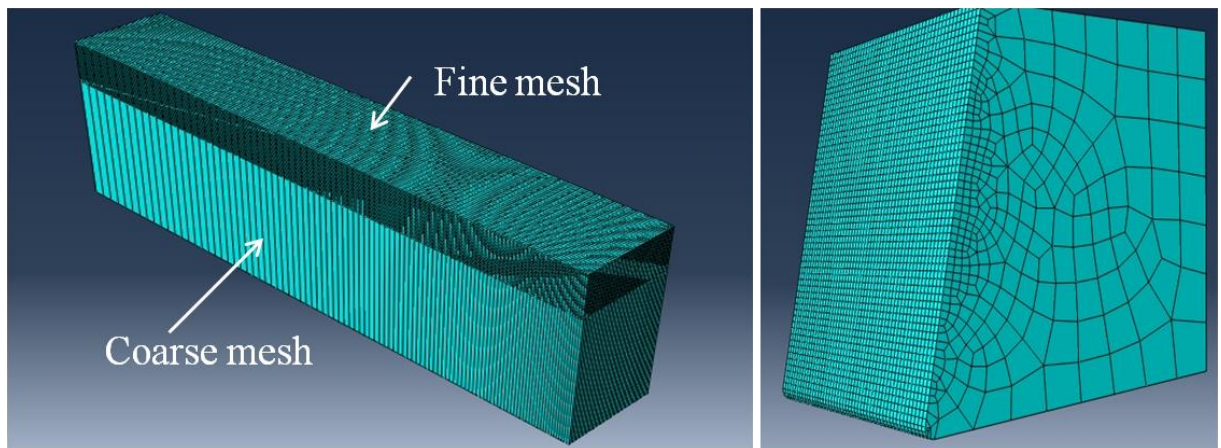
Figure 3.4: Meshing of workpiece and cutting tool

3.2.5 Step selection

In FE simulations, suitable selection of solver plays an important role in success of considered mechanical analysis. In ABAQUS, two types of solvers, names as ABAQUS/Explicit and ABAQUS/Standard are available. In general, ABAQUS/Explicit is used in modeling complex contact problem, materials with degradation and failure, and inherent in metal cutting modeling[143]. Dynamic explicit solver is used to work with dynamic nonlinear problems whereas 'Explicit Temp–disp' is used to solve the coupled thermo-mechanical problems. The required step function is invoked using STEP function in ABAQUS. The selected solver automatically invokes the definition of output request in STEP

function. The necessary modifications in output field can be done to reduce the calculation time.

3.2.6 Contact interaction and Friction

The contact interaction between the tool and workpiece surface have a greater influence on formation of chip in machining process. The contact properties, surface properties and contact formulation for attributes defined in assembly process are defined in interaction definition. In the present FE model, GENERAL CONTACT interaction is defined for chip-tool and tool-workpiece contact pair. The constraint defined in the contact formulation is purely master-slave type. This type of formulation avoids the penetration of slave surface (workpiece) into master surface (Tool). The friction behavior and heat transferred to slave surface are the essential interaction properties. The heat generated due to frictional contact between tool and chip causes the increase in temperature which influence chip formation and tool life in machining process. Hence, it is important to analyze the fractional mechanism occurred in metal cutting to develop accurate models for cutting forces and temperature.

In metal cutting, frictional mechanism is analyzed by considering two contact regions named as sticking and sliding region, along the rake face of the cutting tool. In this mechanism, coefficient of friction is defined with respect to Coulomb friction law in the sliding region while friction stress is assumed in sticking region. If the shear stress is less than frictional stress, there is no relative motion between chip and tool along the rake face of the cutting tool. The sliding occurs in sliding region when the shear stress is equal or greater than the frictional stress. The critical value of the frictional stress value in modified Coulomb friction is given by

$$\tau = \min(\mu p, \tau_{th}) \tag{3.6}$$

where p is the normal pressure, μ is the coefficient of friction and τ_{th} is the threshold value for the Coulomb friction stress. When the value of τ_{th} set to infinity, the equation becomes the original Coulomb's frictional law.

In the current FE model, for the workpiece Ti6Al4V alloy, τ_{th} is takes as 550 MPa which is equal to yield stress in simple stress. The friction between contact surface is defined

with TANGENTIAL BEHAVIOUR with penalty contact to validate the model with literature. The penalty method is based on coulomb friction model where the maximum allowable frictional (shear) stress relates to contact pressure between the contacting bodies. ABAQUS automatically adjust itself the magnitude of the penalty constraint to enforce Coulombs friction condition on contact surfaces. Other properties such as heat generation are also defined considering that 80% of heat generated due to friction is transferred to chip or slave surface.

3.2.7 Boundary conditions

Boundary conditions attribute to the limitation of physical parameters such as fixing of workpiece, displacement, velocity, rotation, acceleration of tool or workpiece, initial temperature or environmental temperature and etc. In this study, the relative displacement between tool and workpiece and boundary conditions used in simulation of UVAT process are shown in figure 3.1. In this model, the workpiece is encastred at bottom surface and surface opposite to the machining zone. The rigid tool is provided with vibrations and workpiece is assigned with cutting speed in x-direction for UVAT process. The vibration motion of the tool in the direction can be written in the following form:

$$x_t = Vt + a \sin \omega t \tag{3.7}$$

where x_t is displacement of tool, V is cutting speed, a and ω are vibration amplitude and angular frequency.

The vibration speed of the cutting tool can be derived by differentiating of displacement,

$$v_t = V + a \omega \cos \omega t \tag{3.8}$$

Here, the angular frequency ω is represented by

$$\omega = 2\pi f \tag{3.9}$$

where f is the frequency of vibration. The tool's vibration speed varies from a minimum of $(V - a \omega)$ at any valley to a maximum of $(V + a \omega)$ at midpoint of each cycle. It is upward and downward motion.

The maximum velocity of the tool is given by

$$v_{t,max} = a\omega = 2\pi f a \tag{3.10}$$

In order to get discontinuous contact between tool and workpiece, the velocity of the tool must be greater than velocity of the workpiece (V) i.e. $v_{t,max} > V$. Hence the critical velocity for UVAT process is given by

$$v_{critical} = 2\pi f a \tag{3.11}$$

In CT process, the relative displacement between tool and workpiece is given by

$$x_t = Vt \tag{3.12}$$

Therefore, the relative velocity between tool and workpiece is constant during deformation

$$v_x = V \tag{3.13}$$

For a frequency of 20 KHz and amplitude of 20 μm, and cutting speed of 1 m/s, the cutting tool displacement and velocity obtained from FE simulation are shown in figure 3.5. From tool motion in UVAT process, the tool is intermittently contact with workpiece material for every cycle motion.
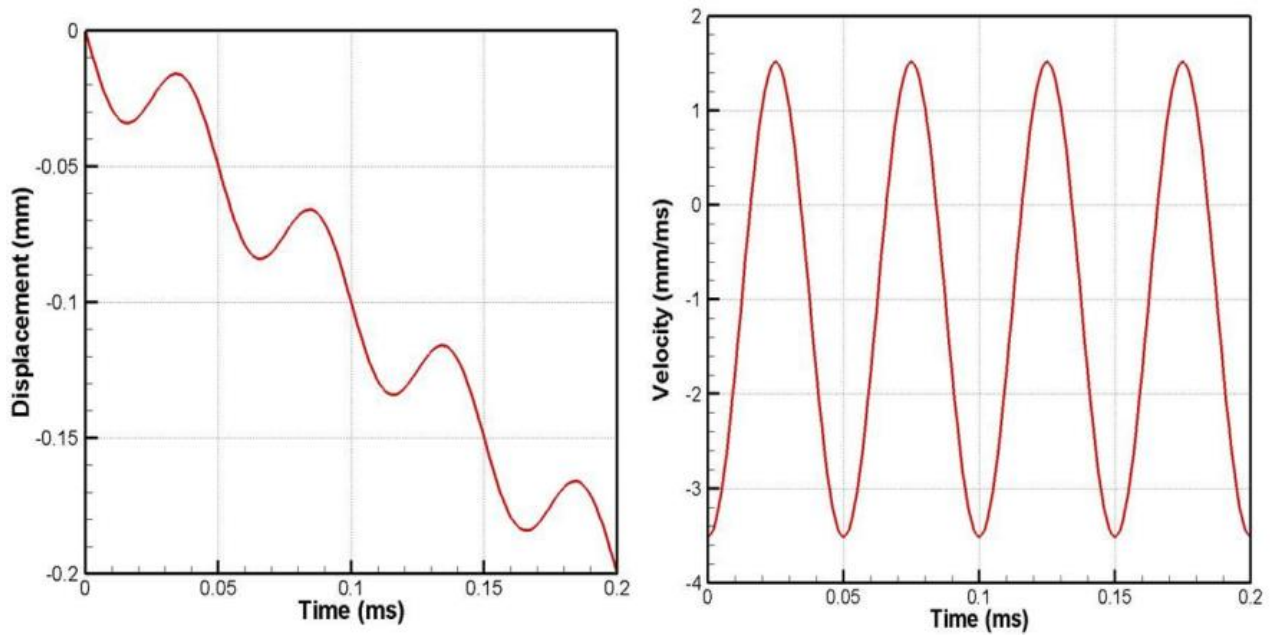
Figure 3.5: Cutting tool displacement and velocity in UVAT simulation

3.3 Validation of FE model

The developed FE model is validated by comparing its results with experimental and simulation results available in literature at same conditions [70]. The geometry of the workpiece and cutting tool, cutting parameters and vibration parameters considered for this simulation are same as the conditions used in literature for validation. The details of cutting conditions and used in the simulations are given in table 3.3. The important simulation parameters used in the present model is given in table 3.4.

Table 3.3: Details of workpiece and cutting tool used in FE simulation of machining process

Materials and cutting conditions	Details
Material	Workpiece:Ti6Al4V alloy
	Cutting Tool: Tungsten carbide
Dimensions	Workpiece : 3.5 mm x 0.2 mm x 0.8 mm (LBH)
	Partition : 3.5 mm x 0.2 mm x 0.2 mm (LBH)
	Cutting Tool: 0.6 mm x 0.6 mm x 0.6 mm (LBH)
Cutting parameters	Cutting speed: 30 m/min
	Depth of cut: 0.1 mm
Tool geometry	Rake angle: 10º
	Clearance angle: 5º
	Tool edge radius: 50 µm
Vibrating parameters	Frequency: 20 KHz
	Amplitude: 20 µm

In order to ensure the accuracy of the developed FE model, cutting force, cutting temperature and equivalent stresses obtained from FE simulation for both CT and UVAT process are validated with experimental results available in the literature[70]. Table 3.5 shows the comparison between simulation and experimental results. Figure 3.6 and 3.7 shows the cutting force, cutting temperature and stresses developed in the FE model for both CT and UVAT process. Variation in cutting force and cutting temperature are observed to be 5.8% and 7.32% respectively in case of CT compared to experimental results, whereas the same are found to be 8.9 % for cutting force and 5.1% for cutting temperature respectively in case of

UVAT. It is observed that the results obtained in the present model are close to the experimental results.

Table 3.4: Setting parameters used for FE simulation

Type of simulation factor	Details
Setting factor	Selected in simulation from the library
Solution procedure	Dynamic-Temp-Disp-Explicit
Element type	Coupled temperature displacement : Explicit type, Geometric order: linear; Element: C3D8RT
Meshing	ALE adaptive mesh : Frequency :100; Remeshing sweeps per increment: 1
Element distortion Control	Length ratio: 0.1
Interactions	General contact type Tool: master surface, workpiece :slave surface
Interface friction	Tangential behavior with penalty contact coefficient of friction: 0.6
Element deletion	Yes
Hour glass control	Default
Heat generation	Inelastic heat fraction: 0.8 ; Gap heat generation: $\eta=1$, f=0.9

Table 3.5: Validation of simulation results with experimental results for CT and UVAT processes

Process	Comparison	Stress (MPa)	Force (N)	Temperature (˚C)
CT	Literature Experiment	-	153	410
	Present simulation (3D)	1078	162	382
UVAT	Literature Experiment	-	110	330
	Present simulation (3D)	872	101	314
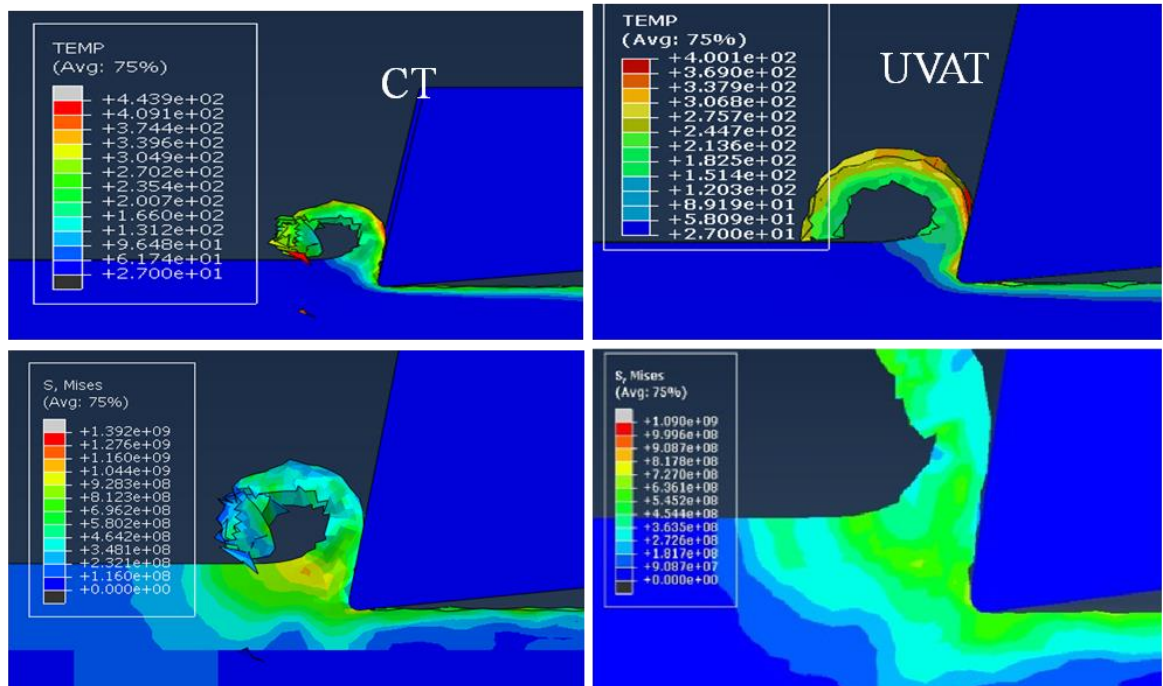
Figure 3.6: Comparison between cutting temperature and equivalent stress in CT and UVAT process
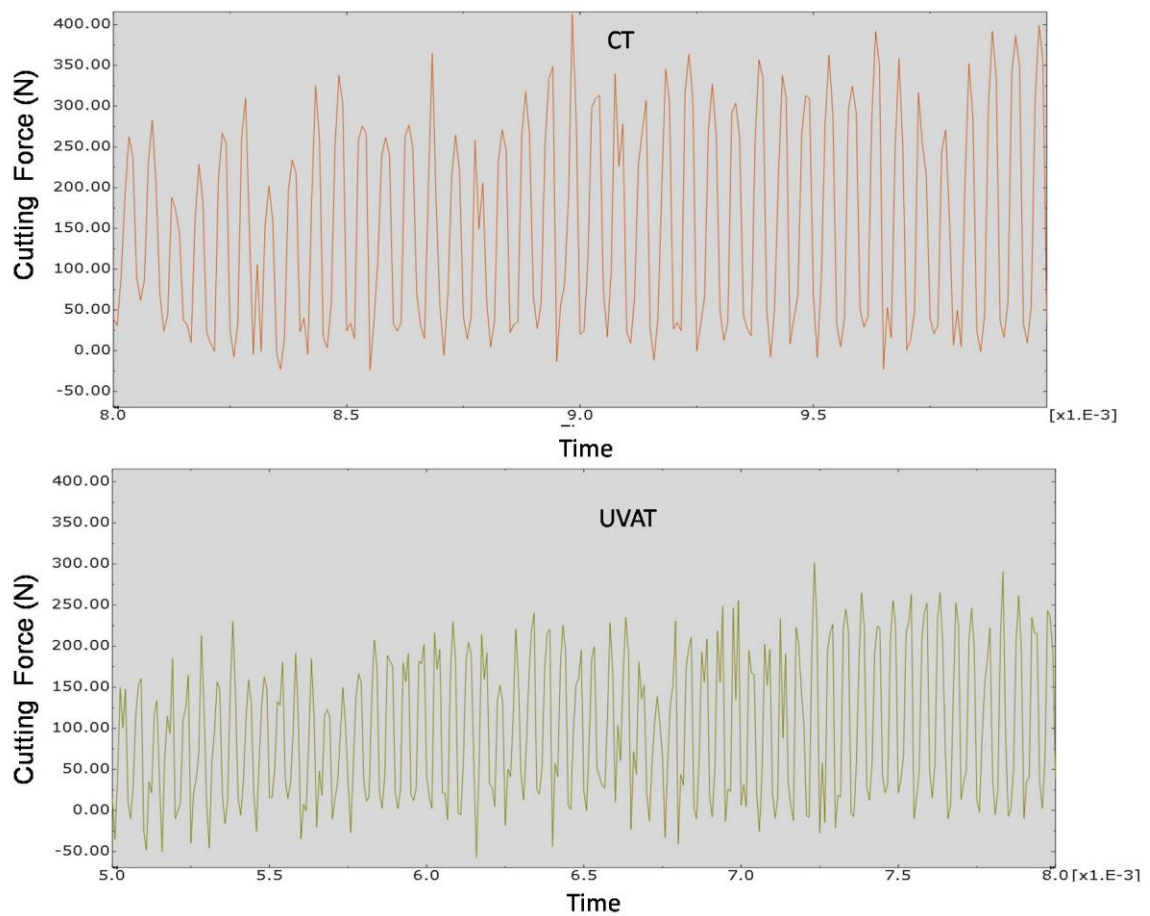
Figure 3.7: Simulation cutting force comparison between CT and UVAT process

3.4. Summary

FE modeling and simulation of machining process is an important tool for analyzing the residual stresses of machined component. In this regard, 3-D orthogonal cutting models are developed for both CT and UVAT processes with necessary tool geometry, cutting conditions and simulation parameters. The developed models are validated with literature results at same cutting conditions in terms of cutting force, cutting temperature and surface roughness and identified that all results are within the limits. Furthermore, it is identified that the accuracy of FE model results can be improved with suitable J-C parameters for machining process.

Chapter 4

Experimentation

4.1 Introduction

In this study, experiments have been carried out under both CT and UVAT processes. The orthogonal experiments have also conducted to evaluate the J-C parameters for Ti6Al4V alloy. The performance of UVAT process is evaluated and compared with CT process at various machining conditions in terms of cutting force, cutting temperature, surface roughness and tool wear. The effect of TWCR on the performance of UVAT process is evaluated from the experimental results. The residual stress profiles of Ti6Al4V alloy components also evaluated at various machining conditions. Finally, HCF tests are conducted to estimate the fatigue life of Ti6Al4V alloy components obtained from both UVAT and CT processes. The details of equipments, tools, workpiece material, measurements of responses adopted in the present study are detailed in this chapter.

4.2 Workpiece material

In the present work, Ti6Al4V alloy is considered as workpiece for both orthogonal, CT and UVAT experimentation. As the cutting velocity is perpendicular to cutting edge of the tool in orthogonal experiments, Ti6Al4V alloy tube is considered and it is shown in figure 4.1. In order to evaluate the suitable Johnson-Cook material for Ti6Al4V alloy, orthogonal experiments have been coducted on cylindrical tube with 84.5 mm outer diameter and 81 mm inner diameter with 1.75 mm thickness is used for orthogonal machining. In order to minimize the chatter during cutting process, experiments are conducted on 100 mm length of workpiece each time.

Similarly, forged Ti6Al4V alloy cylindrical workpiece of 40 mm diameter and 220 mm of length is considered for both CT and UVAT process. Moreover, 20 mm length of cut is considered for each experiment. The chemical composition of Ti6Al4V alloy workpiece is tested by Spectrum analysis and it is shown in table 4.1. In order to ensure stress free condition, Ti6Al4V alloy workpiece is annealed at 590ºC for 2 h and followed by furnace cooling before experimentation.

Table 4.1: Chemical composition of Ti6Al4V alloy workpiece

C	Fe	N_2	O_2	Al	V	H_2	T_i
0.08	0.2	0.05	0.2	6.0	4.0	0.01	Balance
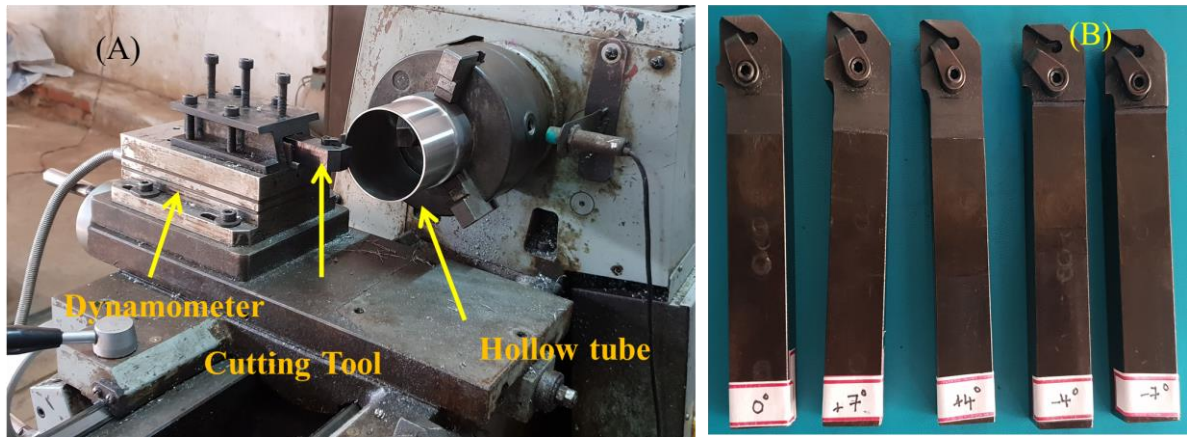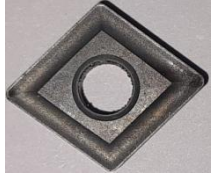
Figure 4.1:Orthogonal machining (A).Experimental setup (B).Cutting tools

4.3 Selection of cutting tools

The performance of Ti6Al4V alloy machining can be increased by selecting suitable cutting tool materials. The cutting tools are selected based on machining process and machining conditions. Orthogonal experiments are carried out under dry condition using uncoated carbide inserts (TPUN160304THM grade) with 11º relief angle and 0.4 mm nose radius. In order to evaluate the effect of rake angle on Johnson-Cook material parameters, orthogonal experiments are performed with (CTGP 2020 K16) five different rake angles (-7º,-4º, 0º, 4º, 7º). Similarly, the uncoated cemented-carbide type inserts (CNMG120408 THM) and Widia tool holders (PCLNR2525M12) are used for machining of Ti6Al4V alloy workpiece for both CT and UVAT process. Additional details of cutting insert are listed in table 4.2.

Table 4.2: Specifications of cutting inserts used for experimentation

	TPUN160304THM	CNMG120408 THM
Tool makers	WIDIA	WIDIA
Tool material	Cemented carbide	Cemented carbide
Nose Radius mm	0.4	0.8
Rake angle	-7º, -4º, 0º ,4º, 7º	-6º
Clearance angle	11º	0º
Cutting edge radius	0.25	---

4.3.1 Tool geometry

In metal cutting, cutting force is greatly affected by tool rake angle. It has an important influence on the tool–chip contact length along with the other factors such as the geometry and dimensions of the chip breaker, cutting edge preparation and cutting speed used during cutting. Generally, the higher the rake angle the lower the forces developed during metal cutting. However, in practical metal cutting operations, there is a limit to the rake angle. Higher rake angle decreases the cutting tool strength and accelerates wear. Therefore, there should be a trade-off between the rake angle and cutting forces. Hence, the present orthogonal experimental work is focused to investigate the effect of rake angle (back rake angle) on the Johnson-Cook material parameters for Ti6Al4V alloy. Specially designed and manufactured tool holders with five different rake angles; -7, -4, 0, 4 and 7 degrees keeping all other parameters of tool geometry constant have been used in the present orthogonal experimental investigations.

4.4 Machine Tool Specifications

Turning experiments are performed with high precision grade 1 accuracy Precision lathe- SSM 1430, featuring flame hardened bed ways with over 300 BHN hardness, hardened and ground alloy steel Spindle running in anti-friction taper roller bearings. It is attached with specially designed and fabricated tool post to accommodate dynamometer and experimental setup. For increasing rigidity of machining system, work-piece material is held between three

jaw chuck for all types of experiments. The specification of precision lathe machine is given in table 4.3.

Table 4.3: Specifications of Precision lathe

Type	Feature	Specification
Make and Model	Company	MAGNUM
	Model	MA-1430
Mechanical system	Swing over bed	356 mm
	Width of bedways	206 mm
	Total length of bedways	1430 mm
	Swing over cross slide	220 mm
	Height of centers	178 mm
	Distance between centers	750 mm
	Variable spindle speed	45-1800 rpm
	Feed rate	0.04-7 mm/rev
	Pitch of the lead screw	6 mm
Electrical system	Spindle motor speed (dynamically variable)	8 KW infinitely variable Speed
	Stabilizer & Transformer	3 KVA
Attachments	Dynamometer for force measurement	yes
	Ultrasonic vibration assistance	yes

4.5. Experimental setup

Experiments have been performed on variable speed precision lathe for both orthogonal and UVAT process. In orthogonal experiments, the cutting edge of the tool is perpendicular cutting velocity as shown in figure 4.1. In orthogonal experimentaion, cutting force (F_c), feed force (F_f) and chip thickness (t_c) are considered as output parameters to evaluate Johnson Cook parameters for Ti6Al4V alloy. Kistler six component 9257 B type dynamometer is used for measring cutting and feed force, Thermal image camera Fluke-Ti200 is used for measuring cutting temperature and chip thickness is measured with vernier calipers in orthogonal experiments.

The experimental setup for UVAT process mainly consists of machine tool, ultrasonic attachment and measuring system. The detailed schematic diagram of ultrasonic assisted vibrating system is shown in figure 4.2.The ultrasonic attachment consist of piezoelectric transducer, booster and horn assembly is mounted on machine tool with help of a specially designed fixture arrangement. The details of ultrasonic attachment is shown in figure 4.3 and 3D view of fixture is shown in figure 4.2.(B).The ultrasonic attachment is connected to ultrasonic generator with high frequency cable. The ultrasonic generator is used to supply electrical energy to piezoelectric transducer at 20 KHz frequency.

The ultrasonic generator consists of various levels of intensity of ultrasonic power to vary the amplitude in UVAT process. The piezoelectric transducer consists of quartz crystal which is used to convert the electrical signal from generator to mechanical vibrations. The displacement and amplitude available at the end of transducer is not enough to produce disengagement between tool and workpiece. Hence, a booster is attached to amplify the vibrations available at the end of transducer and a horn is used to carry these vibrations to the tip of tool with further improvement in amplitude. Moreover, the continuous air cooling is provided to ultrasonic attachment to carry away the heat generated during UVAT process from horn assembly. The specification of ultrasonic attachment is given in table 4.4.
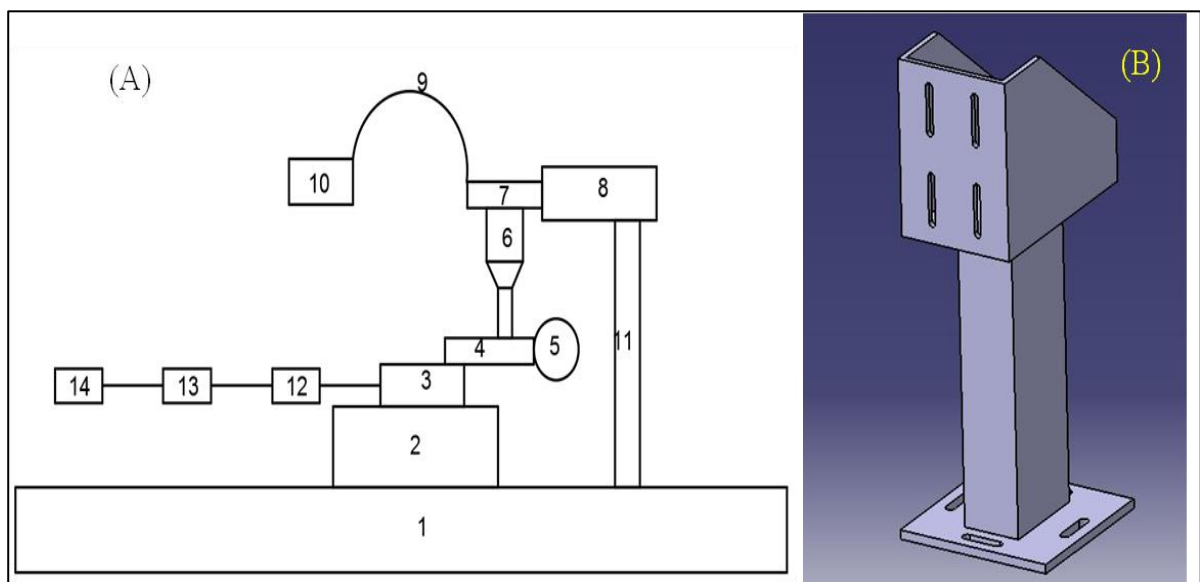
Figure 4.2: Schematic diagram of UVAT process

1. Precision lathe.

2. Cross slide/ compound plate

3. Kistler Dynamometer (9257 B type)

4. Cutting tool system

5. Workpiece

6. Booster and horn

7. Piezoelectric transducer

8. Bracket for holding ultrasonic attachment

9. High frequency cable

10. Ultrasonic generator

11. Fixture for ultrasonic system

12. Charge amplifier for force measurement

13. Data acquisition system for force measurement

14. Display unit for force measurement
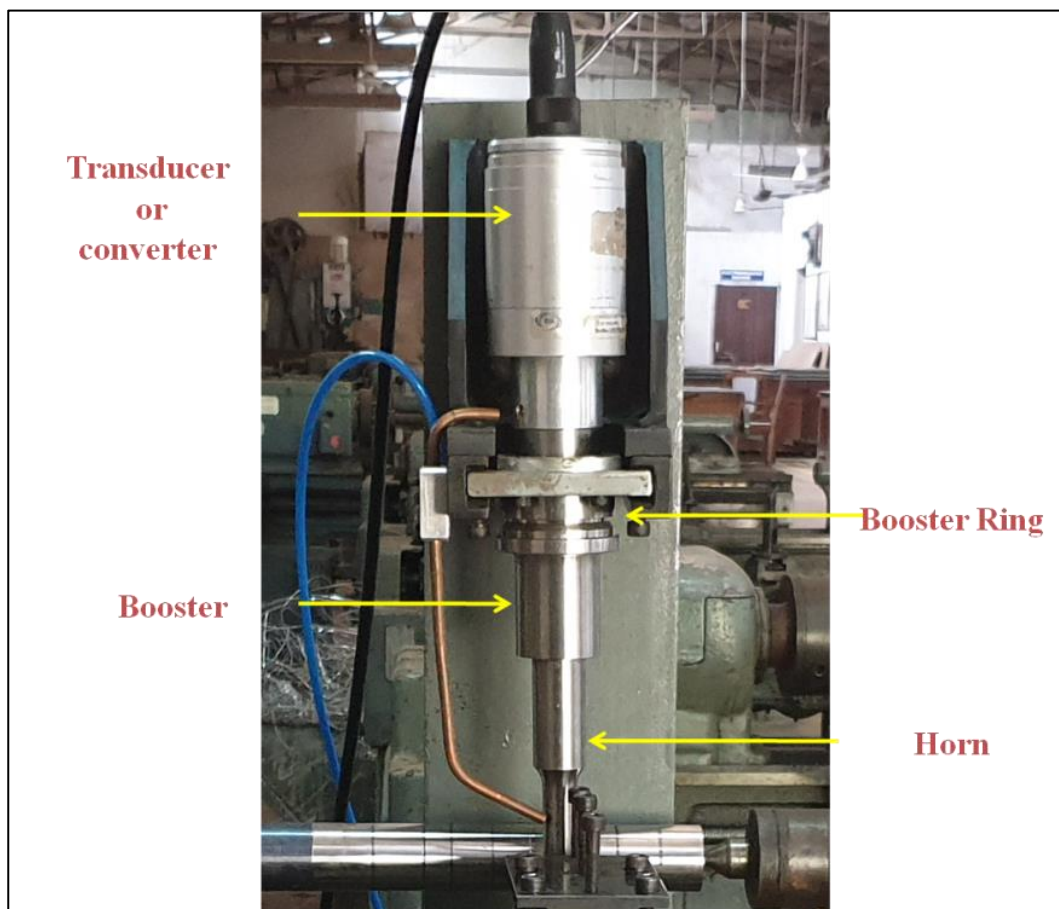
Figure 4.3: Assembly of ultrasonic attachment

In the present work, cutting force, cutting temperature, surface roughness, residual stresse and tool wear have been measured for both CT and UVAT of Ti6Al4V alloy. The experimental setup used for both CT and UVAT is shown in figure 4.4 The details of equipments used for measuring are described below:

Figure 4.4: Experimental setup and measuring system used for UVAT process

Figure 4.5: Kistler six component 9257 B type dynamometer

Table 4.4: Specifications of ultrasonic system

Component	Specifications/Details	
Ultrasonic Generator	Current Input	: 8 Amp
	Working frequency	: 20 KHz.
	Maximum power output	: 4.5 KW.
	Operation mode	: pulse and continuous mode:-on/off & timer mode
	Mode of tuning	: Auto and manual
	Load	: 0-100% overload
	Output control	: Auto tuning with load output power range 30 to 100% of nominal converter amplitude
Converter/ Transducer	Power	: 4.5 KW
	Converter Current	: 6 Amp effective
Booster	Material	: Titanium
Sonotrode/Horn	Material	: Titanium
	Type	: Cylindrical Stepped type with optimum slenderness (L/D)
	Amplitude at the end	:15-25 μm

4.5.1 Force measurement

A. Dynamometer: Kistler make 9257 B type dynamometer was used for force measurement and it is shown in figure 4.5. The dynamometer consists of a four three component force sensor fitted under high preload between a base plate and a top plate.Each sensor consists of three pairs of quartz plates, onse sensitive to pressure in the z direction and other two responding to the shear in x and y direction respectively. The six components (three orthogonal components of a force Fx, Fy and Fz and three torque components Mx, My and Mz) are measured practically without displacement. These precision sensors are featured with high stiffness, high sensitivity, excellent repeatability and long-term stability. They exhibit the inherent ruggedness of bonded strain gage transducers and this is incorporated with rust proof and protected against penetration of splash water and cooling agents. The top mounting surface of the sensor is equipped with mounting tool post to hold lathe cutting tools. The forces and torque acting on the tool are transmitted to the top plate of a six component

dynamometer sensor.. The charges yielded by the quartz plates are collected with electrodes connected to the connector of the sensor.

B. Charge Amplifier: The 5070A, 4 channel strain gage amplifier was used for amplifying the output of the dynamometer from micro-volts to milli-volts. It is cost effective, compact instrument suitable for high resolution measurements. Charge amplifier front panel consists of a rotating knob, adjust and measure push button for setting the ranges of the measuring characteristics. It has both analog and digital capability. In the analog mode, the output signal is rated up to +/- 10 volts and is suitable for input into an A/D convertor or, some other device. In the digital mode, output consists of an RS-232 serial connection. Amplifier inputs and outputs are conveniently provided through single connectors located in the back side of the case.

C. Data Acquisition: DynoWare data acquisition and display software is used for further analysis of the signals that are obtained from the output from the charge amplifier.

4.5.2 Cutting temperature measurement

In this research work, non contact type thermal image camera is used for measuring temperature in orthogonal experiments to avoid the complexity of fixing the thermocouple. However, embedded thermocouple system is used for both CT and UVAT as the tool tip is in contact with workpiece. Embedded thermocouple measurement system is used for measuring cutting temperature during temperature during cutting process. Fine deep holes are drilled in cutting tool with electrical discharge machining (EDM) to insert thermocouple for temperature measurement. Nickel-chromium (k- type) thermocouple of diameter 0.25 mm with an uncertainty of ± 1.1°C is used in this system. In order to provide accurate measurement and tool strength, the hole in cutting tool is positioned as shown in figure 4.6. The thermocouple is calibrated with hot water bath and time constant to reach 63.2 % of total temperature is 0.05 sec. High density polyethylene (HDPE) type thermal glue is selected to fix thermocouple in the tool insert for proper measurement. The variation of cutting tool temperature in standalone condition with vibrating mode is negligible due to continuous contact between the tool and horn. Finally, the cutting temperature is measured with Data Acquisition system as shown in figure 4.4(C).
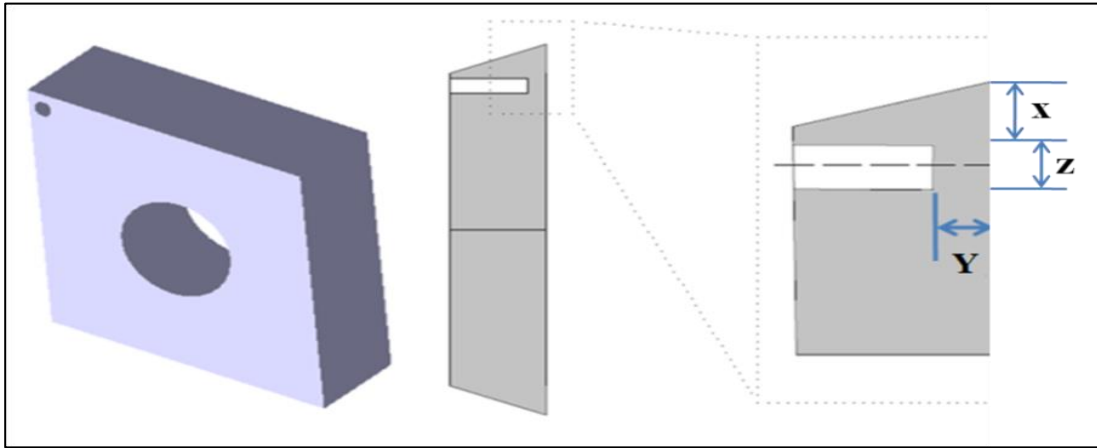
Figure 4.6: Position of the hole in insert for temperature measurement

Table 4.5: Details of temperature measurement

Component	Details
Thermocouple	Type: Nickel-chromium (k- type) thermocouple uncertainty : $\pm$ 1.1ºC Diameter : 0.25 mm
Geometric position of hole in insert	x = 0.72 mm, y = 0.35 mm, z = 0.6 mm

Figure 4.7: Fluke-Ti200 Thermal image camera

In orthogonal experiments, non contact type method is used for measuring cutting temperature in machining of Ti6Al4V alloy tube. This is one of the best method to analyze the temperature generated during the machining process as the edge of the cutting tool is

perpendicular to cutting tool velocity in orthogonal experiments. Hence, high sensitive thermal image camera " Fluke –Ti200" is used for orthogonal experiments. The details of thermal image camera is presented in table 4.6 and figure 4.7. The recorded temperature is analyzed with smart view software by providing required material emmissivity value.

Table 4.6: Details of thermal image camera "Fluke Ti-200"

Temperature measurement range	-20 °C to +650 °C (-4 °F to +1202 °F)
Temperature measurement accuracy	± 2 °C or 2 % (at 25 °C nominal, whichever is greater)
On-screen emissivity correction	Yes
On-screen reflected background temperature compensation	Yes
Detector type	Focal Plane Array, uncooled micro-bolometer, 200 X 150 pixels
Thermal sensitivity (NETD)	≤ 0.075 °C at 30 °C target temp (75 mK)
Total pixels	30,000
Infrared spectral band	7.5 μm to 14 μm (long wave)
Visual (visible light) camera	Industrial performance 5.0 megapixel
Minimum focus distance	15 cm (approx. 6 in)
Level and span	Smooth auto-scaling and manual scaling of level and span
Full screen infrared	Yes
Color alarms (temperature alarms)	High-temperature , low-temperature, and isotherm (user-selectable)
Software	SmartView® full analysis and reporting software

4.5.3 Vibration analyzer

The ultrasonic frequency and amplitude of vibrating system at the end of cutting tool are measured by digital vibrometer. It is used to calibrate the position of ultrasonic vibration system at various ultrasonic powers. The magnetic probe of vibrometer is attached to cutting tool to get the amplitude of ultrasonic system in tangential direction as shown in figure 4.4. The amplitude is varied by changing ultrasonic power intensity as these two parameters are in

direct relation [144]. The amplitude obtained at 100 % ultrasonic power intensity is 25 μm. The detail of vibration analyzer is shown in table 4.7

Table 4.7: Details of vibration analyzer

Type	Details
Transducer	Piezoelectric Accelerometer
Measurements and its range	Frequency:1-20 KHz Displacement: 0.001–4.000mm Velcotiy: 0.01- 40.00 cm/s Acceleration: 0.1- 400.0 m/s RPM: 60-60000 RPM
Probe	Magnetic type

4.5.4 Surface Roughness Measurement

Surface integrity plays a prominent role in fatigue life of a part or component. A significant proportion of component failure starts at the surface due to surface discontinuity or gradual deterioration of the surface quality. Irregular surface finish cause stress concentration, corrosion and fatigue failure. The most important parameter describing surface integrity is surface roughness. In order to ensure the larger life of component, surface roughness must be within acceptable limits.

Marsurf M400 is used to measure the surface roughness of the machined parts and is shown in figure 4.8. This is a contact type measuring sytem, As the stylus moves along the surface, a transducer converts displacement into a signal which is then displayed in terms of surface roghness parameters. In the present work, the surface roughness is measured at three different locations and the average surface roughness value is considered for each each experiment. Each measurement is done at 5.6 mm sampling length by using Marsurf M400 with 0.8 mm as cut-off length. The specifications of Marsurf M400 are given table 4.8.

Table 4.8:Specifications of Marsurf M400

Type	Portable
Roughness parameters:	R_a, R_q, R_v, R_p, R_t, R_z, R_{sk}, R_{ku}
Measurement standards	As per DIN/ISO/JIS
Measuring range:	Min 350 micron
Traversing Length:	Min 1.75, 5.6, 17.5mm
Assesment range:	Min 0.25, 0.8, 2.5 mm
Column & Stand:	Granite base with support stand attachmen
Display unit	LCD, 16 digit x 2 lines

Figure 4.8: Surface roughness measurement using MarSurf

4.5.5 Tool wear measurement

The generation of localized adiabatic zones adjacent to cutting edge of the tool increases the tool wear during machining of Ti-alloy due to its low thermal conductivity. Scanning electron microscope (SEM) is used to measure the flank wear of the tool in machining process.SEM is used to examine the topography, morphology, composition and

crystallographic information. SEM uses electrons rather than light to form an image.The basic principle of SEM is electron beam produced from the tungsten filament is focused with magnetic lenses and hits the specimen. The electron beam collides with top surface of the the specimen and signals are generated by the interaction of the electron beam with the specimen. Each of these signals are sensitive to a different aspect of the specimen and gives a variety of information about the specimen by detecting the signals which are emitted. The SEM setup [TESCAN make, Model: Vega LMU 3] used in this study is shown in figure 4.9 and its specifications are given in table 4.9. Resolution of the SEM is of the order of 3.0 nm at high vacuum mode and 3.5 nm at low vacuum mode. The magnification of SEM can go up to 2x to 100000x which depends on the chamber.

Table 4.9: Specifications of Scanning electron microscope

Component	Details
Make and Model	TESCAN ,Vega LMU 3
Electron gun	Tungsten heated cathode
Resolution	High Vacuum Mode (SE): 3 nm at 30 kV / 2 nm at 30 kV
	Low Vacuum Mode: 3.5 nm at 30 kV / 2.5 nm at 30 kV
Magnification	$2\times - 1,000,000\times$
Scanning Speed	From 20 ns to 10 ms per pixel adjustable in steps or continuously
Chamber Vacuum	High Vacuum Mode: < 10-3×9 Pa
	Medium Vacuum Mode: 3 – 150 Pa
	Low Vacuum Mode: 3 – 500 Pa*
Chamber and Column Suspension	Pneumatic
Specimen Stage	Movements: X = 80 mm (–40 mm to +40 mm)
	$\qquad\qquad$ Y = 60 mm (–30 mm to +30 mm)
	$\qquad\qquad$ Z = 47 mm
	Rotation : 360° continuous
	Tilt : –80° to +80°
	Maximum Specimen Height: 54 mm (with rotation stage)
	$\qquad\qquad\qquad\qquad$ 81 mm (without rotation stage)

Figure 4.9: Scanning electron microscopy

4.5.6. X-Ray Diffraction Technique (XRD)

The residual stresses of machined component are measured by X-ray diffraction (XRD) technique using $\sin^2\psi$ method. The stretching and compressing of material happened when its subjected to stress. This results change in structure of material occurs and distance between crystal planes changes. The X-ray which is incident on sample, diffracted at different angles as shown in figure 4.10 and stress strain relation is used to obtain the stress value. Finally, residual stress induced during machining process g is calculated from elastic strain obtained from inter atomic planes. Panalytical X'pert pro MRD with X'pert stress software is used to measure the residual stress profiles as shown in figure 4.11 and specifications are given in table 4.10.
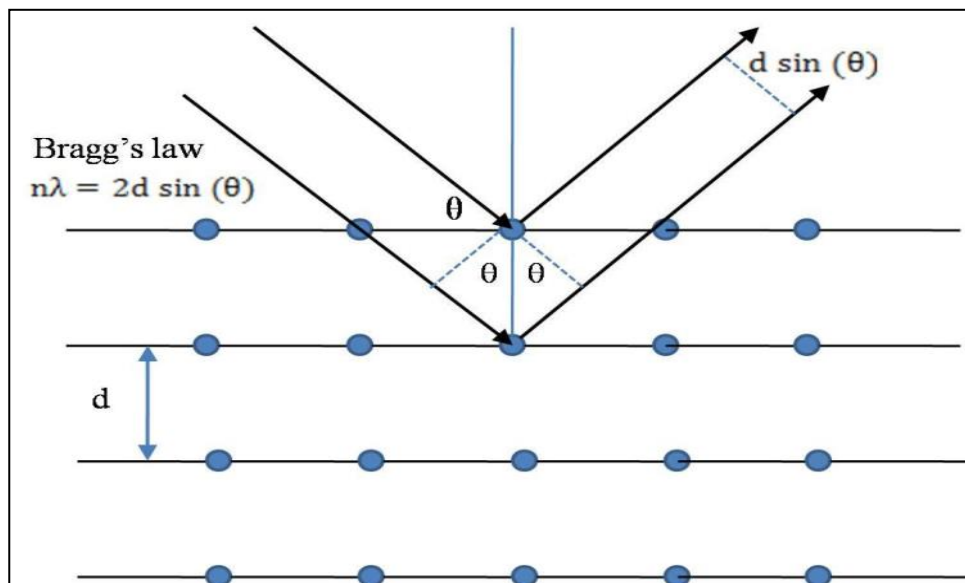
Figure 4.10: Representation of residual stress measurement law

Cu-Kα material is selected for X-ray radiation and XRD system is calibrated with stress free sample. From phase analysis, it is determined that diffraction peaks for the un-machined and machined sample were obtained at 128º and 136º respectively. The mathematical equations used for calculating residual stresses form XRD technique are given below.

$$\sigma = \frac{E}{(1+v)sin^2\psi}\left[\frac{d_\psi - d_0}{d_0}\right] \qquad (4.1)$$

$$\sigma = \left(\frac{E}{(1+v)}\right)m \qquad (4.2)$$

where E and v are young's modulus and Poisson's ratio, d_ψ and d_0 are d-spacing of machined and unmachined sample crystalline planes and m indicates slope of fitted line in d_ψ Vs $sin^2\psi$.

As the residual stress is sensitive to thermo-mechanical loading, the sample (10 mm x 10 mm x 5 mm) for measurement were cut from wire EDM process from cylindrical machined component. The machined sample was polished each time with a step of 15 μm up to 110 μ using electro polishing technique to measure residual stress at various depths of machined component.

Figure 4.11: XRD equipment(Model PANalytical)

Table 4.10: Specifications of X-Ray diffrractometer

Component	Details
Make & model	Panalytical X'Pert Pro
Source of X-rays	Cu-Kα , 1.54 Å wave length
Detector	Pixel and Scintillation detector
Stage for sample	Fixed, with X-Ray source & Detector rotation
Filters	Nickel and copper
Range of masks	2 mm to 20 mm
Measurement range	5º to 140º

4.5.7 High cycle fatigue testing

The estimation of fatigue strength of Ti6Al4V alloy components obtained from CT and UVAT are performed on servo- hydraulic testing machine (Make: BISS) at 15 Hz as shown in figure 4.12 and its specifications are given in table 11.The tests are carried out under sinusoidal load control at room temperature. The uni-axial tension-compression fatigue test are performed with stress ratio ($R = \sigma_{max}/\sigma_{min} = -1$) as suggested by the ASTM 466-15 [23].

Figure 4.12: Setup for Fatigue test machine

Table 4.11: Specifications of HCF testing machine

Frequency range	0-100 Hz
Load range	100 kN
Stroke measurement	150 mm
Load control	Servo hydraulic type
Data acquisition system	32 bit
Frame stiffness	100 kN/mm
Measurement range	5º to 140º

4.6 Summary

Experiments were conducted on Ti6Al4V alloy workpiece for both CT and UVAT process to evaluate its performance based on cutting force, cutting temperature, surface roughness, tool wear, residual stresses and fatigue strength. The standard equipments have been used for every measurement and ASTM standards were followed for each test sample. Orthogonal experiments were also conducted to determine J-C parameters for Ti6Al4V alloy.

Chapter 5

Machining Approach to Determine J-C Material Model Parameters for Ti6Al4V Alloy

5.1 Introduction

The accuracy of numerical modeling of machining process largely depends on material model parameters. The Johnson-Cook material model parameters i.e. A, B, C, n and m describe deformation behavior of material under thermo-mechanical loading. This chapter deals with a machining approach which considers an equivalent strain hardening exponent n_{eq} in place of hardening exponent 'n' for accurate prediction of material model parameters at near orthogonal machining conditions. The effect of strain on secondary deformation zone i.e tool-chip interface is also considered for accurate prediction of material parameters. In the present machining approach, response surface methodology (RSM) and particle swarm optimization (PSO) technique are used to identify material model parameters for Ti6Al4V alloy. Orthogonal experiments are conducted at different rake angles to calculate strain, strain rate and temperature using Oxley's extension theory. J-C constitutive model is used to investigate the effect of strain, strain rate and thermal softening dependency in identifying material model constants.

5.2 Methodology

The orthogonal experiments for Ti6Al4V alloy are conducted as per the experimental design. Second order polynomial models are developed for force components (F_c and F_f) and chip thickness (t_c) using RSM. Analysis of variance (ANOVA) is used to analyze the experimental results and identifying the parameters which have a significant effect on the

machining output responses i.e. cutting force, feed force and chip thickness. The p values or probability values show the level of significance of each parameter on output response. Lower p values indicate that the parameter values have higher probability of falling within the ranges which impact the outcome of the experiment.

The modified Oxley's chip formation theory[144, 145] is used to calculate physical quantities like strain ε, strain rate $\acute{\varepsilon}$ and temperature T on shear deformation zone AB using data obtained from regression models of force components and chip thickness at different rake angles

Shear angle in an orthogonal machining is calculated by

$$\phi = \tan^{-1}\left[\frac{\frac{t_u}{t_c}\cos\alpha}{1 - \frac{t_u}{t_c}\sin\alpha}\right] \tag{5.1}$$

where t_u = uncut chip thickness

t_c = chip thickness

α = rake angle

Equivalent strain on primary deformation zone using von-Misses criteria is given by

$$\varepsilon_{AB} = \frac{\cos\alpha}{2\sqrt{3}\ \sin\phi\ \cos(\phi - \alpha)} \tag{5.2}$$

Equivalent strain rate on the primary deformation zone using von-Mises criteria is given by

$$\dot{\varepsilon}_{AB} = \frac{2\ V_c\cos\alpha}{h\sqrt{3}\cos(\phi - \alpha)} \tag{5.3}$$

where V_c= cutting speed

The thickness of the primary deformation zone is estimated as [124]

$$h = 0.5 \times f \tag{5.4}$$

Equivalent flow stress at the primary deformation zone is given by

$$\sigma_{AB} = \sqrt{3}\sin\phi\ \frac{(F_c\cos\phi - F_f\sin\phi)}{f\ w} \tag{5.5}$$

Temperature along shear plane AB is given by

$$T_{AB} = T_r + \frac{(1-\beta)(F_c \cos\o - F_f \sin\o)\cos\alpha}{\rho\, C_p\, f\, w\, \cos(\o - \alpha)} \qquad (5.6)$$

Where β is the ratio of the heat flowing into the workpiece and can be obtained as

$$\beta = 0.5 - 0.35 \times log(R_T \tan\o) \quad for\ 0.04 \leq R_T \tan\o \leq 10 \qquad (5.7)$$

$$\beta = 0.3 - 0.15 \times log(R_T \tan\o) \quad for\ R_T \tan\o > 10 \qquad (5.8)$$

$$R_T = \frac{\rho\, C_p\, f\, V_c}{K_{th}} \qquad (5.9)$$

Particle swarm optimization (PSO) technique is population based stochastic optimization technique in which system is initialized with a population of random solutions and searches for optima by updating generations. As PSO techniques is less dependent on set of initial values compared to iterative algorithms, PSO technique approaches stable optimum values with less time[147]. A PSO technique is enforced to determine J-C constants with an objective function of minimizing the difference between predicted and measured flow stress. The steps followed in machining approach are shown in figure 5.1.
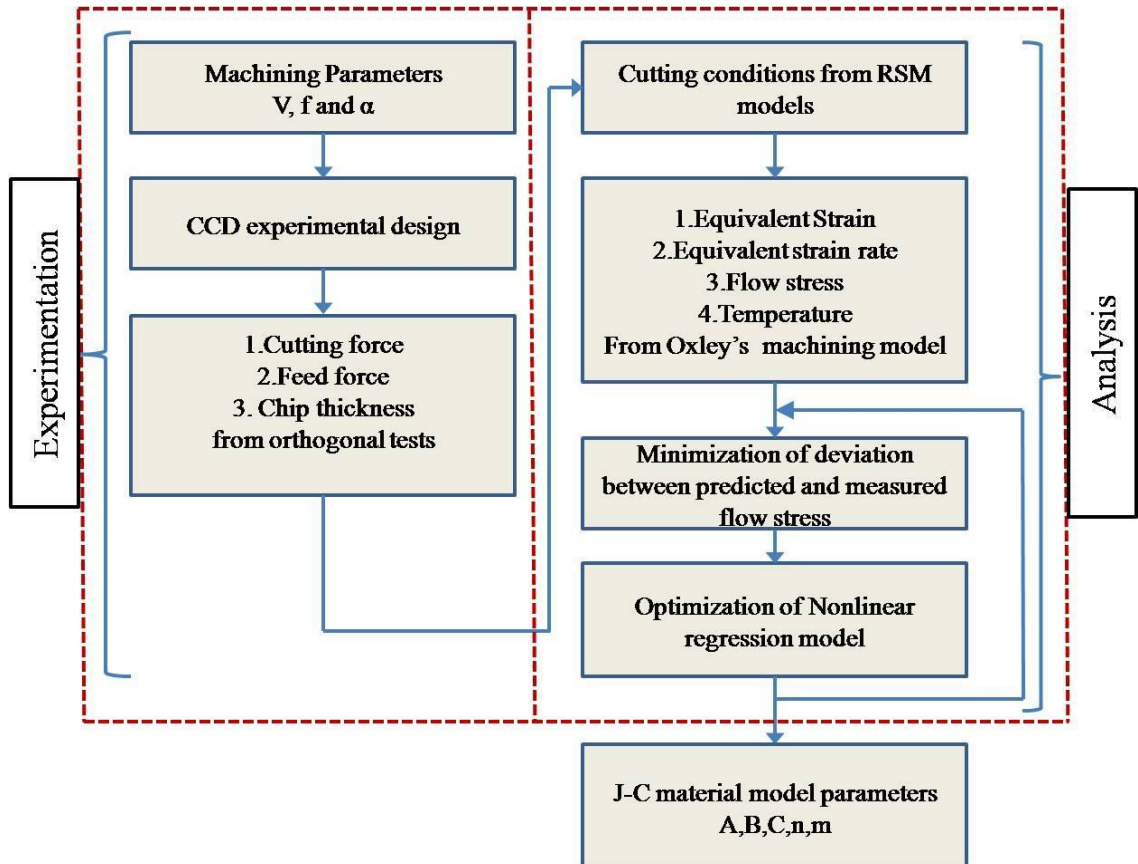
Figure 5.1: Machining approach to determine J-C parameters

5.3 Machining Approach (MA) to Identify J-C Material Constants

In this methodology, J-C constitutive material model is used to determine material constants. The deformation behavior of material under thermo-mechanical loading is expressed as

$$\sigma = (A + B\varepsilon^n)\left[1 + C ln\left(\frac{\varepsilon^o}{\varepsilon_0^o}\right)\right]\left[1 - \left(\frac{T-T_r}{T_m-T_r}\right)^m\right] \qquad (5.10)$$

where σ is the equivalent material flow stress, ε is the plastic strain, ε° is the plastic strain rate, ε°$_o$ is the reference strain rate, T, T$_r$ and T$_m$ represents instantaneous, reference and melting temperature of material respectively, The first term of this equation represents strain hardening where A and B represents yield stress and strain hardening constant of material; second term indicates that flow stress increases with increase in strain rate where C and n represents strain rate coefficient and strain hardening coefficient; third term indicates thermal softening of material with increasing temperature where m represents thermal softening coefficient. In the proposed methodology, equivalent strain hardening exponent n$_{eq}$ [129] which accounts for strain along chip-tool contact is used in place of strain exponent term n. The equivalent strain hardening exponent (n$_{eq}$) is given by

$$n_{eq} = \frac{nB\varepsilon_{AB}^n}{(A + B\varepsilon_{AB}^n)} \qquad (5.11)$$

The proposed MA to determine J-C material constants consists of an experimental and computational phases as shown in figure 1. Initially, orthogonal tests are conducted and force components (F$_c$ and F$_f$), and chip thickness (t$_c$) are measured. In the next step, machining responses F$_c$, F$_f$ and t$_c$ are used to calculate the physical quantities of PDZ. Finally, PSO technique is used to determine J-C constants from following objective function.

$$f(x) = (A, B, C, n, m) =$$

$$min \sum_{i=1}^{N} \sqrt{\left[\left(A + B\ \varepsilon(i)^{neq}\right)\left(1 + C\ ln\left(\frac{\dot{\varepsilon}(i)}{\dot{\varepsilon}_0}\right)\right)\left(1 - \left(\frac{T(i) - T_r}{T_m - T_r}\right)^m\right) - \sigma_{exp}(i)\right]^2} \qquad (5.12)$$

The objective function is minimization of error between predicted equivalent stress and measured equivalent stress. The function f(x) is a vector contains J-C parameters A, B, C, n and m.

The objective function is in the form of min $[f(x)] \rightarrow x_i$

$$x_L \leq x_i \leq x_U$$

x_L and x_U are lower and upper limit of A, B, C, n and m.

The lower and upper limits are in the range of

$$724.7 \leq A_i \leq 1119$$

$$331.1 \leq B_i \leq 1092$$

$$0.011 \leq C_i \leq 0.05$$

$$0.122 \leq n_i \leq 0.93$$

$$0.6437 \leq n_i \leq 1.04$$

5.3.1 Nonlinear models for output response surfaces

The relationship between J-C constants and measured responses from orthogonal cutting are formed using the concept of design of experiments and RSM. RSM is used to develop nonlinear regression models to cover a wide range of machining conditions during optimization procedure. This method is used to establish a relation between desired response variable(Y) and number of independent input variables (x_i) with a number of statistical calculations

$$Y = \alpha_0 + \sum_{i=1}^{N} \mu_i x_i + \sum_{i=1}^{N} \mu_{ii} x_i^2 + \sum_{i<j}^{N} \mu_{ij} x_i x_j + \beta_o \qquad (5.13)$$

where x_i and x_j are machining variables. α_0 is constant while, μ_i μ_{ii} and μ_{ij} are regression coefficients and β indicates experimental error.

In the present work, Central Composites Design (CCD) is used to conduct orthogonal cutting test with reasonable accuracy in the formation of nonlinear responses [148]. Based on literature, it is identified that cutting speed, feed rate and rake angle are the three important

77

variables effecting chip formation model used for determination of J-C Constants. In order to cover wide range of cutting conditions, the cutting parameters levels are selected and given in given in table 5.1. According to CCD, the number of experiments generated for three independent variables(k=3) is 16 including eight factor points(2^k),six axial points (2xk) and two center points with one replication. For rotatable design, the upper and lower limits for each factor are given by ±1.68. In order to avoid the complexity in providing exact upper and lower limit rake angles of 6.72 and -6.72 on cutting tools, these are rounded of to 7 and -7.

Table 5. 1: Machining parameters and their levels for orthogonal cutting

		Low level(-1)	Zero level(0)	High Level(+1)
Cutting speed (V)	m/min	50	75	100
Feed rate (f)	mm/rev	0.051	0.0725	0.094
Rake angle (α)	degrees	-4	0	4

Table 5.2: Experimental run and its output responses for orthogonal cutting

S.No	N (RPM)	f_r (mm/rev)	α (°)	Cutting Force F_c (N)	Feed Force F_f(N)	Chip Thickness t_c(mm)
1	381	0.051	4	955.6	101.9	0.1054
2	190	0.051	-4	446.7	111.5	0.0862
3	290	0.0725	-7	363.4	165.1	0.118
4	190	0.051	4	791.8	225.6	0.094
5	450	0.108	0	324	186.8	0.3042
6	290	0.035	0	280.8	84.7	0.0732
7	125	0.0725	0	394.1	163.5	0.1386
8	381	0.035	-4	140.4	114.4	0.0802
9	190	0.094	-4	525.9	140	0.158
10	190	0.094	4	846.1	185.9	0.18
11	290	0.0725	7	1092	362.7	0.1228
12	290	0.0725	0	324.3	164.7	0.1272
13	381	0.094	4	895	153.2	0.164
14	381	0.094	-4	513.7	176.8	0.1816
15	290	0.0725	0	371.6	170	0.1338

16	290	0.108	0	408.3	151.2	0.179
17	515	0.035	0	334.8	151.9	0.078
18	610	0.051	0	415.26	213	0.0974
19	686.7	0.077	0	520.1	201.8	0.1558
20	762	0.068	0	534.5	219.5	0.1472

Orthogonal experiments with Ti6Al4V alloy workpiece are carried out with five different rake angles (-7º,-4º, 0º, 4º, 7º) to evaluate the rake angle effect on J-C parameters. The details of experimental run and its output responses, F_c, F_f and t_c are shown in table 5.2. Aiming to avoid tool wear and edge radius effect on machining performance parameters, new insert is used for each cutting test. A cylindrical tube with 84.5 mm outer diameter and 81 mm inner diameter with 1.75 mm thickness is used for orthogonal machining. Kistler six component piezoelectric force dynamometer (9257B) is used to record force components for all the experiments. Chips are collected after each experiment and its thickness is measured with digital micrometer. An average of three measurements at different locations of chip samples is considered for estimating final chip thickness.

5.4 Machining parameters

The reliability of J-C parameters determined from MA depends on the selection of range of cutting conditions. In view of this, the cutting conditions at which measured flows stresses are determined must be used for predicted flow stresses. However, the range of cutting conditions to determine J-C constants accurately is not well defined for Ti6Al4V alloy in literature. Hence, the deformation behavior of Ti6Al4V alloy in terms of force components and chip thickness are evaluated at various machining conditions.

5.4.1 Effect of cutting speed on force components and chip thickness

In orthogonal turning of Ti6Al4V alloy, the cutting force decreased with an increase of cutting speed in 50-120 m/min range and increased with increase of cutting speed in 120-250 m/min range. The feed force continuously decreased with increase in cutting speed in a whole range of cutting speed with little change. The amount of heat generated during the machining of Ti6Al4V is accumulated in the vicinity of the cutting tool edge because o flow thermal conductivity of workpiece material and small chip tool contact length. This leads to

high cutting temperature which softens the workpiece material. This softening effect leads to decrease in tensile strength of Ti6Al4V alloy thereby decreasing the cutting force. The work hardening of Ti6Al4V alloy increases with increase in cutting speed. When cutting speed reaches a certain limit within the range of process parameters chosen, the hardening effect of workpiece material dominates thermal softening and hence leads to increase in cutting forces. This may be due to chemical reactivity of Ti6Al4V alloy being high because of which it absorbs oxygen and nitrogen present in air to form hard and brittle surface.

Continuous and segmented chips are produced during machining of the Ti6Al4V alloy. The thickness of the chips decreased with increasing cutting speed and increased with increasing feed rate as shown in Figure 5.2. In addition, chip segmentation increased with increase in cutting speed. The low modulus of elasticity of the Ti6Al4V alloy and the high cutting temperature result in a variation in chip thickness and width.

5.4.2 Effect of rake angle on force components and chip thickness

From Figure 5.3, it is observed that the cutting and feed forces decreased with increase in rake angle. This is due to the increase in the friction and contact pressure between tool and chip while rake angle changes from positive to negative. This leads to increase in energy consumption during machining process for negative rake angle. Hence, more cutting force is observed for negative rake angle for all feed ranges. This requires more energy for plastic deformation of workpiece material for negative rake angle. Moreover, there is a very little variation in chip thickness while changing the rake angle at lower feed rates. Whereas, small decrease in chip thickness is observed when rake angle changes from negative to positive in machining of Ti6Al4V alloy. The increase in temperature due to increase in friction between chip and tool interface with negative rake angle increases thickness of chips produced during machining process.
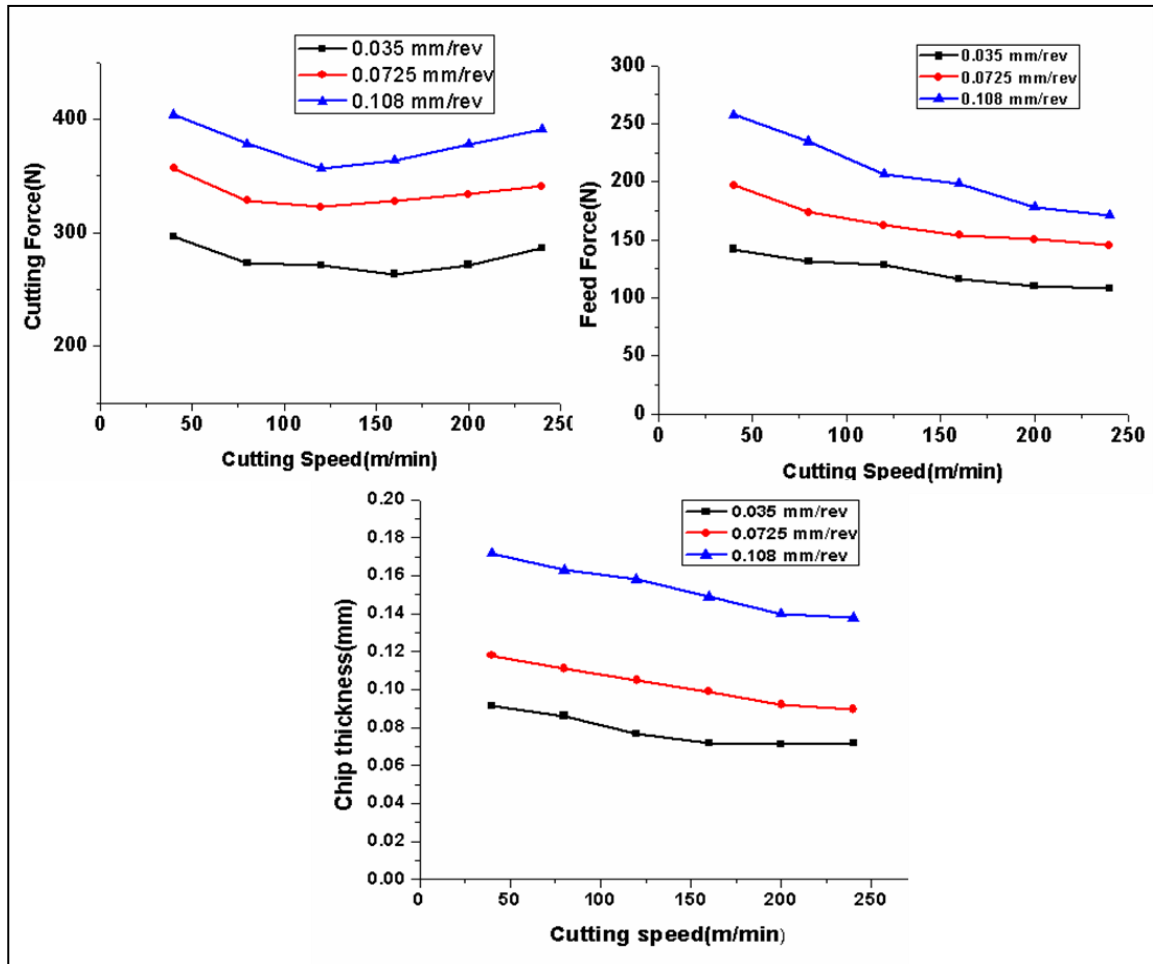
Figure 5.2: Variation of force components and chip thickness with respect to cutting speed at different feed rates
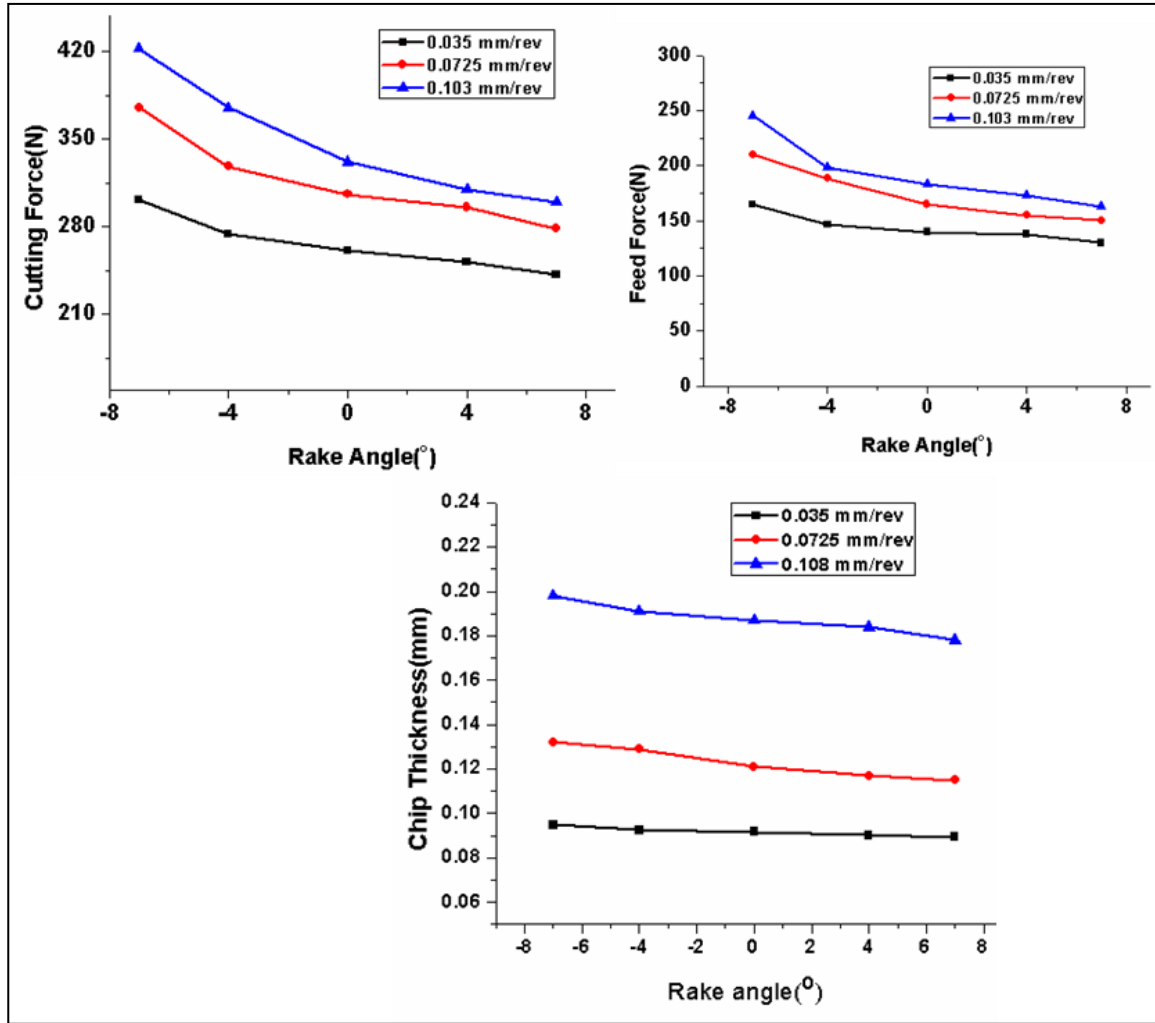
Figure 5.3: Variation of Force components and chip thickness with respect to rake angle at different feed rates

5.5 Response surface model of cutting forces and chip thickness

In order to determine J-C parameters from MA for Ti6Al4V alloy, RSM is used to develop second order models for control factors such as force components (F_c and F_f) and chip thickness (t_c). The CCD of RSM is used for experimental design for orthogonal turning of Ti6Al4V alloy. The second order response surface equations are derived for F_c, F_f and t_c based on CCD. These response equations are obtained in terms of independent variables V, f and α. RSM is used to obtain regression coefficients to form mathematical equations for Ti6Al4V alloy. In order to verify the accuracy of cutting force and chip thickness model, ANOVA is conducted and the results are shown in table 5.3. The P value from ANOVA Table is used to identify the significant factors of the model. In the proposed model, the factors with a less than 5% of P value are considered as significant while the remaining factors are insignificant for a given response Y. In order to improve accuracy, all terms in the

82

response equation are considered to identify J-C constants. Based on this, it is observed that the coefficient of determination R^2, lies between 97.02 and 98.40 % while R_{adj}^2, lies between 92.56 and 96.11 % for all three responses. These results show that the developed nonlinear regression models using RSM predict force components (F_c and F_f) and chip thickness accurately by considering the measurement errors. The developed second order models are validated by four experiments (Experiments 17, 18, 19 and 20) at different cutting conditions. Figure 5.4 shows the comparison between predicted and measured values of force components and chip thickness and the variation observed between these values is less than 10% for all cutting conditions.

Table 5.3: ANOVA for Ti6Al4V alloy

Source	Cutting Force (F_c)		Feed Force (F_f)		Chip Thickness(t_c)	
	Regression coefficients	p-value	Regression coefficients	p-value	Regression coefficients	p-value
Constant	+342.18	0.0003	+167.08	0.0001	0.1308	0.0007
A-Cutting Speed	-14.93	0.0426	+3.73	0.1047	0.0141	0.0026
B-Feed rate	+64.78	0.0001	+22.17	0.0001	0.0321	0.0001
C-Rake angle	-60.56	0.0001	-26.58	0.0001	-0.0008	0.7817
AB	+2.41	0.7618	-0.8625	0.7466	-0.0068	0.1178
AC	-1.69	0.8317	-5.06	0.0942	-0.0099	0.0385
BC	-9.54	0.2564	-5.16	0.0893	0.0035	0.3823
A²	+9.12	0.2442	+3.42	0.1995	0.0152	0.0048
B²	+13.24	0.1101	+4.09	0.1352	-0.0022	0.5431
C²	+26.87	0.0089	+16.59	0.0004	-0.0043	0.2667
R^2		0.9770		0.9844		0.9702
R^2_{adj}		0.9426		0.9611		0.9256
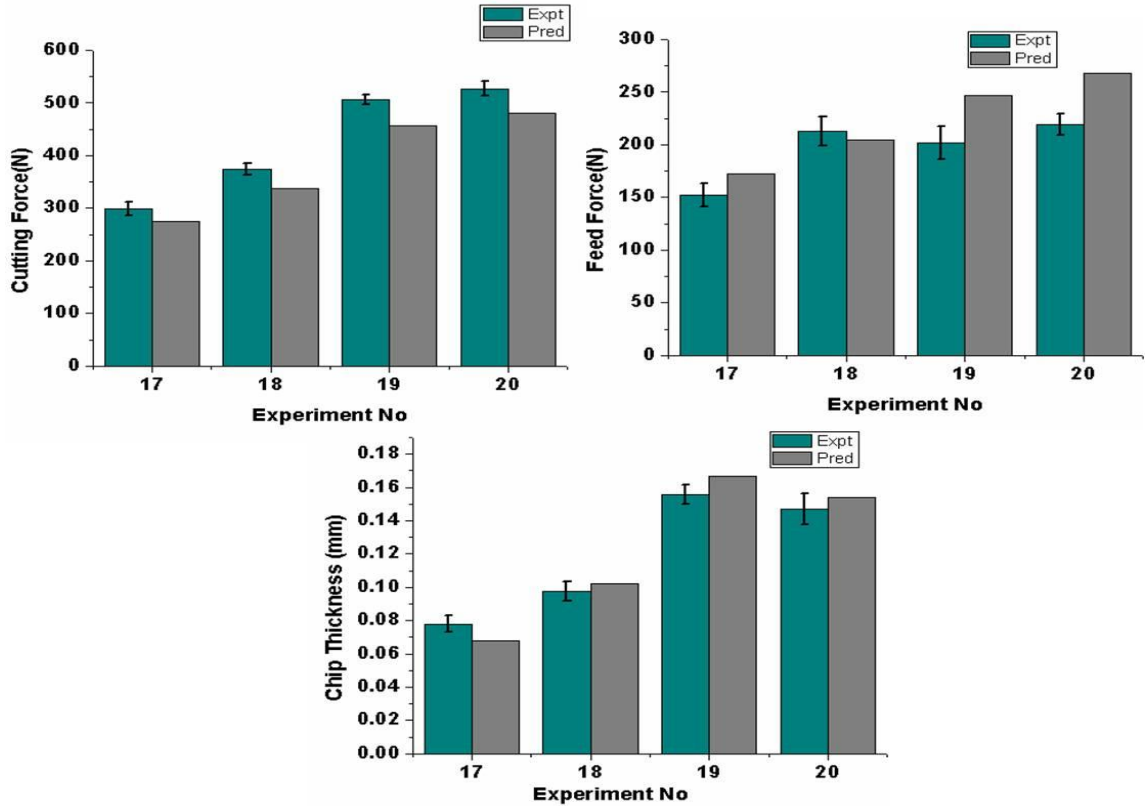
Figure 5.4: Comparison between experimental and predicted parameters

5.6 Effect of rake angle on J-C material constants

The rake angle plays a major role in the development of thermo-mechanical loading along rake face of cutting tool during metal cutting process. The cutting forces are reduced when rake angle changes from negative to positive. From this, rake angle plays a significant role in deformation of material and temperature during machining of Ti6Al4Valloy. Hence, rake angle is considered an important parameter in determination of J-C material constants for Ti6Al4Valloy in MA. The second-order polynomial models are used to obtain cutting forces and chip thickness at defined cutting condition by fixing rake angles. Then, Oxley chip formation model is used to calculate physical quantities (ε_{AB}; ε^o_{AB}; σ_{AB}; T_{AB}) in the PDZ for Ti6Al4V alloy. These physical quantities are used to develop anon-linear polynomial equation which describes the difference between predicted and measured flow stress. A PSO technique is used to identify J-C material constants by minimizing the difference between measured and predicted flow stress. In this PSO, the predicted flow stress is calculated from J-C material model in which the material constants A, B, C, n, and m are randomly taken between lower and upper limit for each iteration. After identification of J-C constants, the effect of rake angle is investigated by comparing the flow stress obtained from equation (5.1) and the material

parameters from table 5.4. Interestingly, it is observed that J-C parameters A, B, C, and n are same for -4º and -7º rake angle and B,C,n and m are same for 0º,4º and 7º rake angle. This indicates that the effect of thermal loading is increased with negative rake angle due to more contact between chip-tool along the rake face of cutting tool. However, the effect of mechanical loading is decreased with increase in rake angle.

The cutting test data used for calculating measured and predicted flow stresses for Ti6Al4V alloy is presented in table 5.5-5.9. The measured and predicted flow stresses are plotted in figure 5.5. The percentage variation between measured and predicted flow stress observed for the rake angles at 0°, 4°, 7°, -4°, and -7° are 31.3, 30.3, 27.2, 36.7, and 78.4 %, respectively. It is observed that the difference with 7° rake angle is comparatively smaller than others. Therefore, this rake angle (7°) is used for further studies.
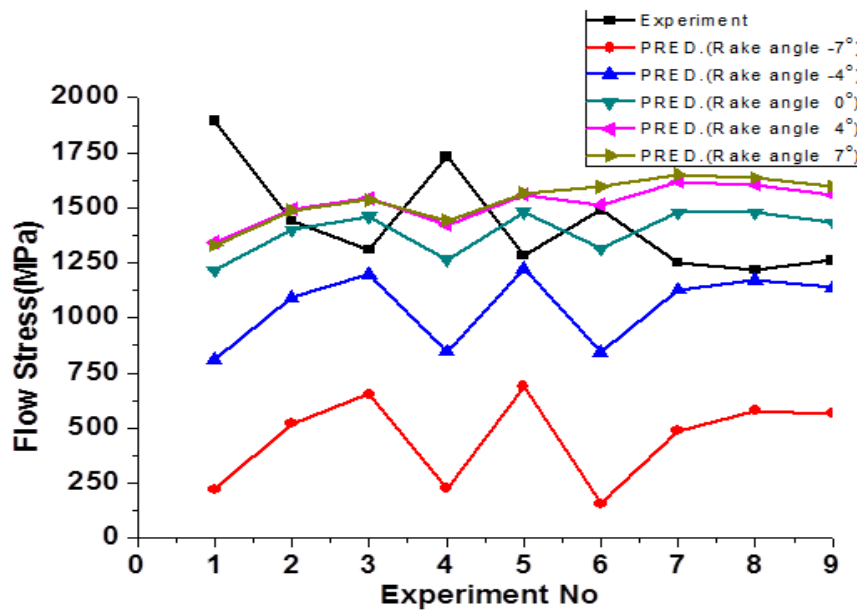
Figure 5.5: Comparison of predicted flow stresses to experimental data

Table 5.4: J-C material constants at five different rake angles

Rake angle α (º)	A(MPa)	B(MPa)	C	n	m
-7	1119	1092	0.05	0.122	0.773
-4	1119	1092	0.05	0.122	1.51
0	1036.4	1092	0.05	0.93	1.51
4	762.092	1092	0.05	0.93	1.51
7	741.139	1092	0.05	0.93	1.51

Table 5.5: Experimental data for Ti6Al4V alloy at -7° rake angle

V (m/min)	f_r (mm/rev)	F_c (N)	F_f (N)	t_c (mm)	Strain (ε)	Strain Rate ($\acute{\varepsilon}$)	T_{AB} (°C)	σ_{AB} (MPa)
42	0.051	497.11	225.45	0.066359	0.6729	42266	1485.3	3093.7
48	0.0725	554.03	254.77	0.102271	0.6873	32984	1260.1	2423.2
53	0.094	640.65	292	0.132237	0.6868	28117	1159.8	2169.2
55	0.051	479.57	228.68	0.069262	0.6799	54483	1481.2	2928.2
65	0.108	705.74	323.13	0.149232	0.6833	30205	1133.5	2074.9
83	0.051	458.56	241.91	0.103067	0.8026	73197	1535.2	2564.6
92	0.0725	526.53	274.51	0.14549	0.7995	57164	1290.4	2083.8
102	0.094	625.49	316.31	0.184628	0.7902	49122	1221.7	1158
110	0.108	707.78	349.37	0.210945	0.7879	46168	1230.5	1928.7

Table 5.6: Experimental data for Ti6Al4V alloy at -4° rake angle

V (m/min)	f_r (mm/rev)	F_c (N)	F_f (N)	t_c (mm)	Strain (ε)	Strain Rate ($\acute{\varepsilon}$)	T_{AB} (°C)	σ_{AB} (MPa)
42	0.051	405.09	180.2	0.081748	0.6847	38514	1210	2541
48	0.0725	454.56	204.7	0.118521	0.6905	30786	1037.1	1992.1
53	0.094	533.77	237.3	0.149646	0.6828	26421	965.25	1818.1
55	0.051	386.89	181.45	0.08079	0.6815	50610	1189.8	2381.3
65	0.108	593.59	264.12	0.164798	0.6716	28569	948.23	1765
83	0.051	364.46	190.42	0.106278	0.7822	71346	1198.5	2044.7
92	0.0725	424.83	217.79	0.148672	0.7749	55814	1023.5	1695.2
102	0.094	516.12	254.20	0.187484	0.7626	48010	992.37	1622.3
110	0.108	593.35	283.52	0.213146	0.7578	45174	1014.9	1644

Table 5.7: Experimental data for Ti6Al4V alloy at 0° rake angle

V (m/min)	f_r (mm/rev)	F_c (N)	F_f (N)	t_c (mm)	Strain (ε)	Strain Rate ($\acute{\varepsilon}$)	T_{AB} (°C)	σ_{AB} (MPa)
42	0.051	329.42	148.88	0.094705	0.6915	36002	957.3	2019.3
48	0.0725	368.94	167.03	0.132628	0.6859	29042	825.9	1595.2
53	0.094	438.28	193.4	0.165298	0.6718	24965	777.7	1485.2
55	0.051	310.34	147.50	0.088599	0.6676	47896	923.8	1891.6
65	0.108	491.08	214.45	0.177993	0.6509	27096	762.7	1467.1
83	0.051	286.02	150.80	0.102999	0.7259	69900	898.2	1631.1
92	0.0725	336.24	171.18	0.145355	0.7227	54581	779.7	1367.9
102	0.094	417.32	200.41	0.183731	0.7119	46915	776.2	1344
110	0.108	487.80	224.74	0.208521	0.7069	44149	808.9	1390

Table 5.8: Experimental data for Ti6Al4V alloy at 4° rake angle

V (m/min)	f_r (mm/rev)	F_c (N)	F_f (N)	t_c (mm)	Strain (ε)	Strain Rate ($\dot{\varepsilon}$)	T_{AB} (°C)	σ_{AB} (MPa)
42	0.051	307.49	150.73	0.099023	0.6704	34629	842.5	1829.9
48	0.0725	337.07	162.51	0.138094	0.6628	27943	719.96	1424.8
53	0.094	396.53	182.76	0.172309	0.648	23985	671.39	1323
55	0.051	287.53	146.72	0.087769	0.6258	46530	792.63	1708.4
65	0.108	442.31	197.96	0.182548	0.62	26072	657.33	1311
83	0.051	261.32	144.35	0.091081	0.6385	69625	737.92	1495.9
92	0.0725	301.40	157.75	0.133397	0.6494	53938	645.54	1240.8
102	0.094	372.27	179.78	0.171339	0.6459	46216	649.27	1221.9
110	0.108	435.99	199.14	0.195256	0.6429	43456	682.49	1272.8

Table 5.9: Experimental data for Ti6Al4V alloy at 7° rake angle

V (m/min)	f_r (mm/rev)	F_c (N)	F_f (N)	t_c (mm)	Strain (ε)	Strain Rate ($\dot{\varepsilon}$)	T_{AB} (°C)	σ_{AB} (MPa)
42	0.051	326.31	173.89	0.09659	0.6335	33993	832	1894
48	0.0725	348.43	180.89	0.13652	0.6312	27358	692	1439
53	0.094	400.49	196.51	0.17190	0.6202	23429	639	1310
55	0.051	305.70	167.91	0.08148	0.5758	46209	755	1732
65	0.108	441.01	207.37	0.18029	0.5889	25511	614	1283
83	0.051	278.07	161.29	0.07647	0.5592	70931	657	1490
92	0.0725	310.54	169.44	0.11876	0.5831	54034	592	1249
102	0.094	373.75	186.09	0.15637	0.587	46060	595	1217
110	0.108	432.41	201.71	0.17964	0.5877	43211	626	1262

5.7 Effect of strain, strain rate and temperature on flow stress

The deformation behavior of Ti6Al4V alloy under different thermo-mechanical loading is analyzed with five different J-C material constants obtained from the proposed methodology. The material flow stresses are calculated for five sets of material constants by varying temperature, strain and strain rate. Figure 5.6 shows the influence of temperature and strain at constant strain rate ($\dot{\varepsilon}=10^5$ s^{-1}) for five sets of J-C parameters. At lower temperature, strain hardening effect is more in case of JC parameters obtained at positive rake angle when compared to JC parameters obtained at negative rake angle. This strain hardening effect is minimized with increase in temperature. Moreover, the predicted flow stress is maximum for positive rake angle J-C sets when compared with negative rake angle J-C sets. Figure 5.7 shows the influence of strain rate and temperature on flow stress at constant strain for five

different sets of JC parameters. The strain rate effect is very small on predicted flow stress, but there is a large variation in flow stresses when rake angle changes from negative to positive.

5.8 Comparison between proposed MA and SHPB technique

The material constants identified by this MA are compared with the one obtained by SHPB techniques for validation purpose. In this regard, five different J-C constants obtained from SHPB technique are taken from literature for validation of JC constant determined from MA are shown in table 5.10. The predicted flow stresses for JC1[135], JC2 [149], JC3[150], JC4[151], JC5 [152] and JC-MA are calculated by using JC flow stress equation (5.1) and are listed in Table 5.11.

Table 5.10: J-C parameters of Ti6Al4V alloy obtained by various methods

Method	Set of JC	A(MPa)	B(MPa)	C	n	m
SHPB	JC1	782.7	498.4	0.028	0.28	1
SHPB	JC2	862.5	331.2	0.012	0.34	0.8
SHPB	JC3	896	656	0.0128	0.5	0.8
SHPB	JC4	968	380	0.0197	0.421	0.577
SHPB	JC5	997.9	653.1	0.0198	0.45	0.7
MA	JC-MA	741.139	1092	0.05	0.93	1.51

Table 5.11: Flow stress data of Ti6Al4V alloy at different cutting conditions

| V (m/min)	f (mm/rev)	Measured flow stress	Predicted Flow Stresses (MPa)					
			JC1	JC2	JC3	JC4	JC5	JC-MA
42	0.051	1894.0	794.1	552.66	688.92	513.08	714.59	1444.4
48	0.0725	1439.0	926.1	655.71	816.97	618.69	853.10	1623.6
53	0.094	1309.6	972.1	693.82	862.86	658.62	903.60	1668.61
55	0.051	1732.4	866.9	607.05	749.80	568.86	784.20	1503.7
65	0.108	1282.7	992.2	710.12	878.69	676.14	923.29	1663.9
83	0.051	1489.8	967.8	682.15	840.42	648.74	886.55	1630.7
92	0.0725	1248.8	1029.3	732.75	906.25	702.87	957.54	1724.7
102	0.094	1216.8	1023.4	729.43	902.64	698.81	952.59	1717.1
110	0.108	1262.0	992.36	705.21	872.73	672.34	918.89	1677.8
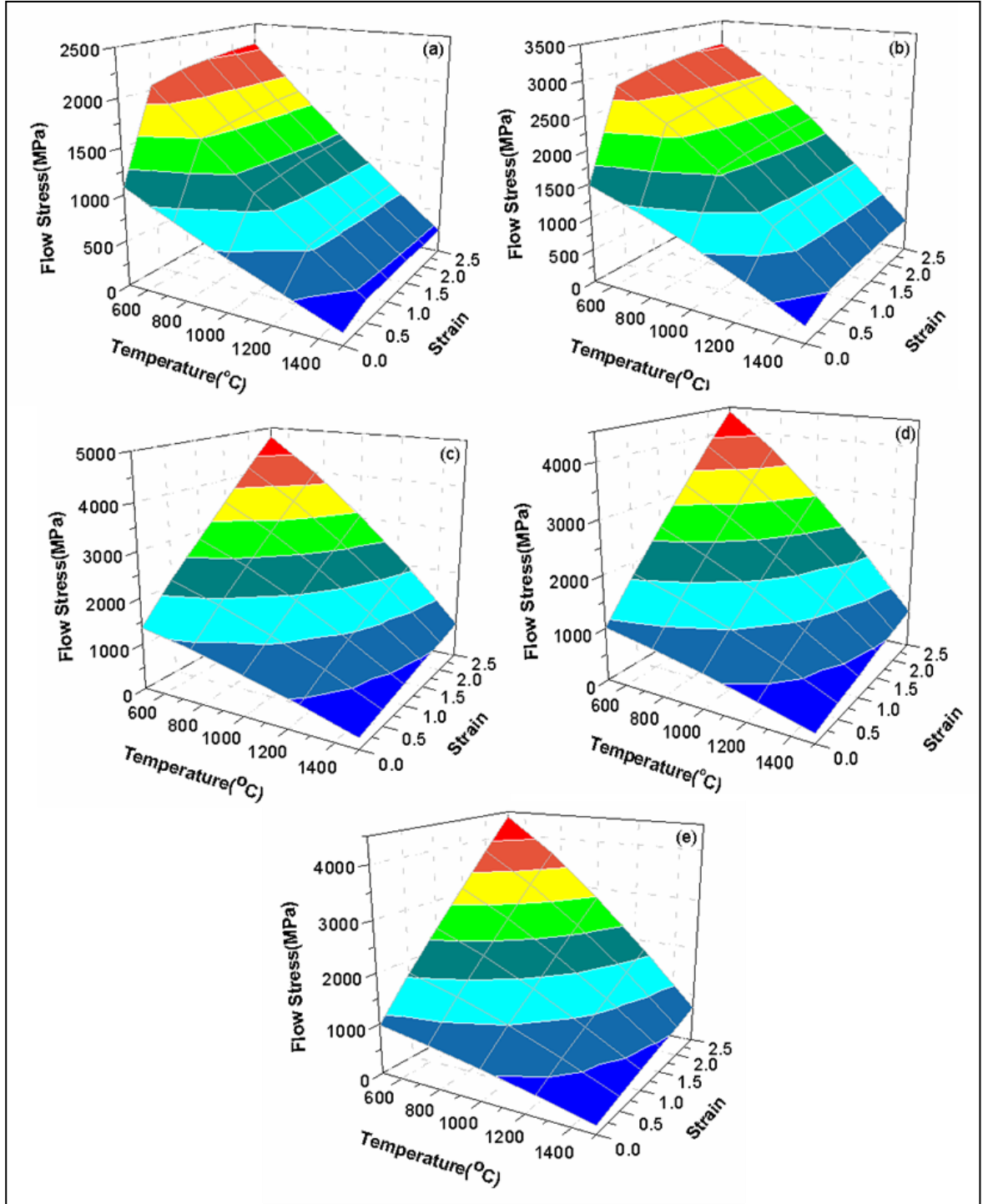
Figure 5.6: Effect of strain and temperature on flow stress ($\dot{\varepsilon} = 10^5$ s^{-1}) at (a).JC(-7) (b). JC (-4) (c). JC (0) (d).JC (4) (e).JC (7)
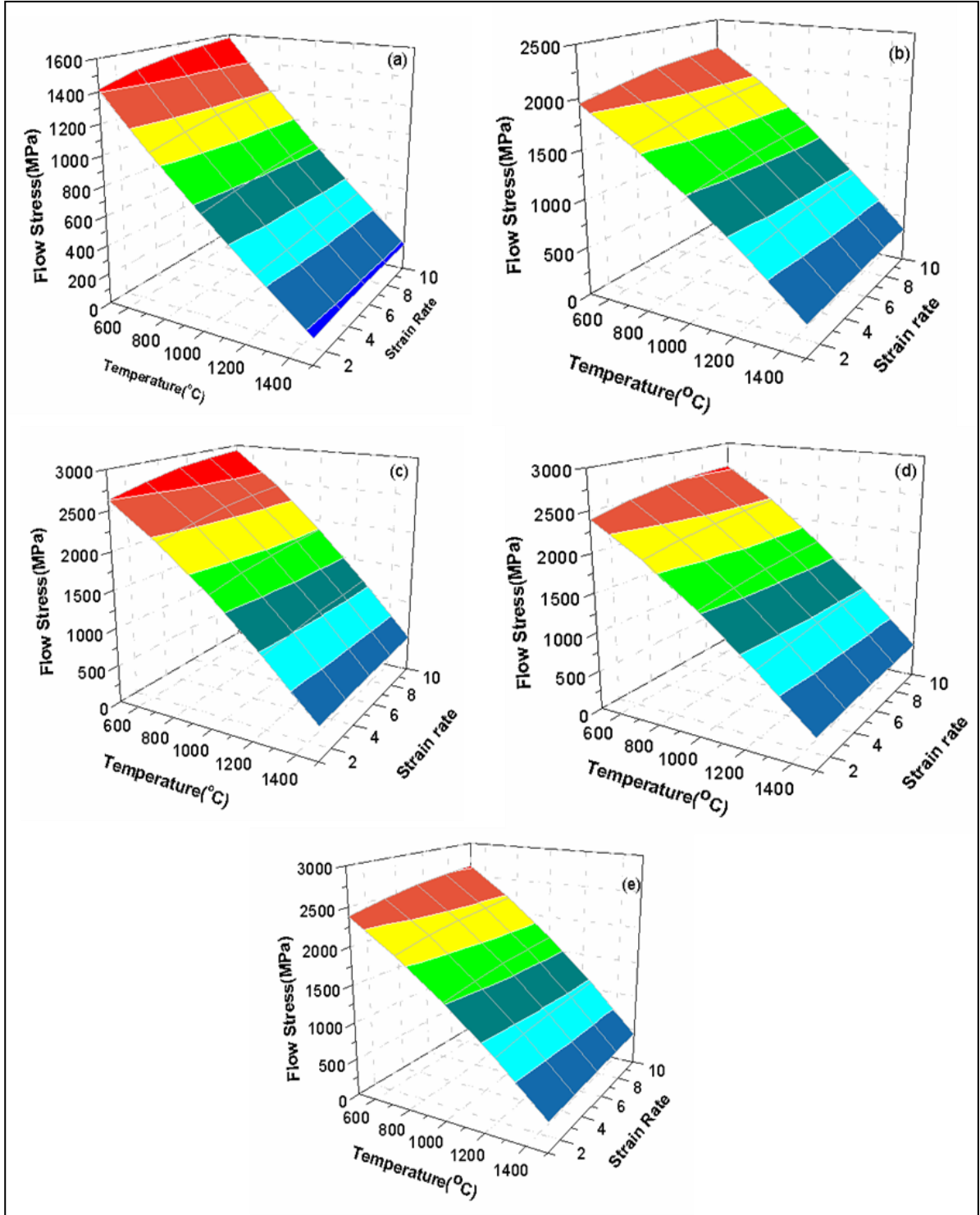
Figure 5.7: Effect of strain rate and temperature on flow stress (ε = 2) at (a).JC (-7) (b). JC (-4) (c). JC (0) (d).JC (4) (e).JC (7)

Table 5.12: Average error between predicted and measured flow stress at different JC parameters

Set of JC	Average Error (%)
JC1	31.3
JC2	51.3
JC3	39.7
JC4	53.7
JC5	36.6
JC-MA	25.4

The efficiency of this approach to identify the material constants for Ti6Al4V alloy is tested by comparison of cutting test data. The average errors of predicted flow stresses when compared to flow stresses obtained with cutting tests data are summarized in table 5.12. Since there are no specific machining conditions available for Ti6Al4V alloy, material constants of JC-MA are verified by the cutting conditions available in Table 5.11. The error reported by JC-MA is lower compared to the remaining material sets. Since the machining conditions used to identify JC-MA are the same as measured flow stress, the relative error associated with JC-MA is small. The flow stresses estimated by the JC-MA material constants are high compared to measured flow stresses from experimental data. This variance could be attributed to errors associated with measurement of F_c, F_f and t_c. Moreover, the predicted flow stress from JC model is the combined effect of strain rate and temperature. Actually, the effect of temperature on strain rate of TI6Al4V alloy is negligible. The assumptions made in Oxley's machining theory also affect the accuracy of model since physical quantities are calculated from the Oxley's model. In view of all these limitations, the error associated with this method is 25.6% which is better than all other JC models. The advantage of this approach is that material constants can be obtained with a large number of cutting conditions at high level. However, material parameters obtained with low level of machining conditions predict flow stresses accurately due to the stability of formation of chip during machining process. Hence, the obtained results from this methodology would be acceptable to predict flow stresses accurately.

5.9 Validation of proposed methodology

The efficiency of proposed machining approach is tested by comparing predicted and measured equivalent flow stresses obtained under similar machining conditions. FEM is used

to predict flow stress at different JC constants available in literature and JC-MA. The cutting conditions used for FE simulations are the cutting speed of 120 m/min, the feed rate of 0.124 mm/rev and the rake angle of 7°.
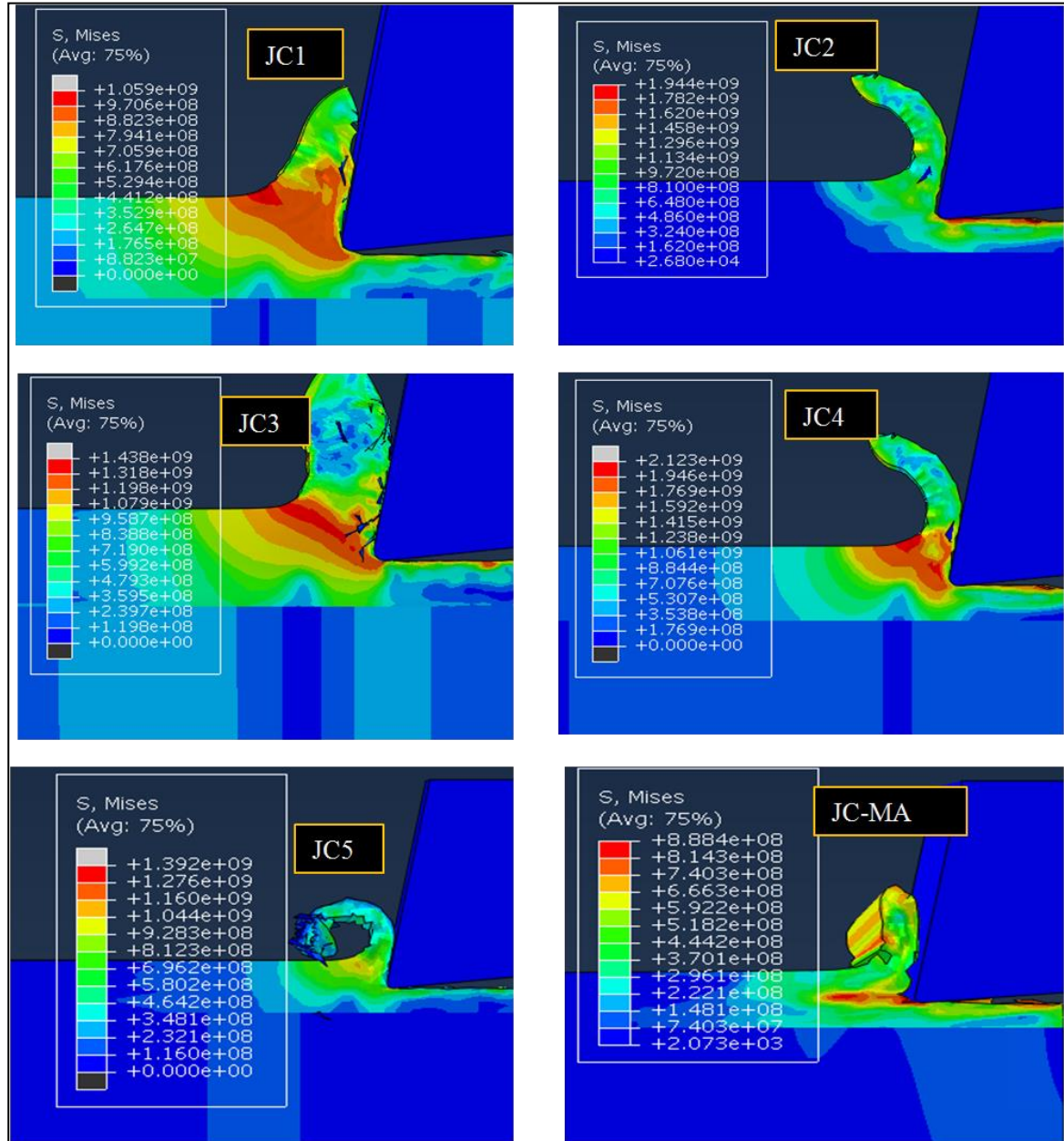
Figure 5.8: Predicted flow stresses for JC1, JC2, JC3, JC4, JC5 and JC-MA

The predicted equivalent stresses for different JC sets are shown in Figure 5.8. Interestingly, the JC constants identified by the proposed approach predicted well compared to JC sets considered for validation. The predicted flow stresses for JC1.JC2, JC3, JC4, JC5 and JC-MA are within 23%, 58.1%, 43.3%, 61.6%, 41.4 % and 8.22% deviation from

experimentally measured flow stresses. Hence, J-C constants identified from this new method can be used for further simulations.

5.10 Summary

In the present study, J-C material constants are determined at near orthogonal machining conditions based on the extension of Oxley's predictive machining theory and PSO technique. The orthogonal cutting conditions and material properties are used as inputs and J-C constants are determined when difference between measured flow stress and predicted flow stress are low. The rake angle effect on J-C constants is also investigated by considering five different rake angles to estimate deformation behavior of Ti6Al4V alloy under thermo-mechanical loading. The J-C constants identified from this machining approach are validated with J-C constants Experimental and simulated values.

Chapter 6

Effect of Tool-Work Contact Ratio in UVAT of Ti6Al4V Alloy

6.1 Introduction

The performance of machining process depends on time of contact of cutting tool with workpiece. High cutting temperatures developed during machining of Ti6Al4V alloy diminishes the tool life by rapid increase in rate of tool wear. The high cutting temperatures increases the chemical reactivity of workpiece with tool material and forms the localized temperature zones at the vicinity of cutting tool edge. The reduced cutting force and temperature improves the tool life in UVAT process due to intermittent cutting process. Hence it is important to evaluate the effect of vibrating and cutting parameters on tool-work contact ratio (TWCR) in UVAT. In this chapter machining performance is measured in terms of average cutting force, cutting temperature and average surface roughness. The performance of UVAT process is analyzed and compared with conventional turning (CT) process at various conditions. Moreover, flank wear of the cutting tool have been evaluated at various cutting conditions for both CT and UVAT processes.

6.2 Study of Ultrasonic Vibration Assisted Turning

In one-dimensional UVAT, low amplitude and high frequency vibrations are superimposed on the movement of cutting tool in tangential direction. The variation of cutting force with respect to cutting tool in UVAT process is shown in figure 6.1. The cutting tool gets separated from the workpiece in regular intervals of time during its oscillating motion. The cutting tool starts its vibration from origin and cuts the workpiece during time period t_{i-j},

$t_{i'-j'}$, in its successive cycles. In UVAT process, cutting tool engages the workpiece in a short period of time in each oscillating cycle. The duty cycle of the intermittent cutting operation in UVAT process is defined in terms of TWCR which can be used to evaluate the effectiveness of UVAT. The relation between TWCR with machining parameters is described in the following sections.

The displacement of tool during vibration is given by

$$x = a \sin \omega t = a \sin 2\pi f t \qquad (6.1)$$

$$\text{where} \quad \omega = 2\pi f,$$

$$f \text{ is frequency and}$$

$$a \text{ is amplitude}$$

The speed of cutting tool during vibrating motion is $v_t = \dot{x} = a\omega \cos \omega t$ (6.2)

$$v_{t, \ min} = 0 \qquad (6.3)$$

$$v_{t, \ max} = 2\pi f a \qquad (6.4)$$

From figure 6.1, it is observed that the tool speed during its vibration varies from zero (at peak or valley) to a maximum value at midpoint of either forward or backward motion except at the origin. In order to get advantage of UVAT process, the cutting tool has to separate from workpiece in each cycle of vibration. Hence, the tool tip velocity must be always greater than the cutting speed of workpiece ($v_{t, \ max} > $ V). As the vibrations are superimposed on movement of cutting tool, critical speed of cutting tool for UVAT process can be defined as

$$v_{t, \ crit} = 2\pi f a \qquad (6.5)$$

The effective parameters which govern UVAT process are known from the following three fundamental equations

$$V + a\omega \cos \omega t_j = 0 \qquad \text{(at t=t}_j\text{)} \qquad (6.6)$$

$$a \sin \omega (T + t_i) - a \sin \omega t_j = V(T + t_i - t_j) \qquad (6.7)$$

$$T_r = t_c / T \qquad (6.8)$$

$$\text{where } T_r \text{ is the tool work contact ratio (TWCR)}$$

$$T = \text{Time period}$$

95

t_c= time of contact

By solving equations 6.6, 6.7 and 6. 8, the final governing equation is obtained as

$$V(1 - T_r) = 2af \sin \pi T_r \cos[\cos^{-1}(-V/(2\pi af)) - \pi T_r] \qquad (6.9)$$

From equation (6.9), it is understood that TWCR is dependent on three important machining parameters frequency, amplitude and cutting speed. Hence, it is important to evaluate the importance of TWCR in UVAT process to improve its performance.
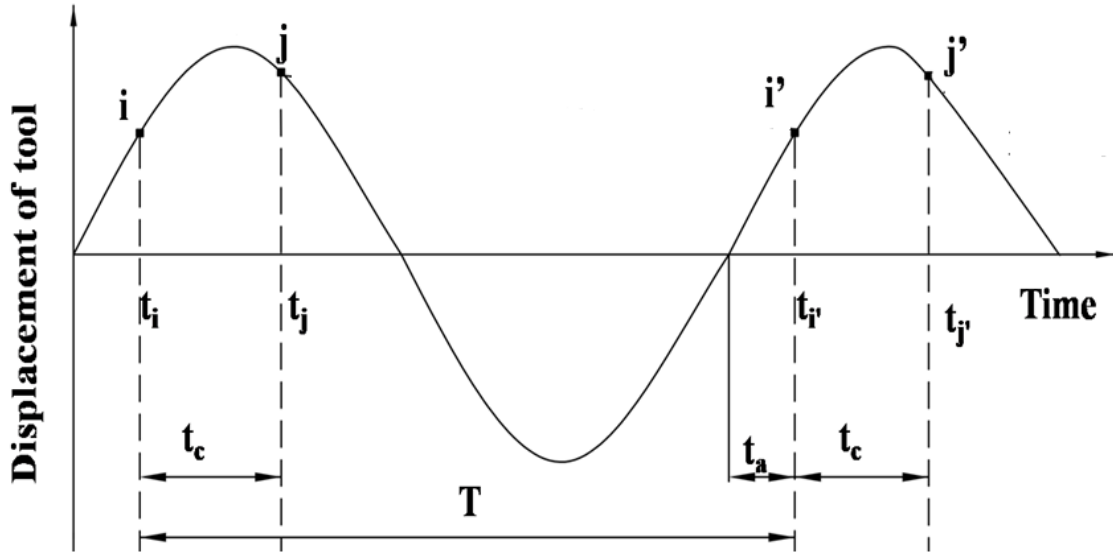
Figure 6.1: Displacement of the tool in UVAT system

6.2.1 Importance of TWCR in UVAT process

TWCR describes the time of contact of cutting tool with workpiece in one cycle of vibration. The performance of UVAT process can be evaluated in terms of TWCR, as less contact period between cutting tool and workpiece of UVAT is influencing factor. TWCR lies between 0 to 1, where 1 indicates complete contact, i.e. CT and zero indicates complete separation, i.e. no cutting process between cutting tool and workpiece. There is a limitation for suitable selection of machining parameters for UVAT process. The performance of UVAT process is very low at low amplitude and frequency[153]. Hence, there is a need to select suitable range of machining parameters for UVAT process where maximum advantage is obtained. TWCR is considered as a performance indicator for selection of optimum range of machining parameters for UVAT process.

6.2.2 Effect of frequency on TWCR

The effect of frequency in UVAT process is theoretically verified by evaluating TWCR using equation (9) at two frequencies f_1=36 KHz and f_2= 20 KHz at 25 µm amplitude and 30 m/min cutting speed. The variation of TWCR during these two frequencies is shown in figure 6.2(A). The cutting period of frequency f_2 is greater than frequency f_1.The decrease in TWCR is observed with increase in frequency in UVAT process. The decrease in TWCR is very low after reaching certain frequency. The benefit of UVAT process is very less over CT process in the range of 0-10 KHz frequency due to larger TWCR. Hence, higher frequency enhances the performance of UVAT process by reducing cutting period.

6.2.3 Effect of Amplitude on TWCR

The effect of amplitude in UVAT process is verified by considering two amplitudes a_1=15 µm and a_2=25 µm at 20 KHz frequency and 30 m/min cutting speed. The variation of TWCR with amplitude is shown in figure 6.2 (B).The time period T at these two amplitudes is same due to same frequency. The cutting tool contact period with workpiece for an amplitude a_1 is higher than a_2. Hence, cutting force required for lower amplitude is more compared to higher amplitude due to more time of contact between the cutting tool and workpiece for each cycle of vibration. Therefore the performance of UVAT process can improve with higher amplitudes. However, it is observed that the reduction in TWCR is not much significant after reaching certain amplitude as the tool moves in sinusoidal path for given frequency and cutting speed.

6.2.4 Effect of velocity on TWCR

The effect of cutting speed in UVAT process is evaluated by considering two cutting speeds of V_1 (30 m/min) and V_2 (100 m/min) at 20 KHz frequency and 25 µm amplitude. The variation of TWCR with amplitude is shown in figure 6.2(C).The increase in contact between the cutting tool and workpiece with increase in cutting speed leads to increase in cutting force. From figure 6.2(C), it is observed that sudden raise in TWCR is noticed at 0 to 20 m/min and 175 to 200 m/min for the given condition. The raise in TWCR is gradual between 20 to 175 m/min. Hence the performance of UVAT process can improve between 20 to 175 m/min range of cutting speed.
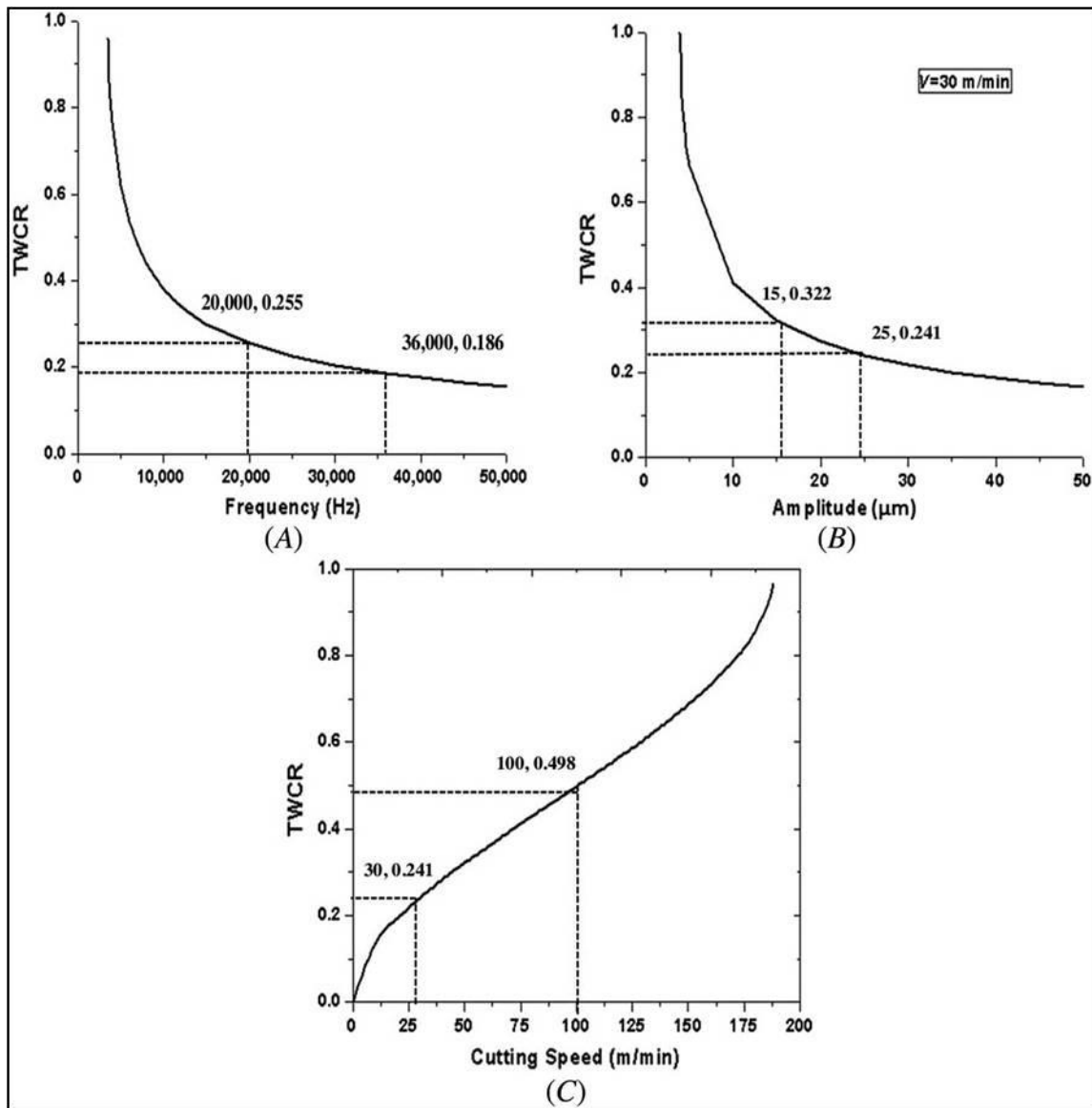
Figure 6.2: Variation of TWCR with respect to (*A*) Frequency, (*B*) Amplitude, and (*C*) cutting speed

6.3. Experimentation

Full factorial experiments are conducted on Ti6Al4V alloy workpiece at different machining conditions shown in table 6.1 for both UVAT and CT process. Vibration is imparted to the cutting tool in tangential direction in UVAT process. The average cutting force, maximum cutting temperature, and average surface roughness are considered to evaluate the performance of both UVAT and CT.

Table 6.1: Experimental details for UVAT and CT

Workpiece details	Ti6Al4V alloy	
Dimension	Φ 40 mm x 300 mm length	
Properties	Young's modulus	114 GPa
	Density	4420 kg/m^3
	Thermal conductivity	7.264 W/m-^{0}C
	Specific heat	526 kJ/kg-^{o}C
Cutting tools	Tool holder	PCLNR2525M12
	Cutting insert	CNMG 120408 THM
Operating conditions	Cutting speed (V)	10,30,50 m/min
	Feed rate (f)	0.055, 0.103, 0.161 mm/rev
	Depth of cut (DOC)	0.1, 0.3, 0.5 mm
	Percentage intensity of ultrasonic power (P_u)	80, 90, 100 %
	Frequency	20 KHz

6.4. Effect of TWCR

The time available for separation of workpiece and tool is one of the important factors which significantly influence the performance of UVAT process. The optimum range of machining parameters for UVAT of Ti6Al4V alloy is selected based on TWCR. For a given frequency and amplitude, the cutting speeds are selected based on critical condition used for UVAT process to get separation between tool and workpiece. TWCR is evaluated from equation (6.9) for the cutting conditions shown in table 6.2. As the percentage intensity of ultrasonic power is directly proportional to amplitude, TWCR is evaluated at 80%, 90% and 100 % intensity of ultrasonic power at 20 KHz frequency and three values of 10, 30, 50 m/min cutting speed. The performance of UVAT process in terms of cutting force, cutting temperature and surface roughness is evaluated with respect to TWCR by conducting experiments at same optimum range of cutting conditions. Later the effectiveness of UVAT process is compared to CT at various cutting conditions.

Table 6.2: TWCR at different machining conditions

Frequency (f), KHz	Cutting speed (V), m/min	Percentage intensity of ultrasonic power (P_u)	TWCR
20	10	80%	0.151
		90%	0.142
		100%	0.136
	20	80%	0.273
		90%	0.251
		100%	0.241
	50	80%	0.365
		90%	0.343
		100%	0.322

6.4.1 Cutting forces

The energy required to shear the material in machining process depends on the time of contact between the cutting tool and workpiece. The continuous contact in CT process requires more F_c whereas intermittent cutting action in UVAT process requires less cutting force. The variation of cutting force with TWCR at different P_u, V, f_r and DOC is depicted in figure 6.3. The cutting force is decreased with an increase in P_u at same machining conditions due to decrease in contact period of the cutting tool with workpiece. The reduction in cutting force with increase in amplitude is not uniform at all cutting velocities, because the variation in TWCR with cutting velocity is nonlinear as shown in figure 6.2(C).

The variation of cutting force with P_u mainly depends on fracture dynamics involved in UVAT process[154]. The ultrasonic vibrations which are imparted to cutting tool leads to cut the material with high impact energy in each cycle of vibration. The stress wave velocity produced due to impact energy has greater influence on material removal in UVAT process. This impact energy is enough to reach the ultimate strength of chip before the tool penetrate into the workpiece. Hence, the force required to cut the material in UVAT process is low compared to CT process. The total impact energy required to shear the material from workpiece depends on the amplitude of vibration, and cutting force reduced with increase in P_u due to increased impact energy. Reduction in TWCR leads to less cutting force, however aerodynamic lubrication (which results due to separation of the cutting tool from workpiece)

increases the cutting force by reducing thermal softening of workpiece. Hence, the variation of cutting force with P_u in UVAT process depends on combined effect of impact energy, TWCR and aerodynamic lubrication.

In Ti6Al4V alloy machining, thermal softening of material plays an important role due to its low thermal conductivity. The thermal softening of material reduces its yield strength which results in easy deformation of material with low cutting force[155]. The rate of thermal softening depends on generation of heat due to machining conditions and the time available for dissipation of heat from cutting zone. In machining Ti6Al4V alloy, higher cutting speeds lead to the formation of adiabatic zone due to less time span available for dissipation of heat from primary shear zone, which results in lower F_c because of thermal softening.

From figure 6.4, it is observed that the cutting force is increased when cutting speed increased from 10 to 30 m/min due to increase in TWCR and low thermal softening at feed rate of 0.055 mm/rev for all depth of cuts. However, cutting force is decreased when speed increased from 30 to 50 m/min due to dominance of thermal softening over TWCR for same conditions. The cutting force is decreased and then remains same with speed increased from 10 to 50 m/min at feed rate of 0.103 mm/rev due to dominance of thermal softening over TWCR. Similarly, the cutting force is decreased and then increased at feed rate of 0.161 mm/rev for increase in cutting speed for all depth of cuts. Therefore, the variation of cutting force in UVAT process depends on TWCR and thermal loading.

The reduction in cutting force is observed with increase in P_u in UVAT compared to CT process. The reduction in cutting force is more at lower cutting conditions than higher cutting conditions. This indicates that the effect of TWCR is gradually reduced with increase in cutting conditions. Moreover, the increased thermal softening at higher cutting conditions reduces the difference in cutting force between UVAT and CT process.

Figure 6.3: Average cutting force Vs TWCR w.r.to feed, cutting speed and percentage intensity of ultrasonic power at different DOC
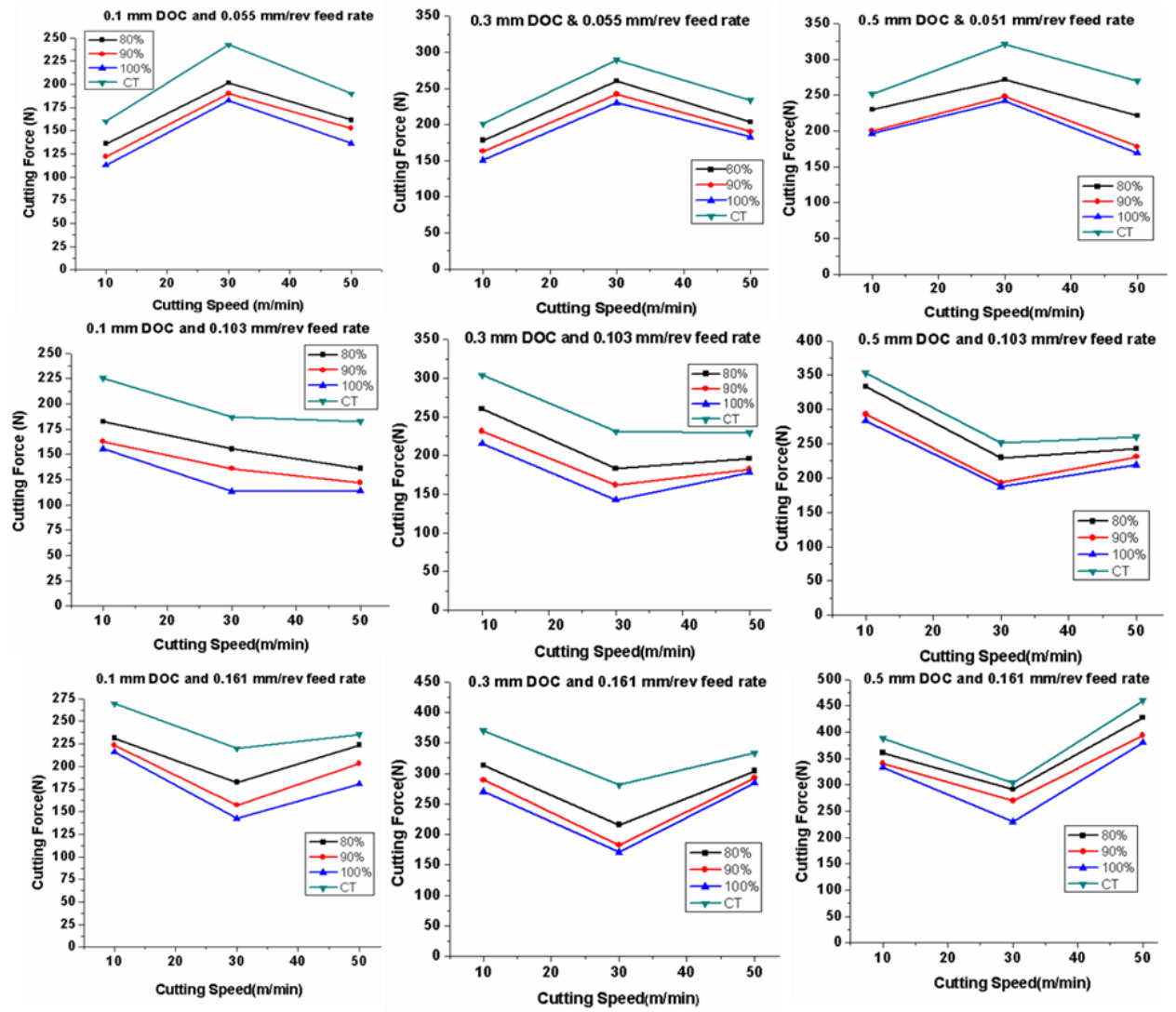
Figure 6.4: Variation of cutting force at different machining conditions

6.4.2. Cutting temperature

The cutting temperature in UVAT process is decreased with increase in P_u due to low TWCR for each cycle of vibration as shown in figure 6.5. Moreover, the increase in P_u increases the level of separation of cutting tool with workpiece which allows some amount of heat to be carried away by air during machining process. TWCR and the heat dissipation by air are responsible for reduction of temperature in UVAT compared to CT process. The amount of heat dissipation by air is less, as the separation between tool and workpiece is in microns. Hence, TWCR plays an important role in reduction of temperature in UVAT process. Another reason for reduction in temperature is the oscillating motion of cutting tool in UVAT process reverse the direction of chip along the rake face of the cutting tool which results in low coefficient of friction.

103

The cutting temperature is increased with increase in cutting speed in machining of Ti6Al4V alloy for both CT and UVAT process. The cutting temperature in UVAT process increased with increase in cutting speed due to increase in TWCR. The amount of heat accumulated in the form of localized temperature zone in machining of Ti6Al4V alloy is increased with increase in cutting speed. This localized temperature zones further softens the material by movement of grain boundaries which results in raise of temperature. The increase in temperature is not uniform at all the cutting speeds. From figure 6.6, it is observed that the temperature increased is more when cutting speed is increased from 10 to 30 m/min compared to 30 to 50 m/min range. From this it is understood that, the rapid increase in TWCR at lower cutting speeds increases cutting temperature significantly in 10 to 30 m/min range of cutting speed. The gradual increase in TWCR reduces the increase in cutting temperature in 30 to 50 m/min range of cutting speed. The cutting temperature is increased with increase in feed rate and depth of cut because of resistance to the movement of cutting tool during cutting process. The rate of increase in cutting temperature is more at higher feed rate and depth of cut.

The decrease in cutting temperature is observed in UVAT process compared to CT process. The reduction in cutting temperature is increased with increase in P_u. The less time of contact between cutting tool and workpiece at higher P_u reduces the cutting temperature. The reduction in cutting temperature is more at lower cutting conditions compared to higher cutting conditions.
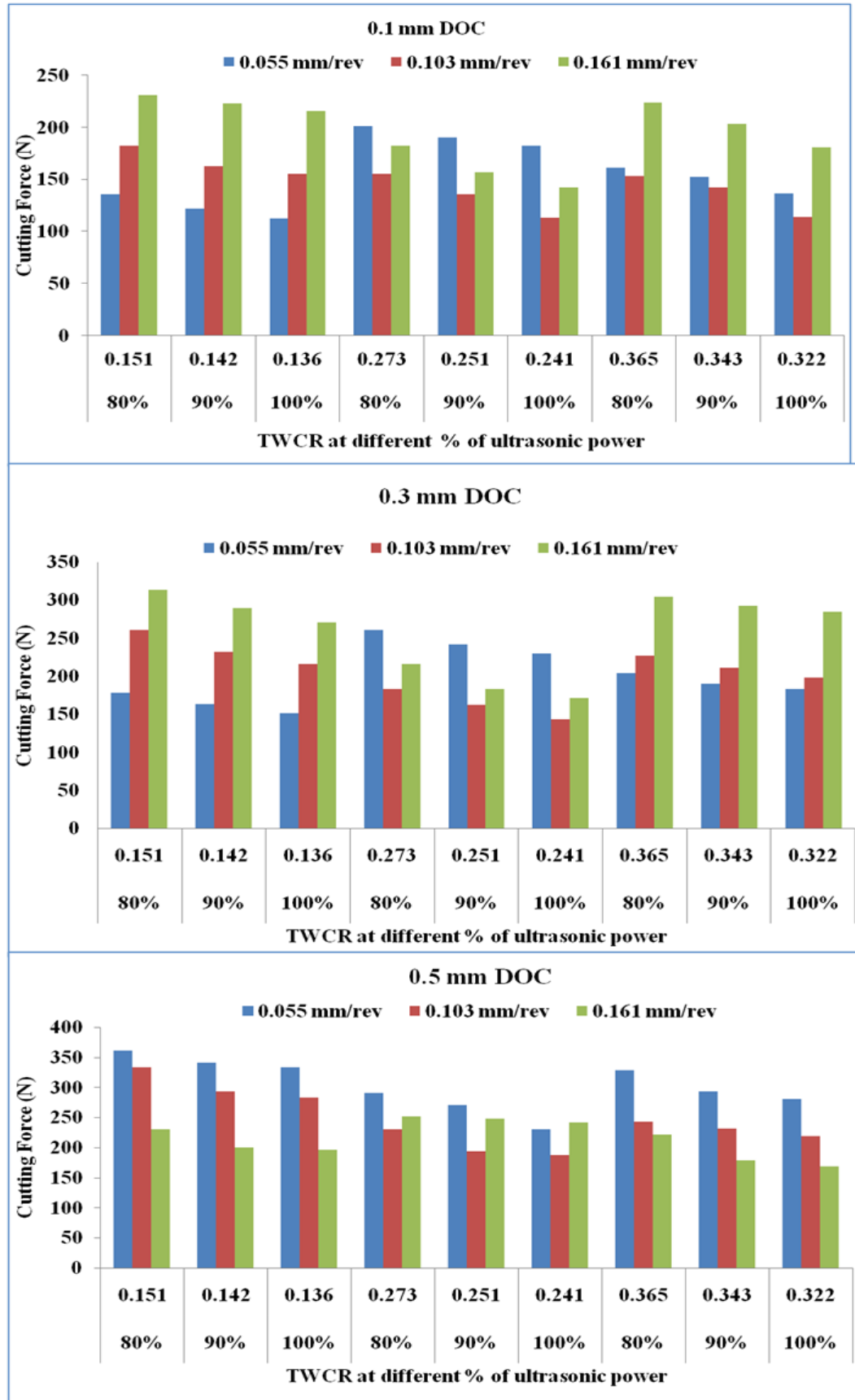
Figure 6.5: Cutting temperature Vs TWCR w.r.to feed, cutting speed and percentage intensity of ultrasonic power at different DOC

105
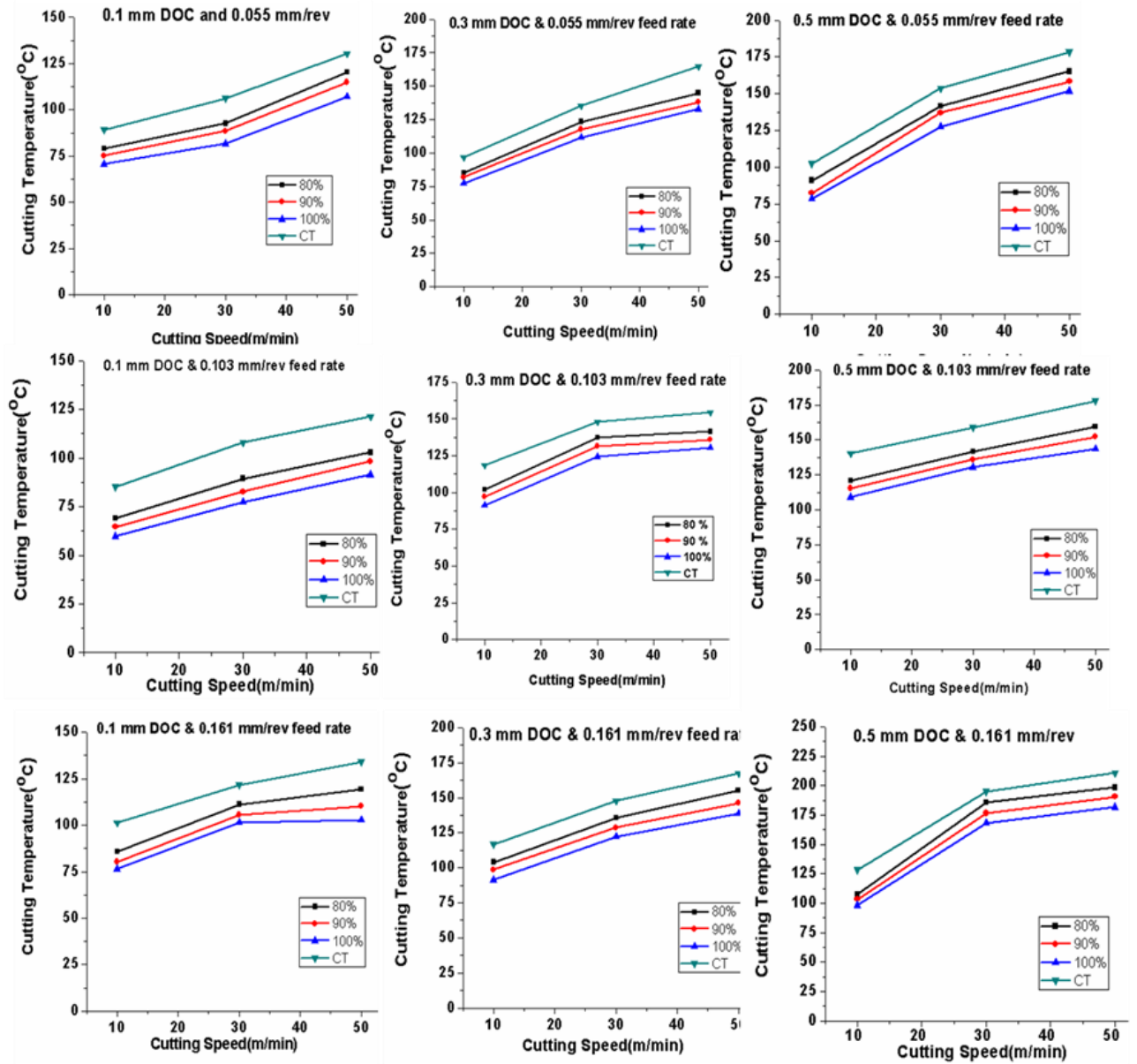
Figure 6.6: Variation of cutting temperature at different machining conditions

6.4.3 Surface roughness

The quality of machined surface depends on the thermo-mechanical behavior of workpiece. From figure 6.7, it is found that surface roughness is decreased with decrease in TWCR for all cutting conditions. The increase in P_u increases the impact energy of cutting tool which results in improved surface finish by having more ironing effect on machined surface. Thermal softening of workpiece due to heat energy also reduces the asperities on machined surface in UVAT process. The decrease in cutting force and cutting temperature due to low TWCR improves the surface quality of machined component in UVAT process.

From figure 6.8, it is found that the surface roughness is reduced in UVAT compared to CT for all machining conditions. The average surface roughness of machined surface is decreased with increase in cutting speed for both CT and UVAT of Ti6Al4V alloy. The ironing effect raised from dynamic action between cutting tool and workpiece improved surface finish in UVAT process. The decrease in surface roughness is high in UVAT compared to CT due to combined effect of thermal softening and mechanical loading. The increase in temperature of CT alone may not be sufficient to obtain better surface finish on machined surface. Even though TWCR is increased with increase in cutting speed, the increase in heat with increase in cutting speed is utilized to get more ironing effect along with impact energy of cutting tool in UVAT process. Hence, it is observed that thermal loading has more influence than mechanical loading at higher cutting speeds. The surface roughness is increased with increase in feed rate and depth of cut for both UVAT and CT process. The distortion of chips produced during UVAT process is less compared to CT process which leads to improve the surface finish. However, the degree of chip distortion is increased with increase in feed rate and depth of cut. Hence, the surface roughness is increased with increase in feed rate and depth of cut.

The large reduction in surface roughness is observed in UVAT process compared to CT process. The combined effect of impact energy and thermal softening is responsible for reduction in surface roughness in UVAT process. The impact of cutting tool on workpiece is increased with increase in P_u in UVAT process which causes reduction in surface roughness.
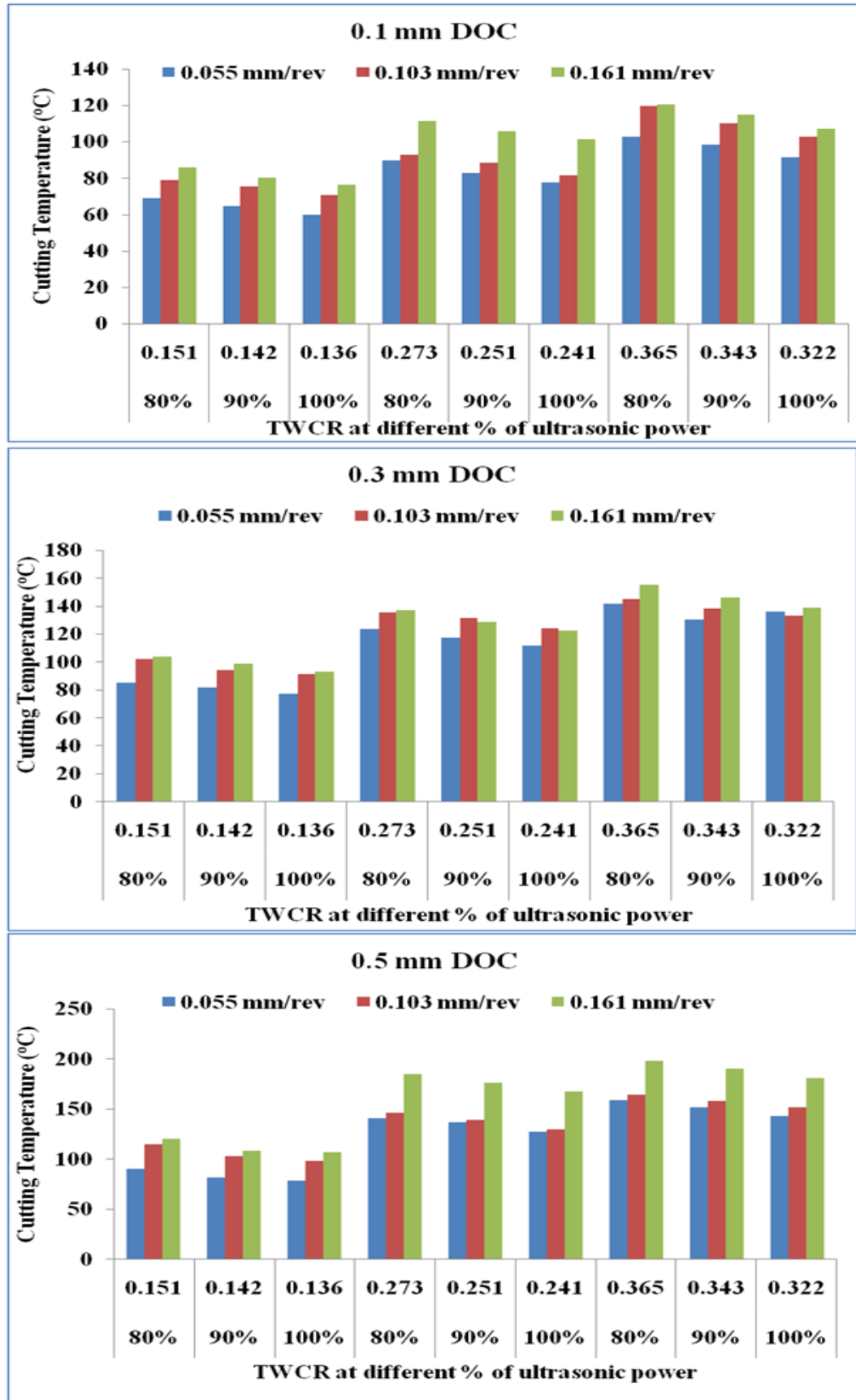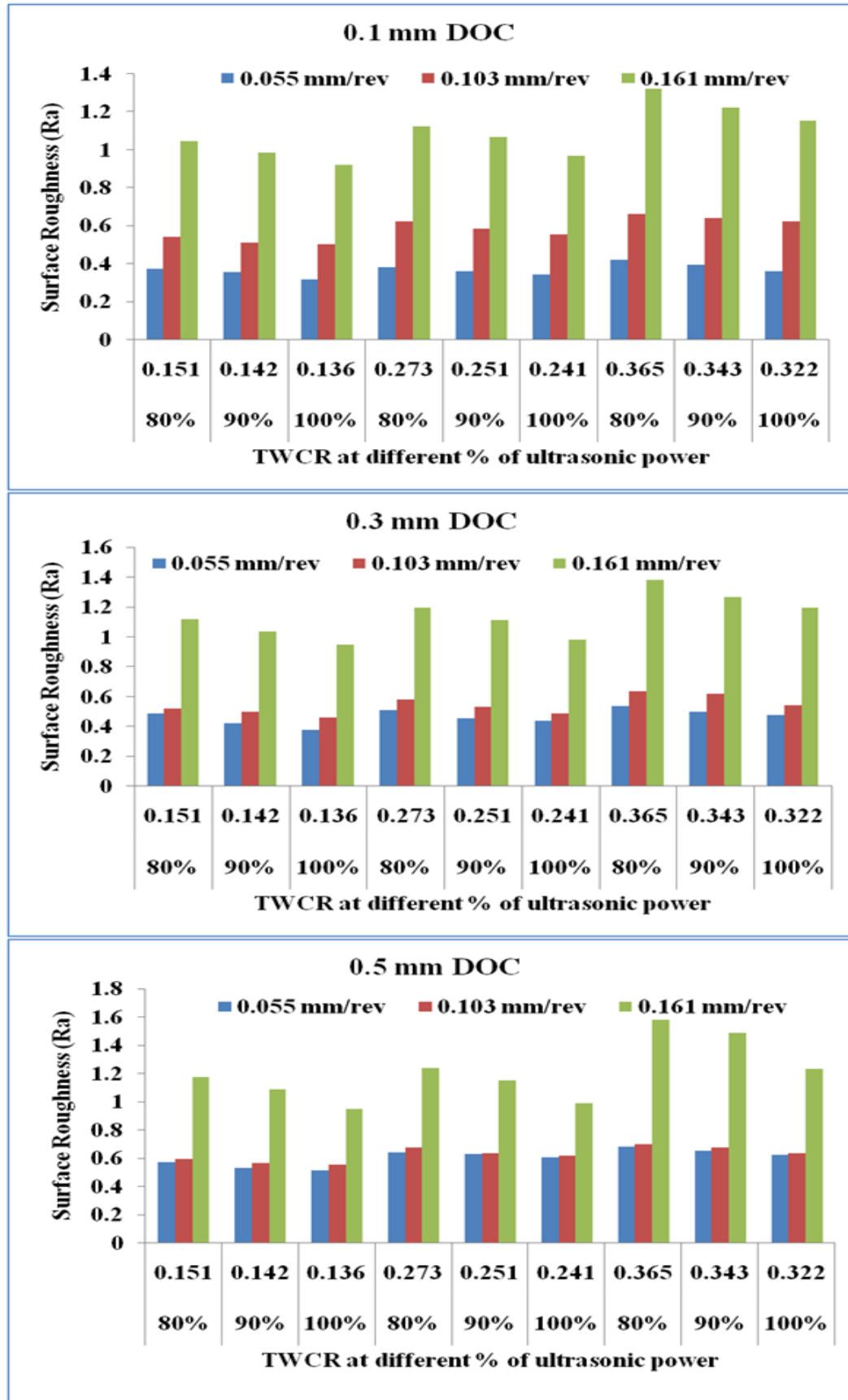
Figure 6.7: Surface Roughness Vs TWCR w.r.to feed, cutting speed and percentage intensity of ultrasonic power at different DOC
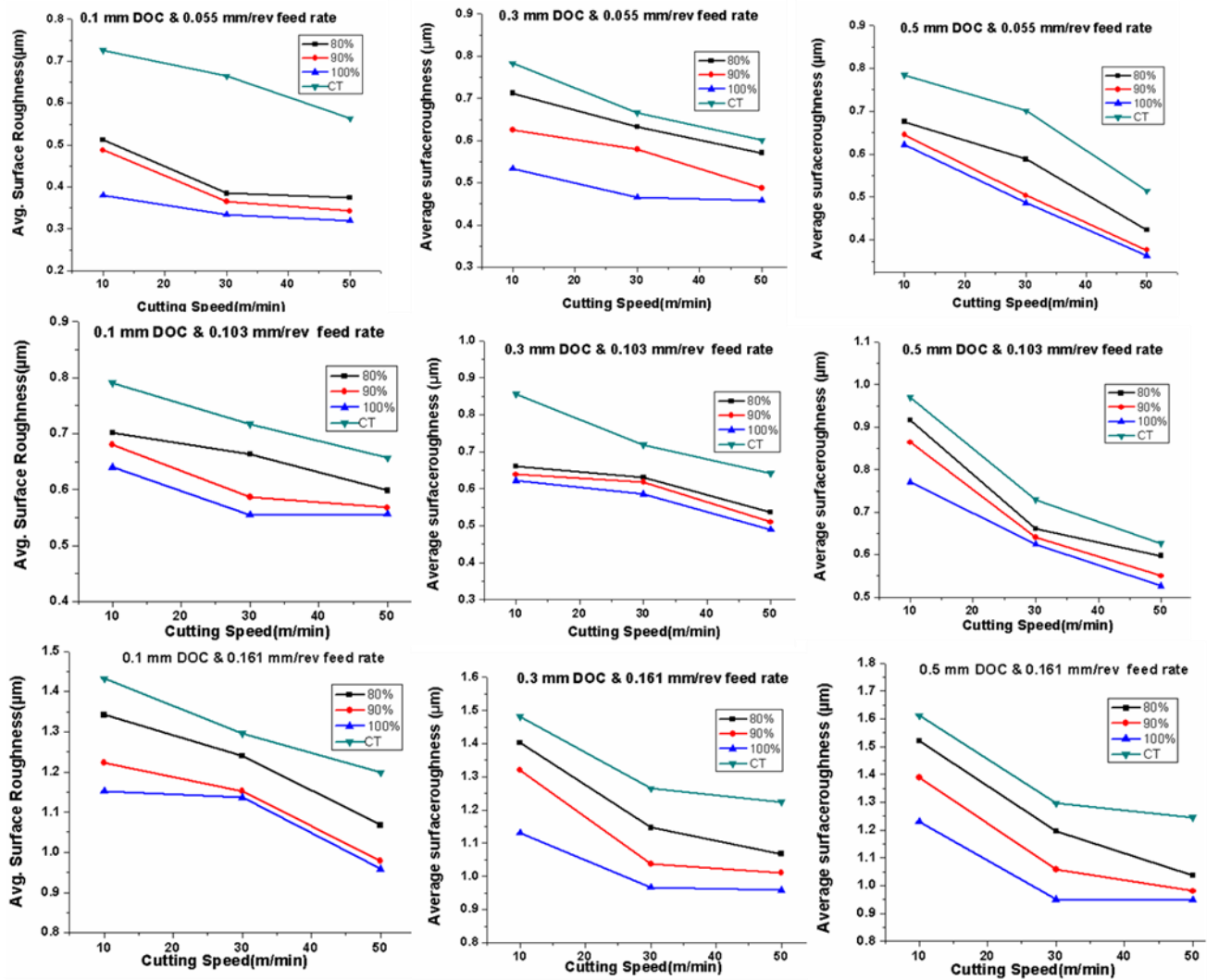
Figure 6.8: Variation of surface roughness at different machining conditions

6.5 Flank wear of the tool in UVAT process

In order to evaluate the growth of flank wear, experiments are performed on Ti-alloy at 90,120 and 150 m/min of cutting speeds, 0.2 mm/rev of feed rate (f_r) and 1 mm of depth of cut (DOC) for both CT and UVAT. Even though, the advantage of UVAT is maximum at low cutting and high vibrating conditions, the higher cutting speeds are selected within the critical speed limit of ultrasonic system ($v_{critical} = 2\pi f a > V$) to study the tool wear mechanism. The ultrasonic frequency and P_u used for UVAT are 20 KHz and 100 % respectively. As the tool vibrates in tangential direction, the rates of flank wear needs to evaluate in UVAT method. Scanning electron microscope (SEM) is used to measure the flank wear of the tool.

The growth of flank wear of the tool is analyzed by considering two important wear parameters i.e. V_B and V_M at 90 m/min, 120 m/min and 150 m/min of cutting speeds and 80 %, 90 % and 100 % of ultrasonic power. The measurement of V_B and V_M from SEM images is shown in Figure 6.9.The growth of tool wear in both CT and UVAT process is evaluated with respect to V and P_u. In order to compare both CT and UVAT process, the tool life criteria considered for this study is 300 μm for V_B [156].
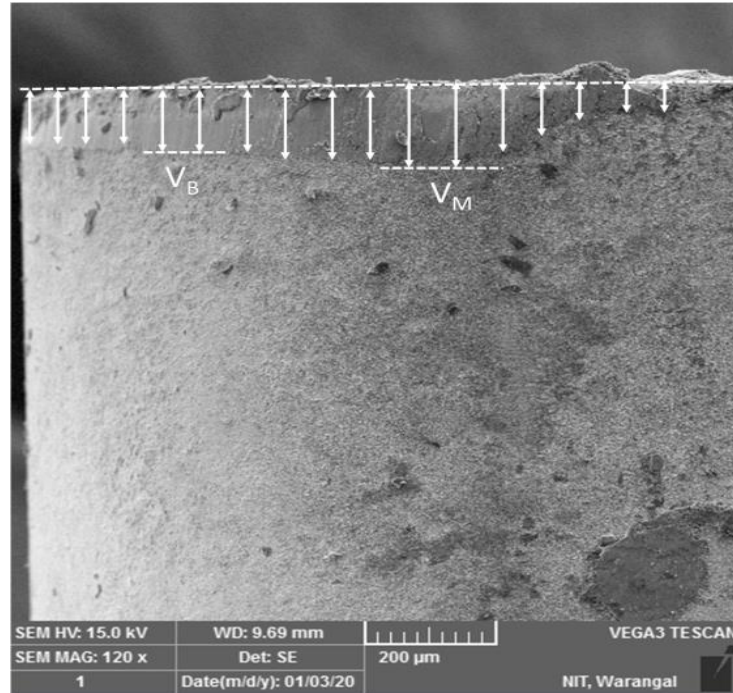
Figure 6.9: Flank wear measurement from the cutting edge of the tool

6.5.1 Development of flank wear

In metal cutting, the raise in T_c depends on cutting conditions, and tool and workpiece material properties. At the same cutting conditions (f_r and DOC) in machining of Ti6Al4V alloy, cutting speed and coefficient of friction between tool and chip plays a significant role in raise in temperature. In UVAT, the oscillating motion of tool causes the reversal of direction of chip for each cycle of vibration. Hence, the raise in T_c in UVAT process is low compared to CT due to less coefficient of friction at secondary deformation zone.

In machining of Ti6Al4V alloy, the rate of tool wear occurs due to abrasion, adhesion and diffusion. The raise in temperature causes the chip to make an intimate contact with rake face with an interfacial layer. The intimate contact between chip and tool causes the continuous shearing of material from rake surface. Furthermore, the chemical reactivity of

110

chip with tool enhances with high cutting. This leads to transfer of tool particles into adherent layer of chip material through abrasion, adhesion and diffusion. However, the intermittent cutting action between tool and workpiece and reversed direction of chip reduce the T_c in UVAT compared to CT process. Hence, the degree of chemical reactivity between layer of chip and tool material is low in UVAT process.

The rate of flank wear is increased with increase in machining time due to increase in F_c and T_c in both CT and UVAT process as shown in figure 6.12. However, this rate of tool wear is low in UVAT compared to CT process. Figure 6.10 (A) Indicates the flank wear of the tool after volume of material being removed for 2 min for both CT and UVAT process. The continuous cutting action between tool and workpiece in CT increases the wear rate and initiates to form BUE whereas the intermittent cutting action in UVAT reduces the rate of flank wear in UVAT. In UVAT, initiation of wear and adhering of chip are observed after material being removed for 2 min of machining due to reversed direction of chip on the rake face of the tool. However, in CT, the initial raise in temperature due to continuous contact increases the wear rate flank face of the tool and begins to form the BUE on the cutting edge. From figure 6.10. (B), it is found flank wear of the tool is increased and smooth after 5 min of machining in UVAT process. The rapid growth of wear is due to abrasive action between tool and workpiece and formation of interface layer between rake face and flow of chip at higher F_c and T_c. In CT, the growth of flank wear and size of BUE formation is increased due to increase in T_c. Similarly, fracture of cutting edge of the tool is observed after 7.5 min of machining in CT process. The continuous cutting action increases the flank wear of the tool rapidly due to increase in T_c. Moreover, thickness of interface layer between tool and workpiece increases with prolonged machining in CT process. At some point of time, this adhered layer torn and moved from the cutting edge by flow of the chip. This leads to wear of cutting edge of the tool due to transfer of grains of the tool as shown in figure 6.10. (C). In UVAT, the raise in temperature with reversal of chip direction for each cycle increases the wear rate and ensures the smooth wear on the flank surface.

6.5.2 Effect of ultrasonic power on flank wear of the tool

As ultrasonic power is directly proportional to amplitude of the vibration, increase in P_u reduces TWCR in UVAT process. This leads to reduction in F_c and T_c in UVAT compared to CT process at same cutting conditions. The developed T_c and TWCR plays a significant

role in growth of wear of the tool. Hence it is important to evaluate the effect of P_u on tool wear in UVAT process. The tool wear is analyzed by considering 80%, 90% and 100% of P_u in UVAT and compared with CT process at V = 90 m/min, f_r = 0.2 mm/rev and DOC = 1mm.
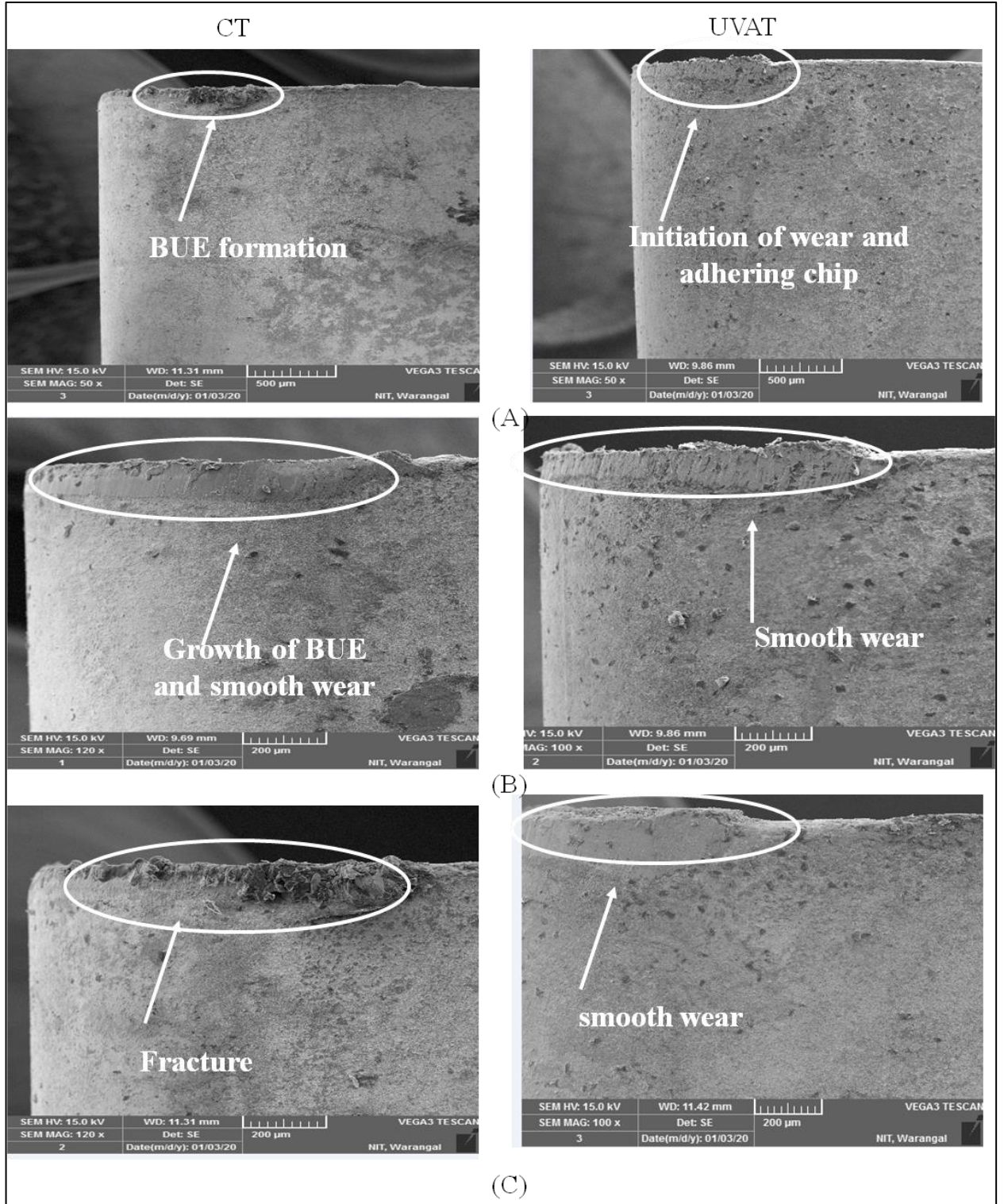
Figure 6.10: Progression of flank wear of tool in CT and UVAT after (A). 1.75 min (B). 5 min and (C). 7.5 min of machining
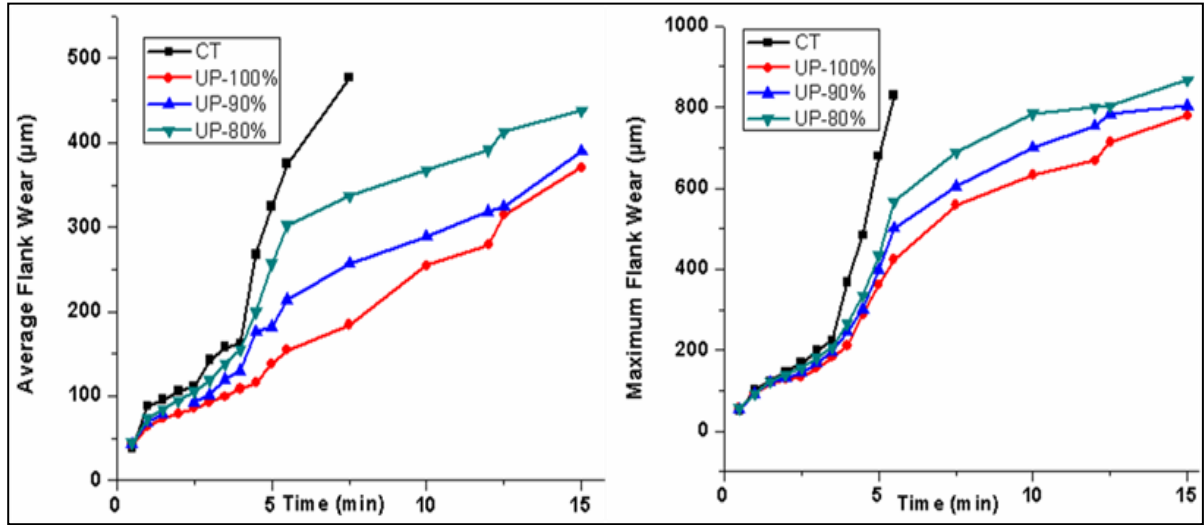
Figure 6.11: Effect of ultrasonic power on flank wear of the tool

Figure 6.11, shows the growth of V_B and V_M at different ultrasonic power and its comparison with CT at same cutting conditions. The initial rapid growth of flank wear is higher in CT compared to UVAT and it decreases with increase in ultrasonic power. Moreover, maximum material is being removed with gradual wear rate at higher ultrasonic power. This leads to improve the performance of machining process by increasing the tool life. For a tool life criteria of V_B= 300 μm, the tool life obtained in CT is 4.75 min whereas 6 min for 80 %, 11.5 min for 90% and 12.5 min for 100% of ultrasonic power in UVAT process. As P_u increases, the contact between tool and workpiece decreases. This leads to improvement on tool life because of lower F_c and T_c. Moreover, the coefficient of friction between tool and chip reduce with increase in P_u due to reversal of chip direction on the rake face of the tool. This improves the tool life by reducing chemical reactivity between the tool and the workpiece. Moreover, steep raise in V_B is observed after 4.75 min of machining time in CT process due to sudden raise in T_c and faster plastic deformation. This enhances the chemical reactivity between tool and workpiece which results in sudden raise in V_B is observed. This sudden raise in V_B is substantially reduced with increase in P_u due to reduced T_c and F_c.

6.5.3 Effect of cutting speed on flank wear of the tool

Figure 6.12 depicts the growth of flank wear features V_B and V_M with machining time at 90, 120 and 150 m/min of V for both CT and UVAT of Ti-alloy. It is found that the rate of growth of both V_B and V_M are less in UVAT compared to CT for all cutting speeds. However,

the advantage of reduction in rate of growth of flank wear in UVAT process seems to be a function of V and P_u. The reduction in T_c with increase in P_u decreases the growth of the tool
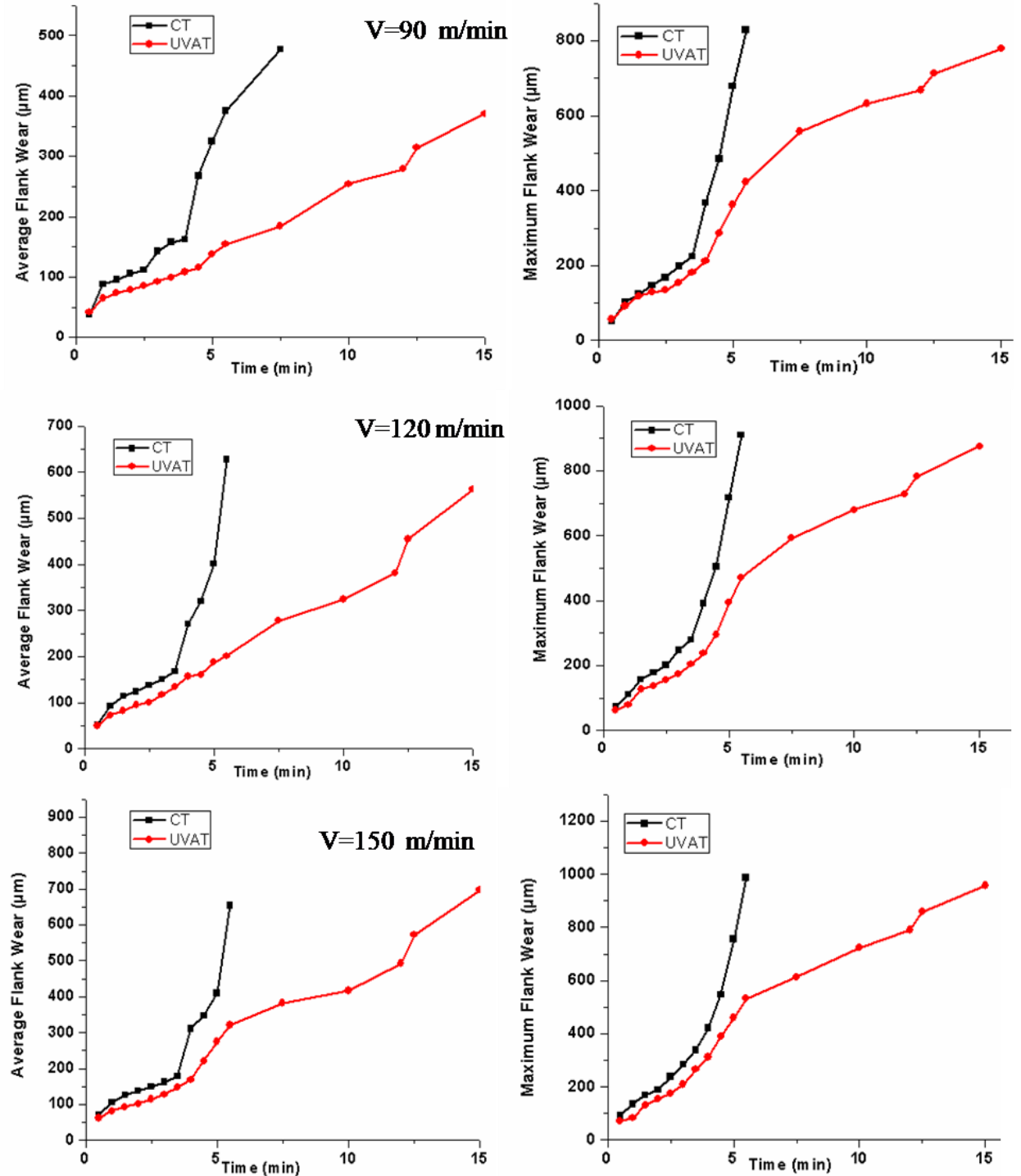
Figure 6.12: Growth of average and maximum flank wear with cutting time various velocities.

wear due to low TWCR in UVAT. However, the growth of the tool wears increases with increase in V due to to increase in T_c as shown in figure 6.13. For V_B of 300 μm, the tool life

obtained in CT is around 4.75 min for 90 m/min against 12.5 min obtained in UVAT process. The considerable improvement in tool life is observed in UVAT due to reduction in F_c and T_c enabled by reducing TWCR. As the V increases, the flank wear grows much faster due to large plastic deformation and higher T_c. However, the decrease in TWCR in UVAT process substantially retarded the growth of tool wear. The effect of TWCR decreases with increase in cutting velocity in UVAT process. Hence, the chatter suppression due to ultrasonic vibration could affect the flank wear in UVAT process at higher cutting speeds[157]. At higher cutting speeds, the advantage obtained from ultrasonic power is low due to high TWCR. Hence, it is always beneficial to work at lower cutting speeds and higher ultrasonic power for maximum tool life in UVAT process.
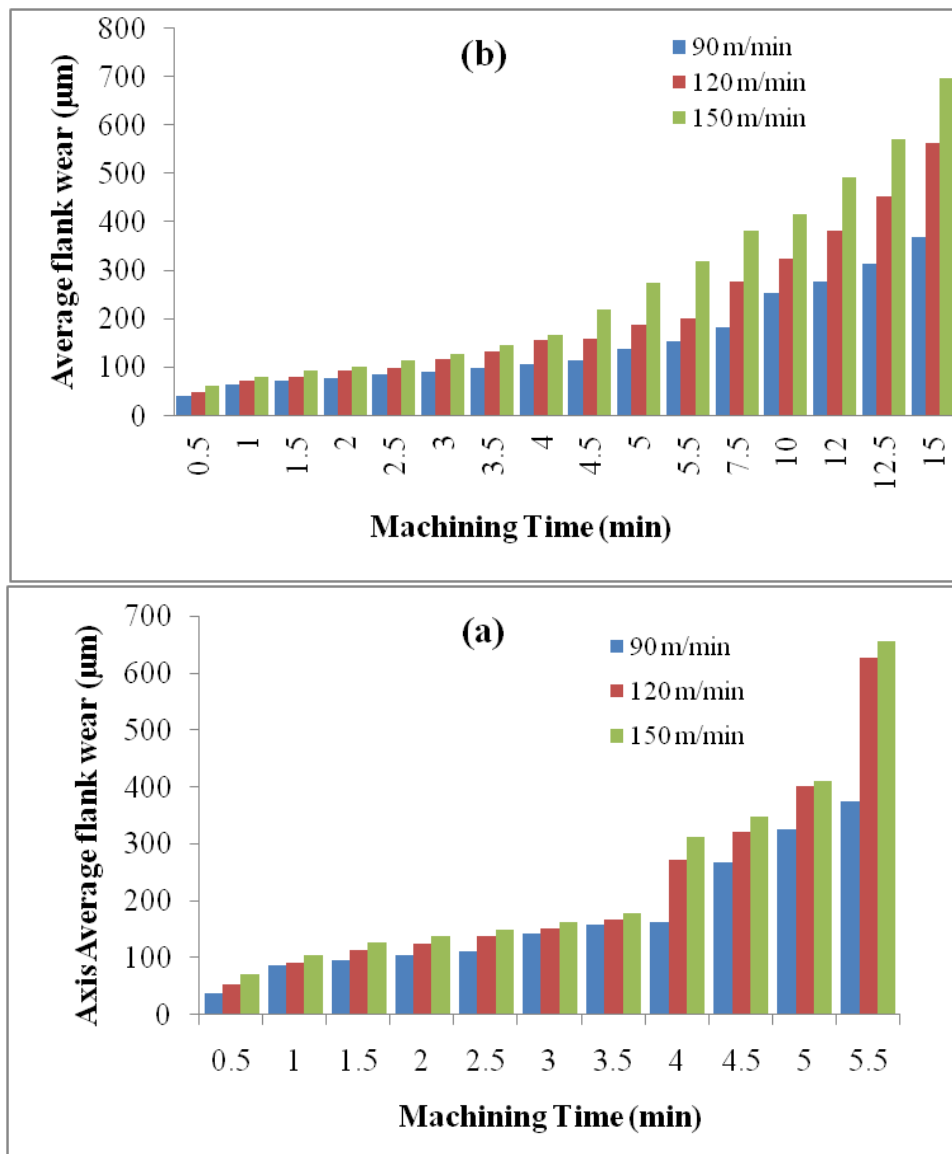
Figure 6.13: Growth of tool flank wear at various cutting speeds in (a). CT and (b). UVAT

6.5.4 Effect of flank wear on cutting forces
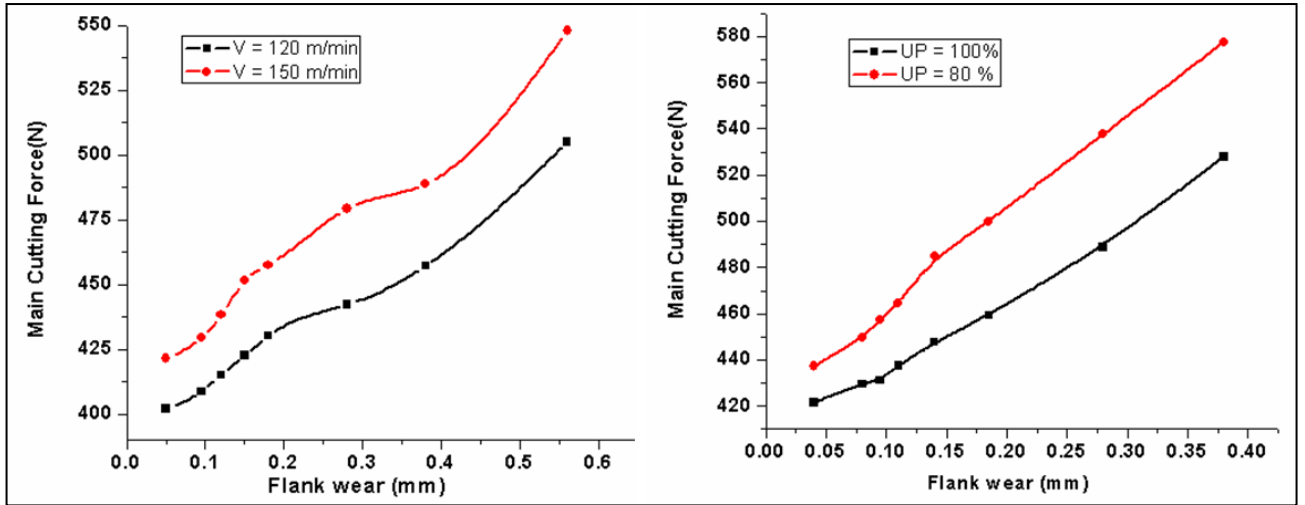
Figure 6.14: Variation of cutting force with flank wear at different cutting speeds and ultrasonic powers

Cutting force is increased with increase in V_B for both 120 and 150 m/min of V as shown in figure 6.14. The increase in F_c is low up to about 0.2 mm of V_B and thereafter, F_c is rapidly increased with increase in V_B for both cutting speeds. The increased abrasive action between tool and workpiece with increase in flank wear increases F_c rapidly. Moreover, the increased TWCR with increase in V increases F_c speed. The variation of F_c with flank wear for both ultrasonic power of 80 and 100% is shown in figure 6.14. The variation of F_c between 80 and 100 % of ultrasonic power is increased with increase in V_B. This variation is low up to 0.1 mm of V_B and thereafter, the difference is increased with increase in V_B rapidly. The reduction in abrasion between tool and workpiece with increase in ultrasonic power slowdown the increase in F_c with increase in flank wear.

6.6 Summary

Experiments are conducted on a Ti6Al4V alloy for both UVAT and CT processes under various machining conditions. The performance of the UVAT process was evaluated in terms of cutting force, cutting temperature, and surface roughness at various machining conditions by considering TWCR. Similarly, the growth of flank wear on the cutting tool is analyzed during machining of Ti6Al4V for both CT and UVAT. The progression of tool flank wear in both CT and UVAT is analyzed at the same cutting conditions. The effect of ultrasonic power and cutting velocity on tool flank wear is also analyzed.

Chapter 7

Evaluation of Surface Integrity of Ti6Al4V Alloy in UVAT Process

7.1. Introduction

The study of residual stresses induced during machining is of considerable importance due to their effect on fatigue life of machined components. The metallurgical changes occurred due to thermo-mechanical phenomenon in cutting process affects the distribution of residual stress in machined components. In this chapter, experimental and finite element (FE) studies are conducted to study the circumferential and axial residual stress distribution in UVAT of Ti6Al4V alloy. The Johnson-Cook parameters determined from machining approach which is discussed in the chapter 5 has been used in FE analysis of residual stresses for accurate results. The effect of vibrating parameter (ultrasonic power intensity) and cutting parameters (cutting speed, feed rate and depth of cut) on the residual stress profiles of machined surface are evaluated. The circumferential and axial surface residual stresses obtained from FE simulation are also compared with experimental results using X-ray diffraction method. The effect of thermo-mechanical loading on residual stress distribution is analyzed with respect to force components (cutting force and feed force) and cutting temperature. Finally, the effect of each cutting parameter on subsurface layer of machined component is analyzed.

7.2. Experimentation

Forged Ti6Al4V alloy workpiece of 40 mm diameter and 220 mm length was considered and cutting length of 20 mm was used for each experiment. In order to ensure stress free, Ti6Al4V workpiece was annealed at 590ºC for 2 h and followed by furnace cooling before experimentation [158]. The cutting parameters and their levels considered for this study are shown in table 7.1. The change in amplitude in UVAT process was obtained by varying ultrasonic power intensity as these two parameters are in direct relation (Sharma). In order to analyze the thermo-mechanical loading in UVAT process, the cutting force and cutting temperature are measured at the same cutting conditions used for measurement of residual stresses.

As the residual stress is sensitive to thermo-mechanical loading, the sample (10 mm x 10 mm x 5 mm) for measurement were cut from wire EDM process from cylindrical machined component. The machined sample was polished each time with a step of 15 µm up to 110 µm using electro polishing technique for measuring depth residual stress profiles.

Table 7.1: Details of measuring system and experimental conditions

Measuring system	Details of measuring system
Ultrasonic system	Frequency of ultrasonic generator : 20 KHz Amplitude at 100% ultrasonic power : 25 µm
Force measurement	Dynamometer : 9257 B Kistler 6-component type Data acquisition system : 5070 A type
Temperature measurement	Thermocouple : Nickel-chromium (k type) Diameter : 0.25 mm Uncertainty : ± 1.1ºC Position of hole in insert (in mm): x = 0.72 y = 0.3 z = 0.6
Cutting parameters and their levels	Ultrasonic power intensity (P_u) : 70, 80, 90, 100 % Cutting speed (V) : 30, 50, 70, 90, 110 m/min Feed rate (f_r) : 0.055,0.103,0.161 mm/rev Depth of cut (DOC) : 0.5, 0.75, 1, 1.25 mm

7.3 Residual stresses in UVAT process

The analysis of residual stresses developed during machining process through experimentation is costlier and time consuming. FE modeling is one of the powerful tool available to analyze residual stresses completely. In developed FE model, residual stress along the tangential direction i.e Circumferential residual stress (CRS) is S11 and perpendicular to cutting direction i.e Axial residual stress (ARS) is S33 as shown in figure 6. FE simulation results are used to study the effect of machining parameters on CRS and ARS in UVAT process. As the residual stresses is dynamic in nature in UVAT, the average residual stress is evaluated by considering residual stress at three equidistant sections as shown in figure 7.1.
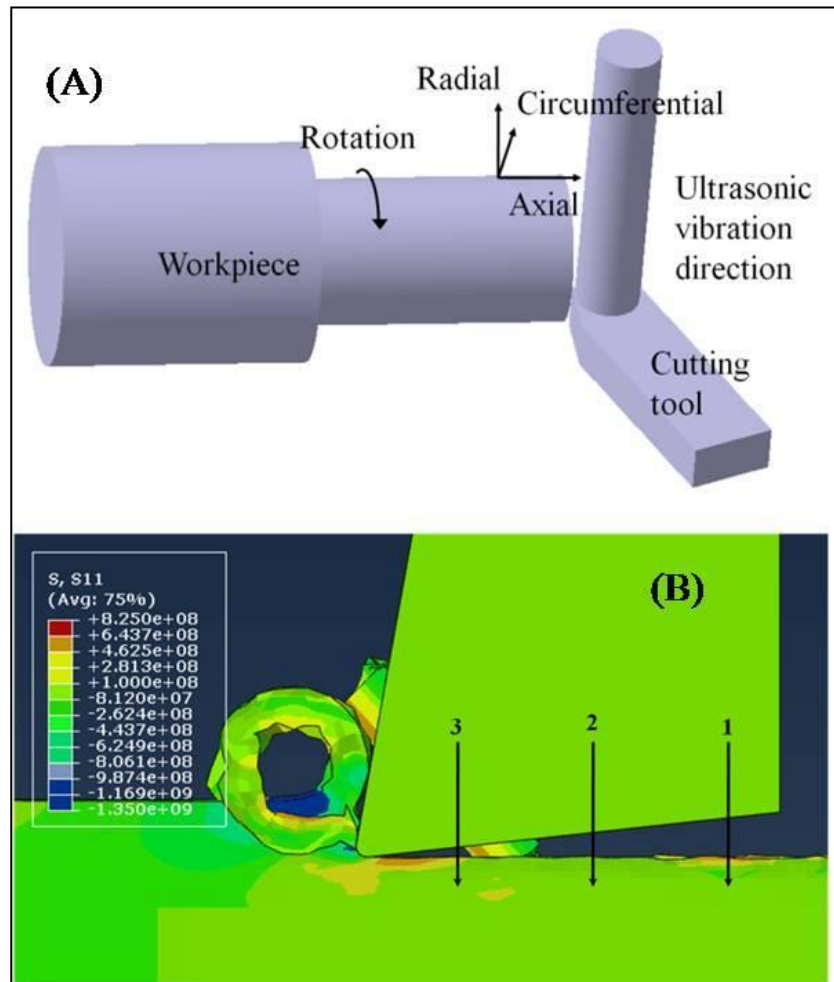
Figure 7.1: FE simulation of UVAT process (A).Directions of residual stress state and (B).Measurement of residual stresses.

The residual stress distribution in UVAT process is analyzed in four stages for each cycle of vibration and its variation is shown in figure 7.2 and 7.3. The FE simulations for this analysis are conducted at V=30 m/min, f_r = 0.055 mm/rev, DOC = 0.5 mm and P_u = 100%. In stage I, average residual stress observed is 425 MPa (tensile) when cutting tool contacts the chip and its nature changes to compressive at a depth of approximately 50 μm. In second stage, tensile residual stresses are observed at each section and maximum observed on surface is 580 MPa when cutting tool penetrates into workpiece. The maximum plastic deformation of material occurs in this stage and thermal loading resulted from plastic deformation causes tensile CRS at this stage. In stage III, average tensile residual stress on surface is 260 MPa and its nature changes to compressive at a depth of 35 μm as the tool retracts from workpiece. In stage IV, an average residual stress on surface is 192 MPa (tensile) when tool is about to start for next cycle and its nature changes to compressive at a depth of 20 μm.
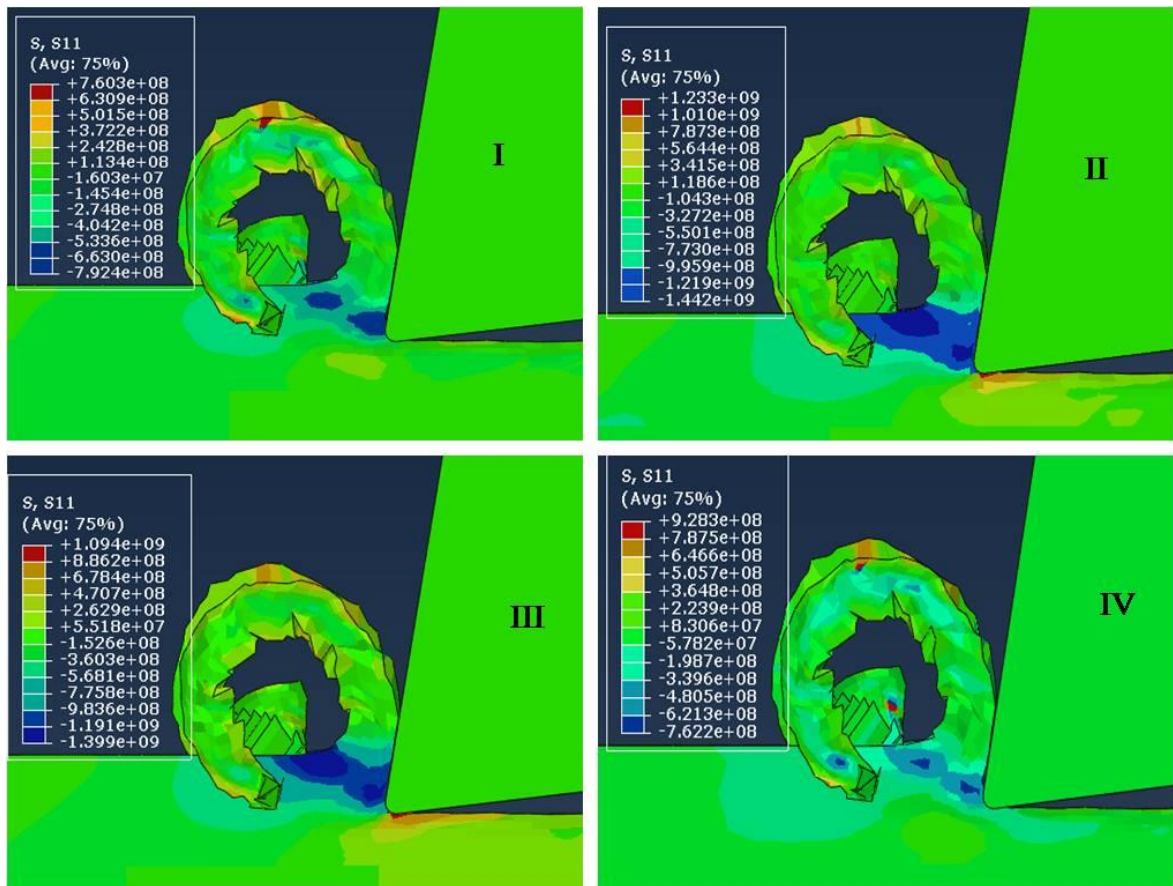
Figure 7.2: Residual stress distribution in various stages of UVAT process.
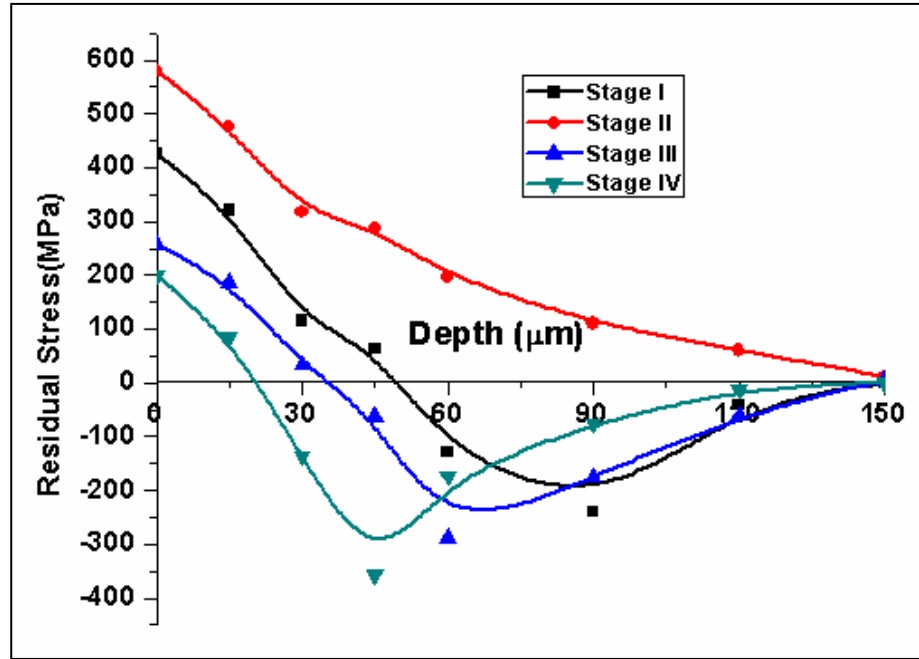
Figure 7.3: Depth profile of residual stress in various stages of one UVAT cycle.

7.4 Model validation

The developed FE model for UVAT process is validated with experimental results at 30 m/min of V, 0.103 m/min of f_r, 0.5 mm of DOC and 100 % of $P_{u..}$ The comparison between FE and experimental results of cutting force and residual stresses are shown in figure 7.4 and 7.5. The percentage variation of cutting force and cutting temperature between simulation and experimental results are within the permissible limit. In order to validate the same FE model with respect to residual stresses, CRS and ARS obtained from simulation results on the surface are compared with experimental results at the same cutting conditions. However, the surface residual stresses obtained from simulation are dynamic in nature; hence the average residual stress obtained from simulation is compared with constant residual stresses obtained from experimentation. The variation between simulation and experimental results are within permissible limit as shown in table 7.2. Hence, the developed FE model is used for further analysis of residual stress along the depth at various machining conditions. The interaction between chip and cutting tool in UVAT is difficult to evaluate due to dynamic effect of ultrasonic vibration. Probably, this could be the reason for having error between simulation and experimental results.

121

Table 7.2: Comparison of simulation and experimentation results of UVAT process

Parameter	Simulation	Experimentation	Percentage Variation (%)
Cutting force (N)	165	175	5.7
Cutting Temperature (°C)	155	169.3	8.4
Circumferential Residual stress (MPa)	-185.3	-177.5+7.9	4.3
Axial residual stress (MPa)	-202.1	-192.2+7.9	5.1
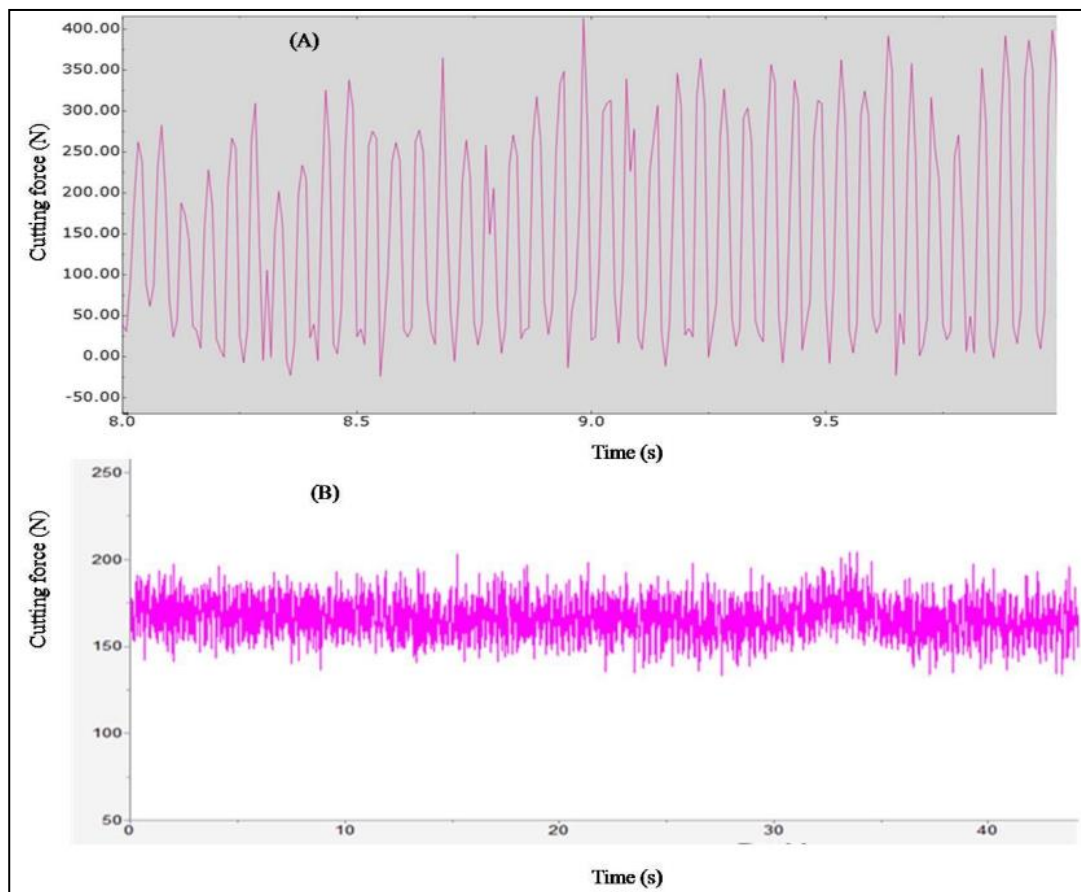
Figure 7.4: Cutting force comparison between (A). Simulation and (B). Experimental results.
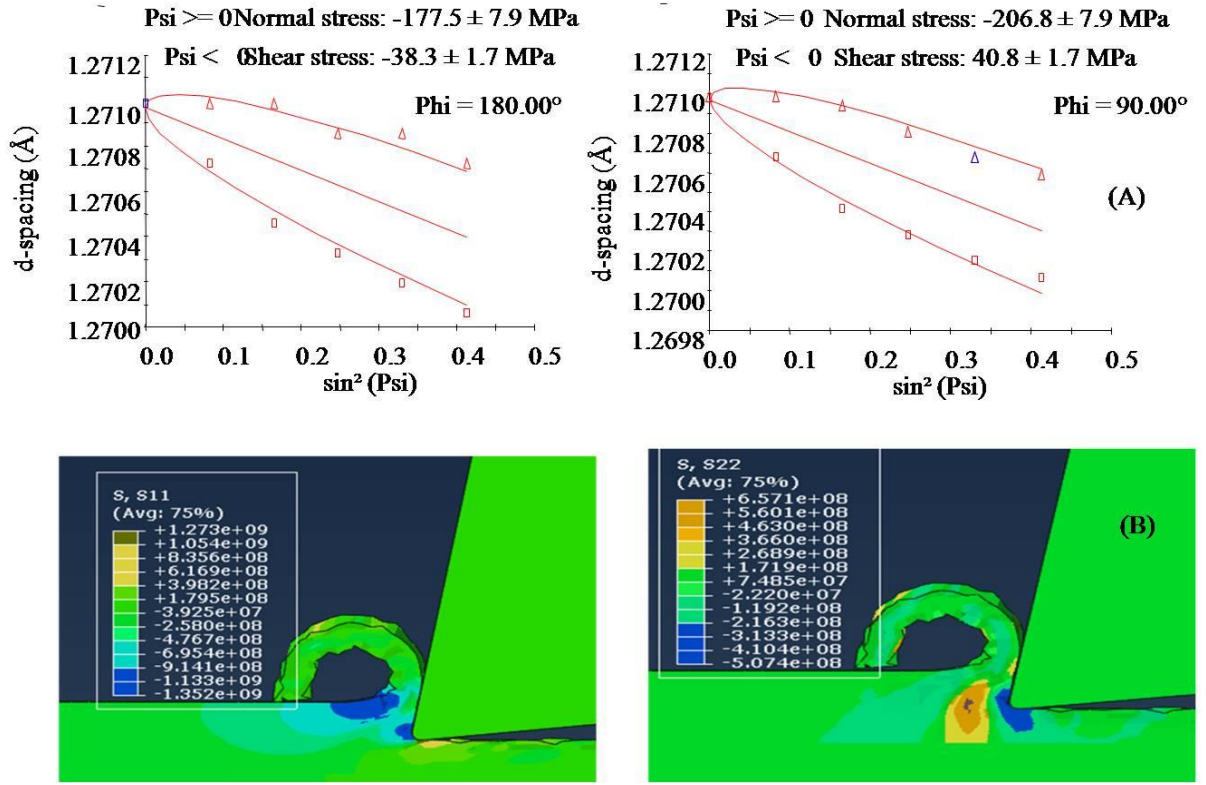
Figure 7.5: Residual stress comparison between (A).Experimental and (B).Simulation results.

7.5. Evaluation of residual stresses

In this section, the machining parameters effect on residual stresses is analyzed with respect to thermo-mechanical loading in UVAT process[159]. The thermo-mechanical aspects in UVAT process are analyzed by force components and cutting temperature from experimentation. Furthermore, residual stress distribution of machined components is analyzed with respect to thermo-mechanical phenomenon at same cutting conditions.

7.5.1 Effect of machining parameters on thermo-mechanical loading

The level of machining induced residual stresses are directly affected by heat generated due to plastic deformation and friction between chip and cutting tool [158, 159]. In order to describe the effect of thermo-mechanical loading on residual stress formation during UVAT of Ti6Al4V alloy, the force components (F_c and F_f) and cutting temperature are analyzed by conducting experiments at various cutting conditions where residual stresses are analyzed and the results are shown in figure 7.6. The level of machining induced residual stresses are directly affected by heat generated due to movement of chip along rake face of the tool and plastic deformation[160].

The type of residual stress and its affect on subsurface layer of machined components depends on thermo-mechanical loading in cutting process. From figure 7.6 (a), it is found that the force components and T_c are decreased with increase in P_u from 70 to 100%. The reduction in F_c and F_f with increase in P_u is mainly due to fracture dynamics of UVAT process [154]. The intermittent cutting action between tool and workpiece generate high impact energy per each cycle of vibration. This impact energy produces high stress wave velocity which affects the ultimate strength of chip before cutting action between tool and workpiece in UVAT process. Furthermore, the intermittent cutting action in UVAT reduce the larger strains produced on the machined surface which results in reduction of heat due to severe plastic deformation compared to CT [70]. Moreover, the yield strength of the material decreases with increase in thermal softening which leads to separation of chip from cutting zone with low cutting force. The increased separation between tool and workpiece with increase in P_u reduces the cutting time and increases the aerodynamic cooling during machining process. Hence, the reduction in thermo-mechanical load with increase in ultrasonic power significantly influences the distribution of residual stress. From figure 7.6(b), it is found that F_c and F_f are decreased due to increase in thermal softening and T_c is increased due to adiabatic temperature zones with increase in V from 30 to 110 m/min in UVAT. The variation of thermo-mechanical loads due to increase in cutting speed also plays a major role residual stress distribution.

The variation of force components and cutting temperature at different f_r and DOC is shown in figure 7.6 (c) and (d). The increased resistance to movement of cutting tool with increase in f_r and DOC increases force components and cutting temperature. The increased thermo-mechanical load due to increase in f and DOC affects the residual stress generation in machining process. Hence, it is important to evaluate the variation of residual stresses on the machined surface and subsurface layer with variation of cutting conditions.
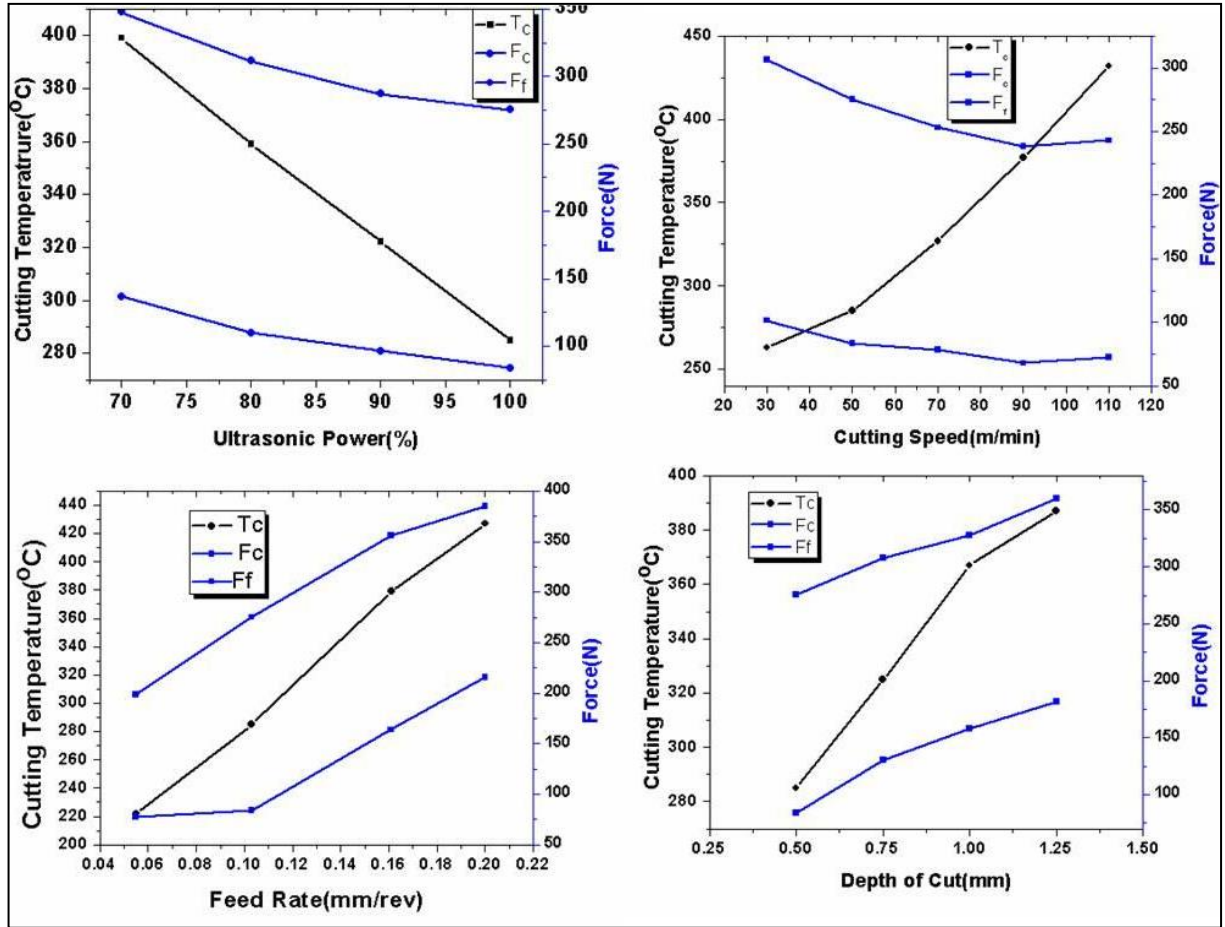
Figure 7.6: Evolution of cutting force and cutting temperature with machining regime.

7.5.2 Influence of machining conditions on Residual Stress distribution

7.5.2.1 Influence of ultrasonic power

The influence of ultrasonic power on surface residual stress in UVAT process is analyzed at V = 50 m/min, f_r = 0.103 mm/rev and DOC =0.5 mm. From figure 7.7.(A), it is observed that the surface CRS is changed from 50 MPa (tensile) to 28 MPa (compressive) when ultrasonic power is increased from 70 to 100 %. Similarly, the surface ARS is changed from 125 MPa (compressive) to 221 MPa (compressive) for the same range of ultrasonic power. The state of residual stress on surface depends on dominance of either thermal or mechanical load. The dominance of thermal load over mechanical load is decreased with increase in ultrasonic power which results surface CRS is changed from tensile to compressive. However, compressive nature of surface ARS is increased with increase in ultrasonic power due to effect of thermal load in axial direction is negligible compared to mechanical load.
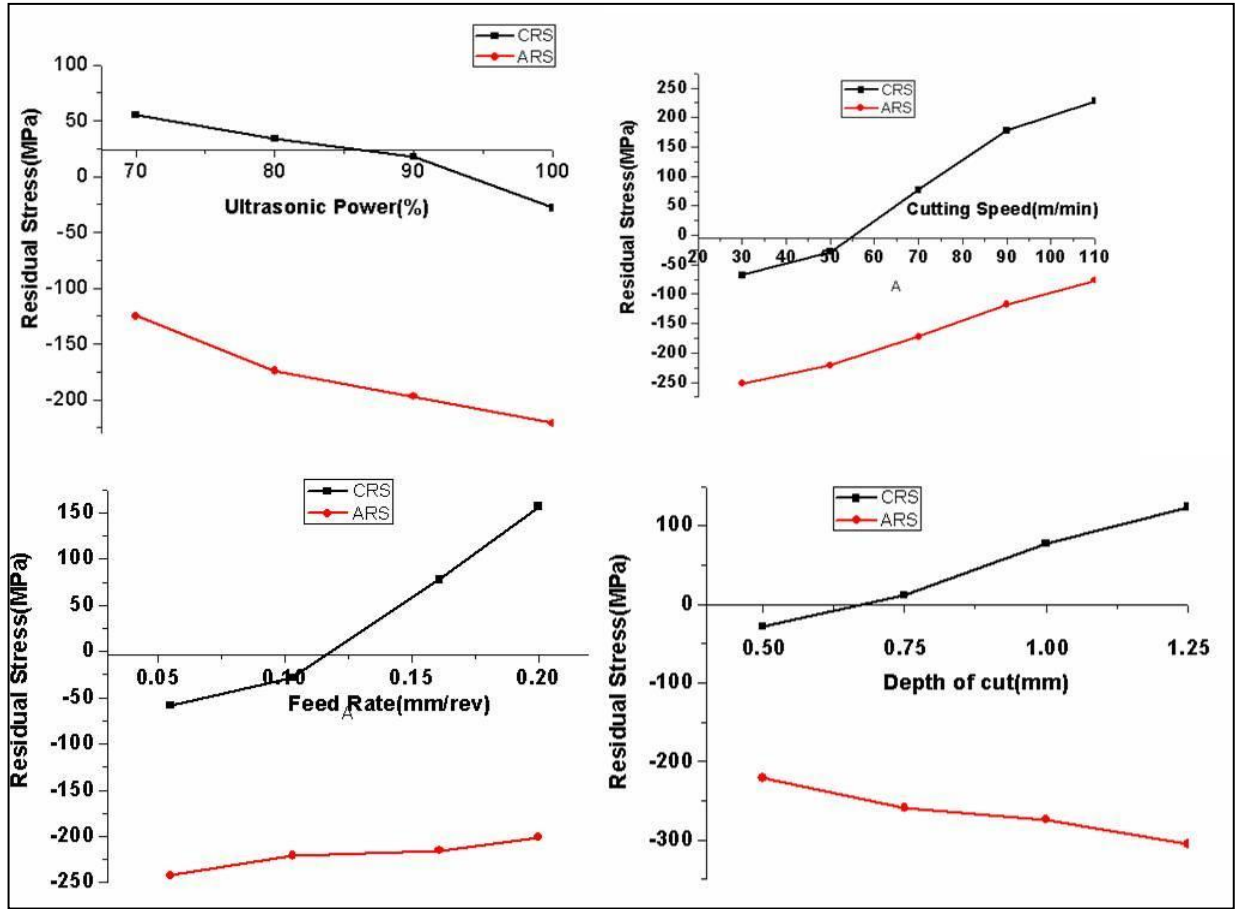
Figure 7.7: Evolution of surface residual stresses with respect to Ultrasonic power intensity, Cutting speed, Feed rate and Depth of cut.
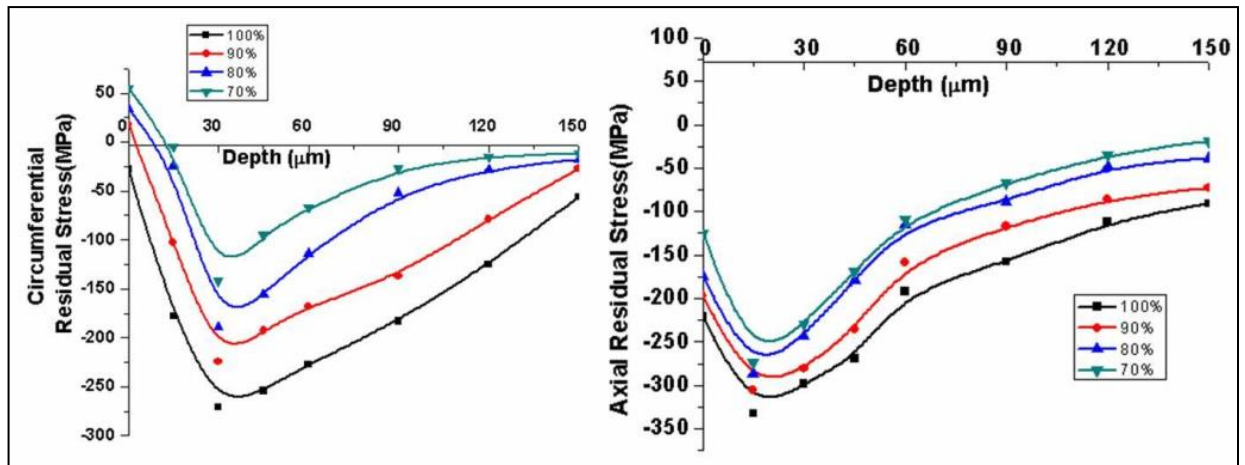
Figure 7.8: Evolution of CRS and ARS at different ultrasonic power intensity.

Depth profiles of CRS and ARS are obtained at various ultrasonic powers as shown in figure 7.8. From CRS distribution, it is observed that, the tensile layer thickness is decreased with increase in P_u from 70 to 90% and becomes zero at 100%. Similarly, the compressive layer thickness is increased with increase in P_u. The variation of residual stress depth profiles mainly depends on thermo-mechanical phenomenon involved in UVAT process. The

reduction in thermal softening with increase in ultrasonic power decreases the impact of thermal load in generation of residual stress. And also, the reduction in cutting force indicates the decrease in mechanical loading effect with increase in ultrasonic power. However, the reduction in thermal loading is more significant compared to mechanical loading on CRS and hence, the magnitude of compressive CRS is increased with increase in P_u. However, the decreased mechanical load effects the maximum residual stress profiles. Hence, the maximum compressive stress is increased with increase in P_u. Similarly from ARS distribution, it is observed that, the maximum compressive stress is increased with increase in ultrasonic power due to reduction in thermal load. Moreover, the compressive layer thickness is increased with increase in P_u due to dominance of mechanical load.

7.5.2.2. Influence of Cutting speed

The influence of cutting speed (V) on surface residual stresses is analyzed at f_r = 0.103 mm/rev, DOC= 0.5 mm and P_u = 100% as shown in figure 7.7.(B). The surface CRS is changed from 68 MPa (compressive) to 228 MPa (tensile) when V is increased from 30 m/min to 110 m/min. Similarly, the surface ARS is changed from 252 MPa (compressive) to 77 MPa (compressive) for the same range of V. The variation of both CRS and ARS on surface can be described with respect to force components (F_c and F_f) and cutting temperature. The decrease in F_c and F_f and increase in T_c with cutting speed increases the effect of thermal load over mechanical load in generation of residual stress. Hence, the surface CRS and ARS are increased with increase in V.
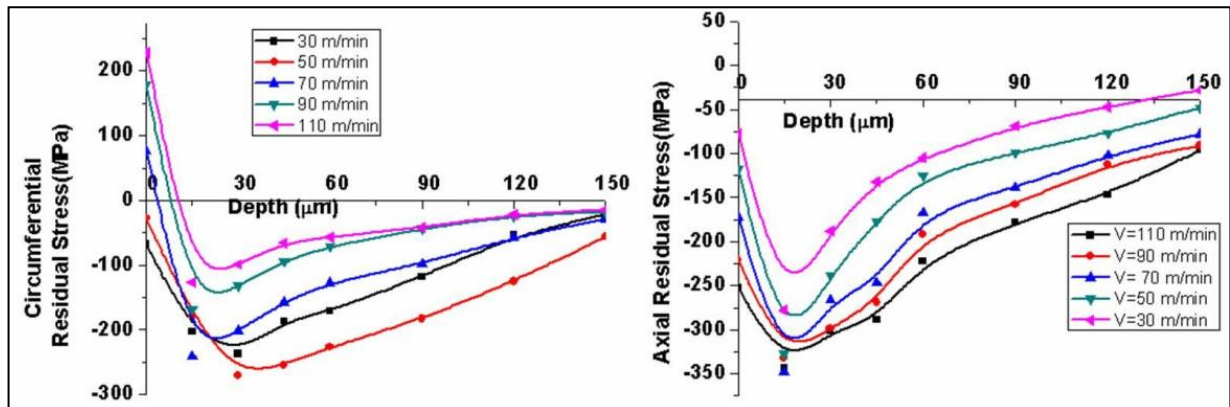
Figure 7.9: Evolution of CRS and ARS at different cutting speeds

The influence of V on depth profiles of CRS and ARS are shown in figure 7.9. From the depth profiles of CRS, it is observed that tensile layer thickness is increased and

compressive layer thickness is decreased with increase in V. The increase in cutting temperature and decrease in force components (F_c and F_f) with increase in cutting speed induces more thermal load than mechanical load on the machined surface. This result in more heat effected layer of machined surface increases with increase in V. Hence, tensile layer thickness is increased. Moreover, the maximum compressive CRS is increased with decrease in V and its location is moves away from the surface. Similarly, the compressive layer thickness of ARS is increased with increase in V and maximum compressive ARS is also increased with cutting speed.

7.5.2.3 Influence of Feed rate

The influence of f_r on surface CRS and ARS is analyzed at V=50 m/min, DOC = 0.5 mm and P_u =100%. From figure 7.7.(C), it is observed that the surface CRS is increased from 58 MPa (compressive) to 157 MPa (tensile) when f_r is increased from 0.055 mm/rev to 0.103 mm/rev. Similarly, surface ARS is changed from 242 MPa (compressive) to 201 MPa (compressive) with increase in f_r. From the analysis, it is observed that the effect of f_r on surface CRS is more compared to surface ARS. The increased force components (F_c and F_f) and cutting temperature with increase in f_r induces more thermal load than mechanical load which results nature of surface CRS is changed from compressive to tensile. The nature of surface ARS is compressive due to negligible effect of thermal load compared to mechanical load. However, the effect of thermal load is increased with increase in f_r which results in reduction of compressive surface ARS.
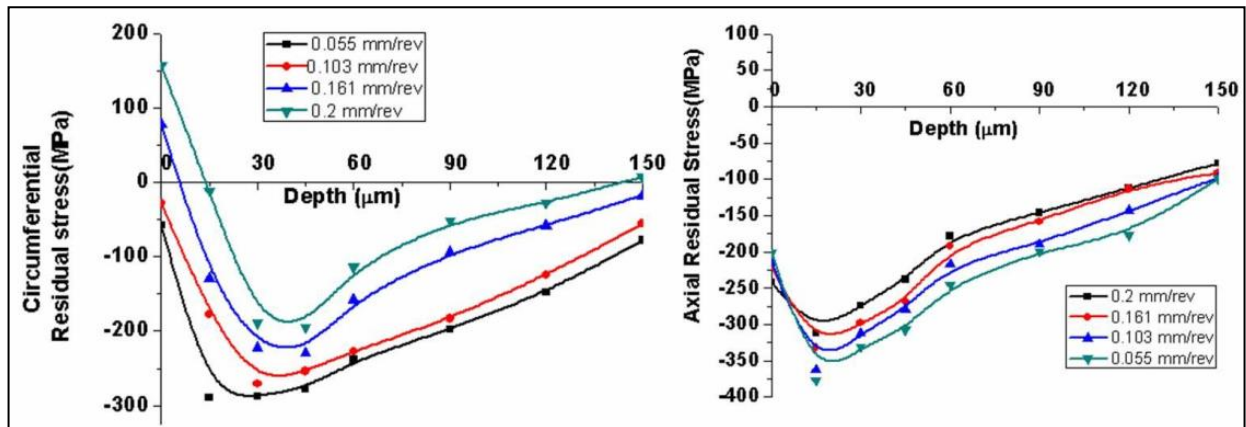
Figure 7.10: Evolution of CRS and ARS at different feed rates.

Depth profiles of residual stress along circumferential and longitudinal direction at various f_r are shown in figure 7.10. From CRS depth profiles, it is observed that tensile layer thickness is decreased with increase in f_r and becomes zero for 0.2 mm/rev of f_r. The compressive layer thickness and maximum compressive CRS is increased with f_r and maximum compressive CRS location is shifted towards the surface. The resistance to movement of cutting tool induces large compressive region in primary deformation zone which is just below the cutting edge and influence the effect of mechanical load on generation of residual stresses. Similarly, from depth profiles of ARS, it is observed that the maximum compressive ARS is decreased with increase in f_r and compressive layer thickness of ARS is not changed much with f_r.

7.5.2.4 Influence of depth of cut

Influence of DOC on surface CRS and ARS is analyzed at V=50 m/min, f_r= 0.103 mm/rev and P_u =100%. From figure 7.7.(D), it is found that the surface CRS is increased from 28 MPa (compressive) to 124 MPa (tensile) with increase in DOC from 0.5 mm to 1.25 mm. The surface ARS is changed with increase in DOC from 221 MPa (compressive) to 305 MPa (compressive). The increase in force components (F_c and F_f) and cutting temperature with increase in DOC increases the thermal load on the surface which results in larger tensile surface CRS. The effect of DOC on surface ARS is less compared to CRS.
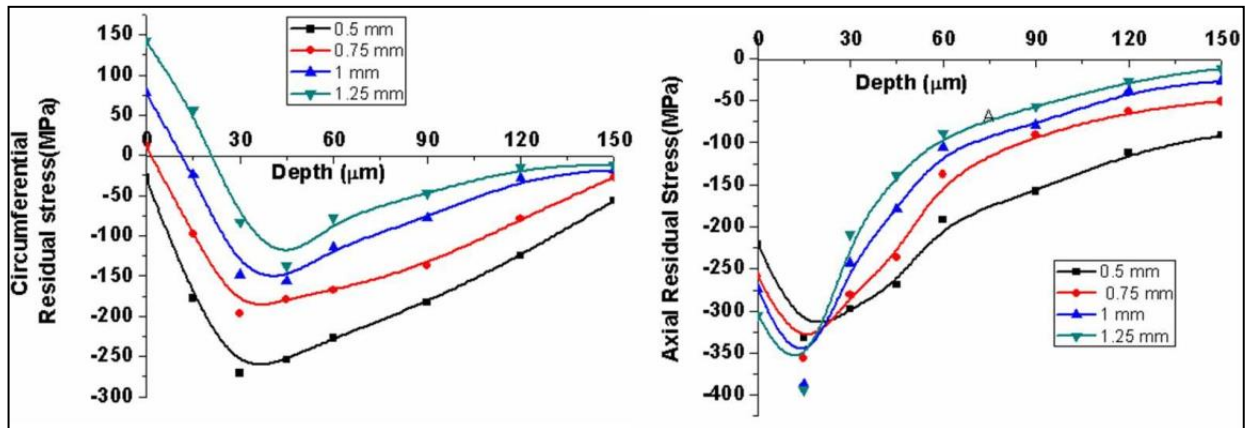
Figure 7.11: Evolution of CRS and ARS at different depth of cuts.

Depth profiles of CRS and ARS at various DOC are shown in figure 7.11. From CRS depth profiles, it is observed that the tensile layer thickness is increased with increase in DOC whereas compressive layer thickness is decreased with same DOC conditions. Moreover, the maximum compressive CRS is also decreased with increase in DOC. The increased heat generation with increase in DOC affects the subsurface layer which results in tensile CRS are

formed in subsurface layers. Similarly, from depth profiles of ARS it is found that the compressive layer thickness is decreased and maximum compressive ARS is increased with increase in DOC.

7.5.3. Interaction effects

From above discussion, it is observed that the variation of CRS and ARS with each machining parameter depends on the thermo-mechanical phenomenon occurs during cutting process. The contact time between tool and workpiece decides the thermo-mechanical loading in UVAT method. From the fundamentals of simple harmonic motion, it is identified that f, a and V are the three important cutting parameters which effect the contact time in UVAT process[113]. The interaction effects of vibrating parameter i.e ultrasonic power with machining parameters such as V, f_r, and DOC are discussed in this section.

7.5.3.1. Interaction between ultrasonic power and cutting velocity

The time of contact between tool and workpiece is rapidly increased at lower and higher cutting speeds whereas moderately increased at medium cutting speeds. However, the time of contact is decreased with increase in P_u. The decreased time of contact promotes better aerodynamic lubrication which results in increased heat removal from the surface in UVAT. Hence, the mechanical load dominates over the thermal load at higher ultrasonic power and moderate cutting speeds which generates the compressive residual stresses. Moreover, at constant ultrasonic power, shear angle is increased with increase in V which results in increased rate of heat conduction from chip to workpiece. This leads to the generation of tensile residual stress due to high thermal effect.

7.5.3.2 Interaction between ultrasonic power, feed rate and depth of cut

The effect of f_r and DOC are similar in cutting process with respect to thermo-mechanical phenomenon. The f_r and DOC, and P_u have opposite trend in generation of residual stress. From figure 7.7, it is observed that thermal effect is more at higher f_r and DOC, and lower P_u which results in generation of tensile residual stress on machined surface. Hence, the advantage of intermittent cutting in UVAT process is predominant at higher ultrasonic power. Moreover, the raise in thermal effect enhances the ironing effect with increase in ultrasonic power which results in improved machined surface.

7.6 Fatigue Life of Ti6Al4V alloy components

Fatigue strength of Ti6Al4V alloy components is evaluated with HCF testing and it is correlated with the surface properties like surface roughness and surface residual stresses. Experiments are conducted on Ti6Al4V alloy for both CT and UVAT processes to evaluate the surface roughness and surface residual stresses at various machining conditions. The optimum condition for UVAT is also obtained based on surface residual stresses to evaluate the fatigue strength.

7.6.1 Residual stress modeling

Response surface methodology has been used to evaluate the residual stress in UVAT of Ti6Al4V alloy. Experiments are designed based on Box-Behnken technique to evaluate the optimum condition for minimum residual stresses. This method performs the less number of experiments to obtain accurate results. The machining parameters and their levels selected for this study are given in table 7.3. Experimental design for residual stress measurement is given in table 7.4.

Table 7.3: Machining parameters and their levels for UVAT experiments

		Low level	High level
Cutting speed	(m/min)	50	90
Feed rate	(mm/rev)	0.055	0.161
Depth of cut	(mm)	0.5	1
Intensity of ultrasonic power (%)		80	100

The regression analysis has been carried out to develop second order model for predicting residual stress over a wide range of parameters. The residual stress data is analyzed based on the analysis of variance (ANOVA). ANOVA data for CRS is presented in table 7.5. In order to find the optimum condition for minimum residual stress, desirability approach is followed. From this analysis, the minimum residual stress is 43 MPa (compressive) and it is obtained at V= 50.5 m/min, fr= 0.06 rev/min, DOC= 0.615 mm and intensity of ultrasonic power is 99.6% as shown in figure 7.12 .

Table 7.4: Experimental run for residual stress measurement

Cutting speed (m/min)	Feed rate mm/rev	Depth of cut mm	Intensity of ultrasonic power %	Circumferential residual stress MPa
90	0.103	0.5	80	195
90	0.161	0.75	90	181
70	0.103	0.5	80	92
70	0.055	1	90	81
90	0.103	0.75	100	186
90	0.103	1	90	193
70	0.103	0.75	90	88
70	0.161	0.5	90	94
50	0.103	0.75	100	-28
70	0.103	1	100	-7
50	0.161	0.75	90	2
50	0.103	0.75	80	42
70	0.161	0.75	80	63
50	0.103	0.5	90	18
70	0.161	1	90	91
90	0.055	0.75	90	75
70	0.103	0.75	90	69
70	0.055	0.75	100	-11
50	0.103	0.5	100	-28
70	0.103	0.5	100	-19
50	0.055	0.75	90	15
70	0.055	0.5	90	42
90	0.103	0.5	90	63
70	0.103	0.75	90	56
70	0.161	0.75	100	-22
70	0.055	0.75	80	87
70	0.103	1	80	111

Table 7.5: ANOVA Table for CRS

Source	Sum of Squares	DOF	Mean Square	F-value	p-value	
Model	43131.67	4	10782.92	21.76	< 0.0001	significant
A-Cutting Speed	14770.08	1	14770.08	29.81	< 0.0001	
B-feed rate	310.08	1	310.08	0.6258	0.4378	
C-Depth of cut	1260.75	1	1260.75	2.54	0.1256	
D-Intensity of ultrasonic power	26790.75	1	26790.75	54.06	< 0.0001	
Residual	10406.22	21	495.53			
Lack of Fit	10206.22	20	510.31	2.55	0.4616	not significant
Pure Error	200.00	1	200.00			
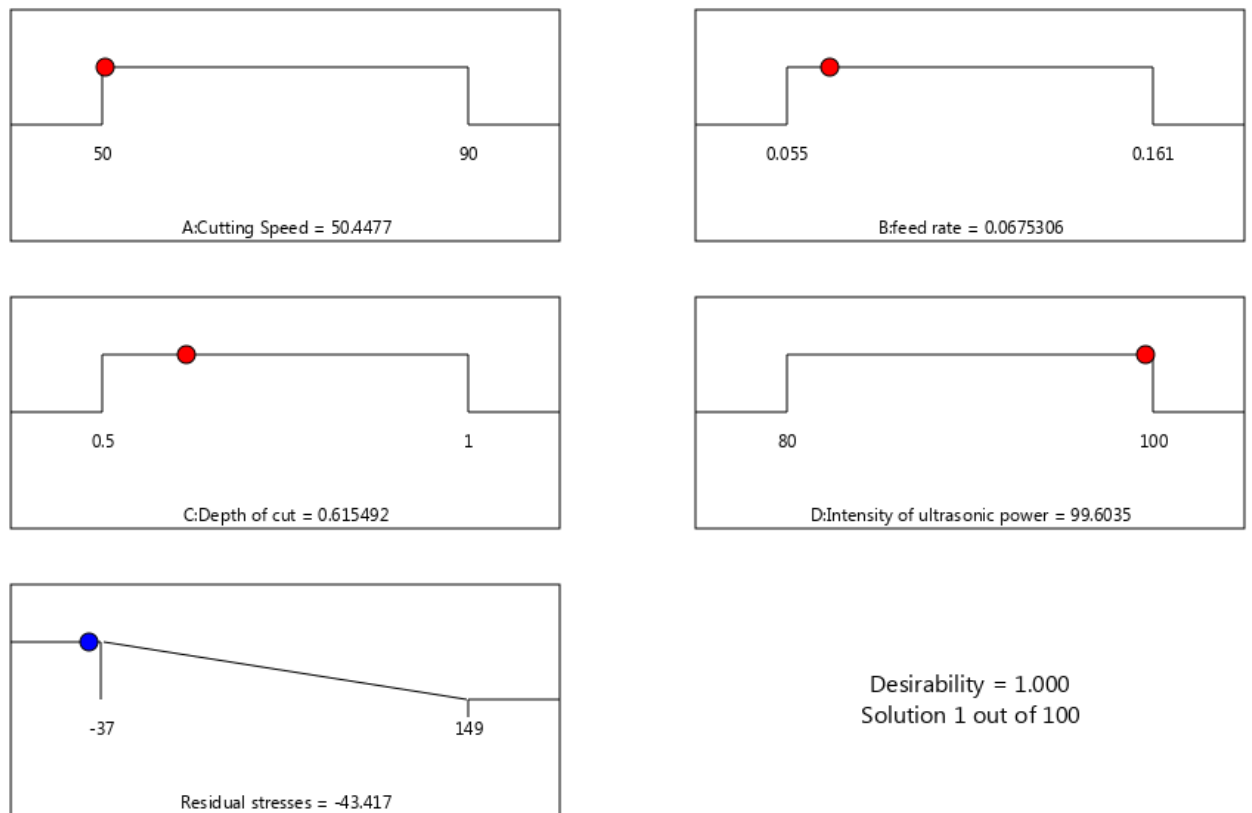
Figure 7.12: Optimum condition for minimum residual stresses

133

7.6.2 High cycle fatigue testing

In order to evaluate the fatigue strength, the fatigue test samples are prepared at three machining conditions and their levels are given in table 7.6. The effect of surface roughness and surface residual stresses on fatigue life of samples is evaluated at same levels where HCF test samples are prepared.

Table 7.6: Machining parameters and their levels for fatigue testing samples

Type of machining process	Levels of machining parameters
CT	V= 50 m/min, f_r= 0.05 mm/rev, DOC=0.5 mm
UVAT	V= 50 m/min, f_r= 0.05 mm/rev, DOC=0.5 mm P_u=100 %
Optimum UVAT	V= 50.5 m/min, f_r= 0.05 mm/rev, DOC=0.5 mm P_u=99.6 %

7.6.3 Effect of Surface roughness

The surface roughness is measured for each test sample for three times at different positions along the surface. The variation of mean surface roughness (R_a) of test samples for both CT and UVAT are shown in figure 7.13. The improved surface finish with UVAT process generally retards initiation of crack under cyclic loading. The R_a value for UVAT process is consistently superior to those obtained in CT process. The roughness values are also helpful to understand the role of residual stress. In fact, it is well know that residual stresses play a significant role on fatigue life as the value of R_a affects the surface residual stresses. Furthermore, relaxation of residual stresses occurs rapidly in the early stages of cyclic loading. Moreover, it is confirmed that the initiation of crack occurs at grain boundaries with low values of R_a.
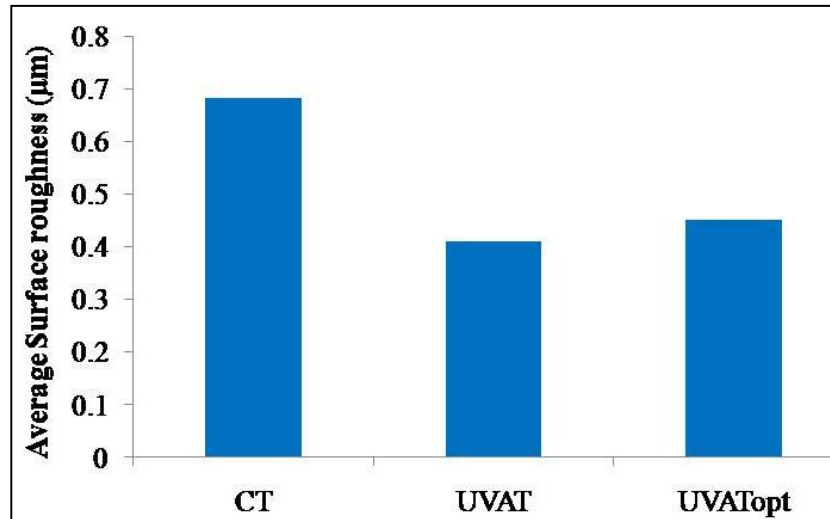
Figure 7.13: Comparison of average surface roughness of CT, UVAT and UVAT$_{opt}$

7.6.4 Effect of surface residual stresses
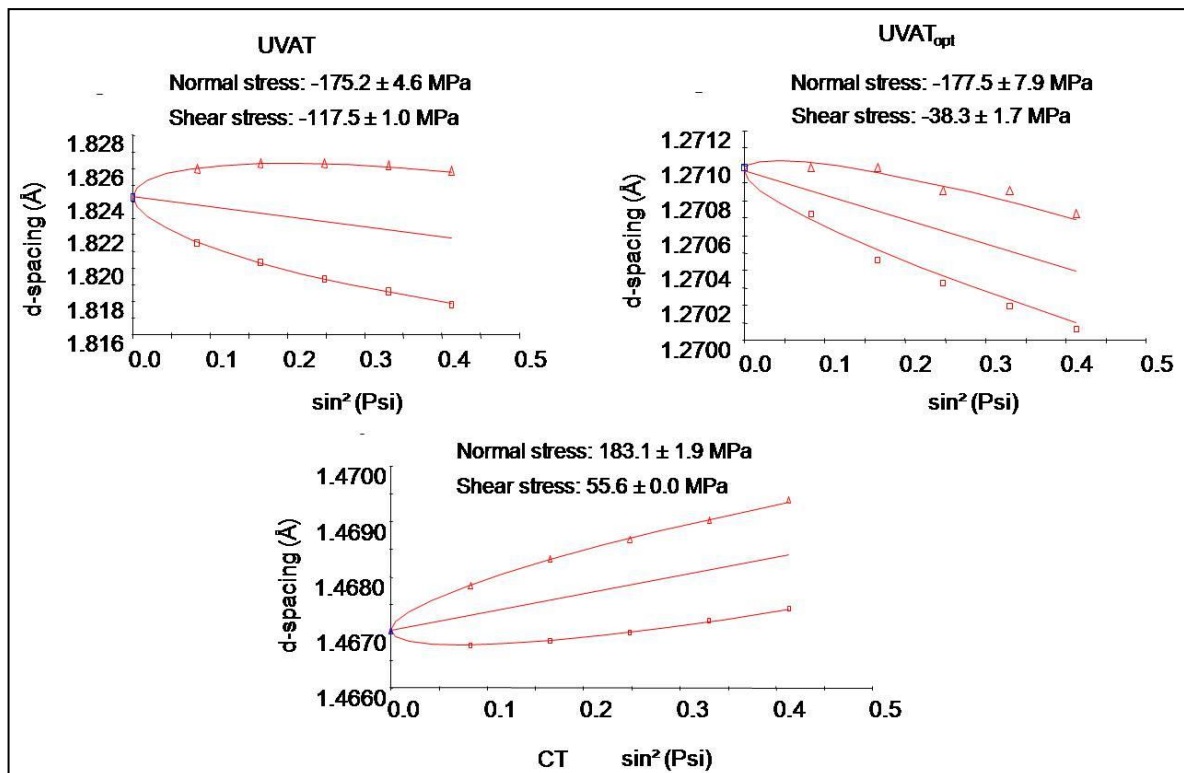
Figure 7.14: Comparison of residual stresses between CT and UVAT samples

The surface residual stresses for CT, UVAT and UVAT$_{opt}$ samples are measured with X-Ray diffraction technique is shown in figure 7.14.. The surface residual stresses play a significant role on initiation of crack in fatigue life testing. As the relaxation of residual stresses occurs at initial stages of cyclic loading, compressive residual stresses resist the

initiation of crack while the tensile residual stresses promotes the crack during fatigue life testing. Finally, it is confirmed that the compressive surface residual stresses in UVAT process improves the fatigue life of Ti6Al4V alloy component compared to CT process.

7.6.5 Fatigue strength

In order to evaluate the fatigue strength, up and down method has been used and its procedure is show in figure 7.15. The initial stress amplitude at which fatigue test has to run, is identified from the tension test and stress- strain curve is shown in figure 7.16. The yield strength of the Ti6Al4V alloy is 960 MPa. Then, fatigue test has conducted at 60%, 70%, 75% and 80% of yield strength as per the ASTM 139 [162]. At first step, the cyclic stress amplitude of the first sample is tested at 825 MPa which is 85% of yield stress of Ti6Al4V alloy and it is tested for fixed number of cycles (N_{limit} =10^7 cycles). If the specimen fails, then it is not considered for further analysis and the initial stress amplitude is reduced by $\Delta\sigma$. If specimen does not fail with in the N_{limit} of cycles, the test is repeated by increasing the stress of $\Delta\sigma$. This procedure is repeated until fracture of sample occurs which defines the end of the test at corresponding failure. Thus fatigue limit is calculated using equation 7.1. The fatigue failure of the sample commonly initiates from the surface and propagates into material with time. The crack initiation and propagation of machined samples depends on surface properties and microstructure of the material and it is shown in figure 7.17. The fatigue failure occurs suddenly after running some number of cycles.

$$\sigma = \frac{N_{failure}}{N_{limit}} (\sigma_n - \sigma_{n-1}) + \sigma_{n-1} \qquad (7.1)$$
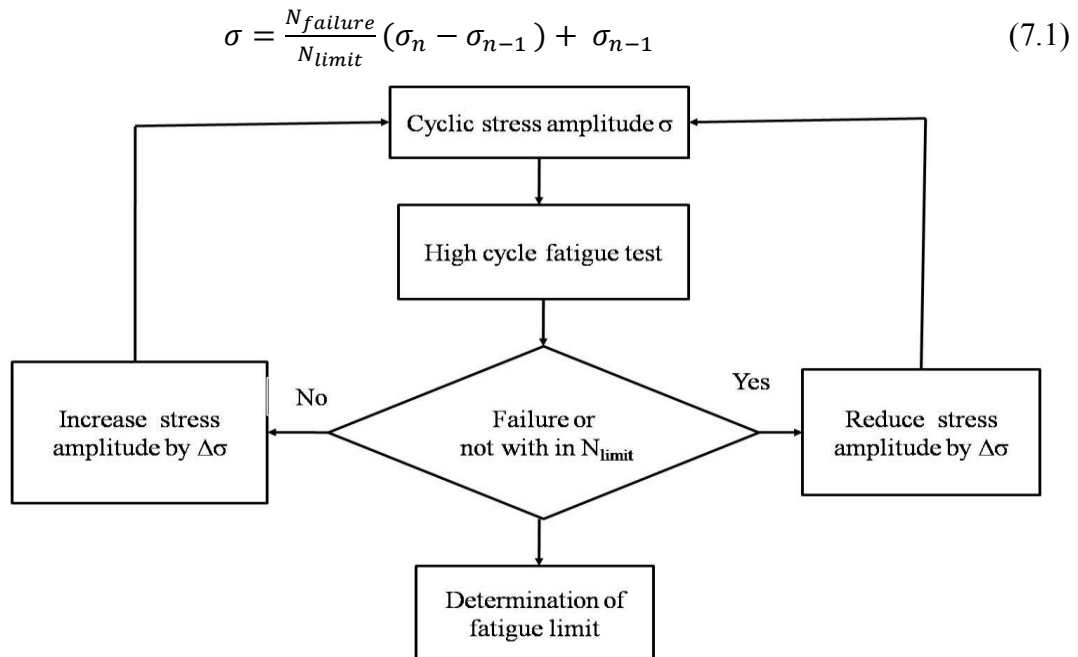
Figure 7.15: Step by step method to determine the fatigue limit

136
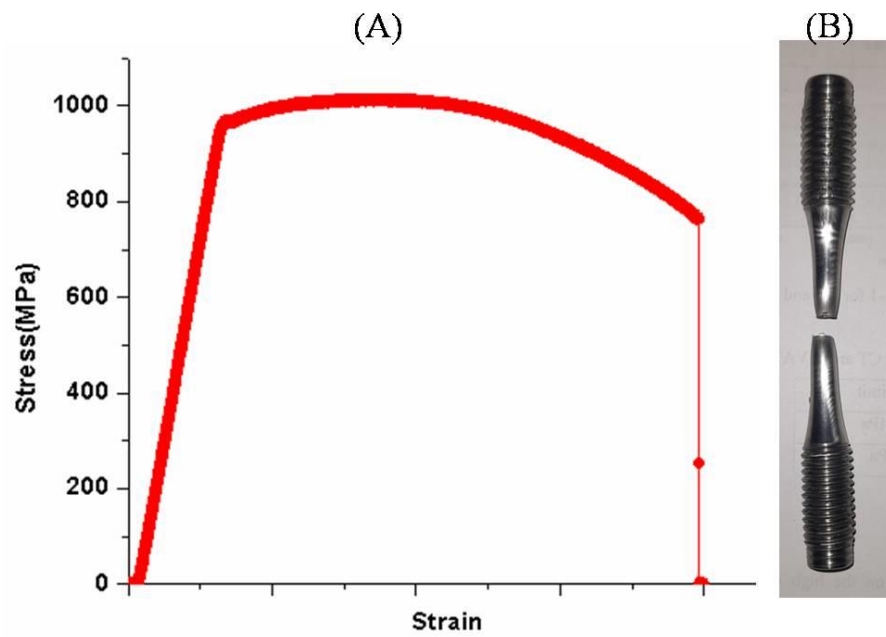
Figure 7.16: Tension test (A).Stress- strain diagram for Ti6Al4V alloy (B). Failed sample
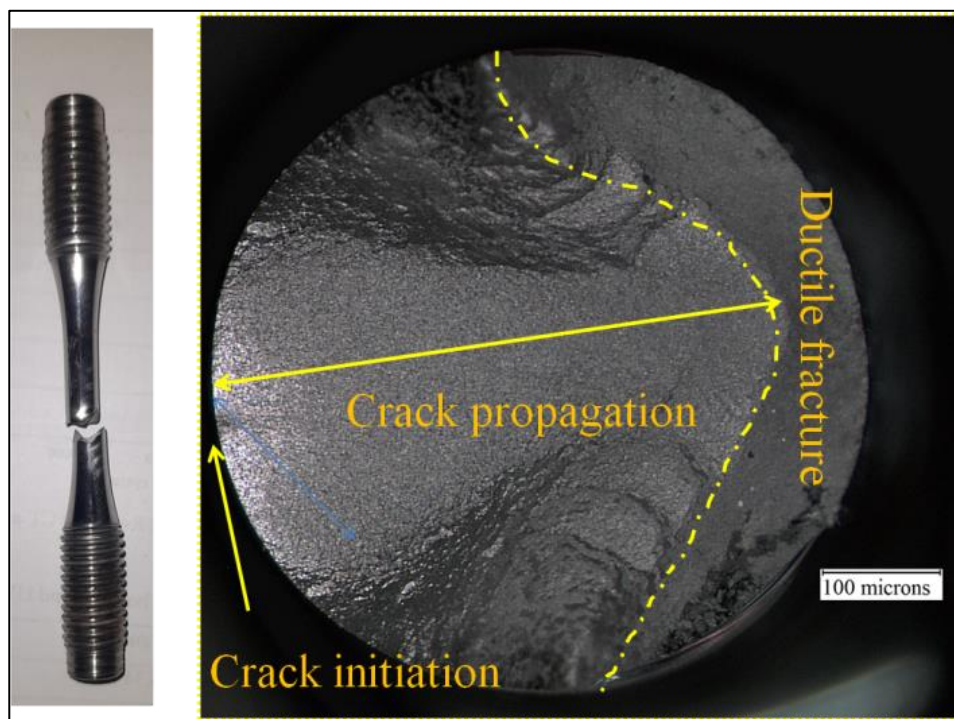
Figure 7.17: Fatigue fracture of Ti6Al4V alloy sample
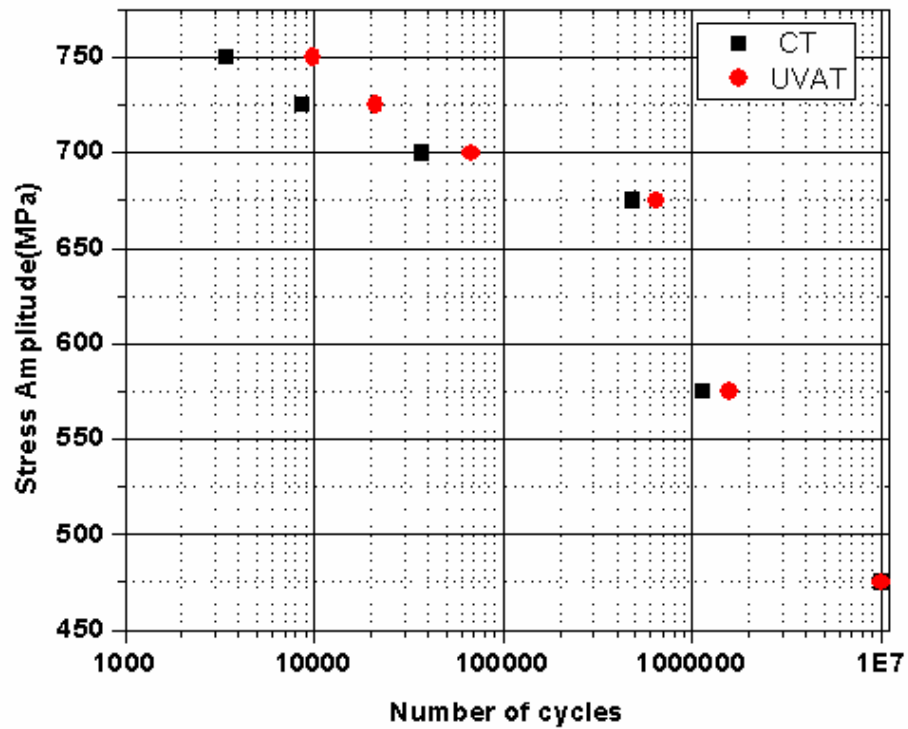
Figure 7.18: S-N curves for Ti6Al4V alloy at R= -1 for CT and UVAT process

Figure 7.18 shows the S-N curve for CT and UVAT of Ti6Al4V alloy in the high cycle fatigue range. The fatigue life of Ti6Al4V alloy sample obtained from UVAT process has shown significant improvement compared to CT process due to improved surface properties. The failure is observed at 575 MPa for both samples, however more number of cycle are registered for UVAT process compared to CT process. The intermittent contact between tool and workpiece improves the surface properties in UVAT process which leads to better results for all stress amplitude compared to CT process. However, the run out at 1E7 cycles occurred at 475 MPa for both processes. Thus, fatigue limit of Ti6Al4V alloy for both CT and UVAT process are evaluated using equation 7.1 and it is shown in table 7.7.

Table 7.7: Fatigue limit of Ti6Al4V alloy samples for both CT and UVAT process

	Fatigue limit
CT	486.34 MPa
UVAT	490.7 MPa

7.7 Summary

FE model is developed for both CT and UVAT using J-C parameters determined from machining approach. The developed FE model is used to analyze the variation of residual stresses on surface and subsurface levels of machined components at various machining conditions. The circumferential and axial residual stresses are analyzed at different ultrasonic power intensity, cutting speed, feed rate and depth of cut. Similarly, the effect surface integrity on fatigue strength of Ti6Al4V alloy is evaluated for both CT and UVAT processes and compared.

Chapter 8

Conclusions and Future Scope

In the present study, orthogonal experiments were conducted to evaluate J-C parameters for Ti6Al4V alloy in MA. The determined J-C parameters are validated with J-C parameters available in literature to predict the accurate results from FE simulation. The effect of ultrasonic vibrations on surface integrity of Ti6Al4V alloy is evaluated using both experimental and finite element simulation. The intermittent cutting action in UVAT method is evaluated in terms of TWCR and its performance is evaluated at certain range of machining conditions in terms of cutting force, cutting temperature and surface roughness. The tool life is estimated in machining of Ti6Al4V alloy for CT and UVAT process. Furthermore, machining induced residual stresses are analyzed on surface and subsurface layers of machined components at different machining conditions using finite element method with J-C parameters determined from MA approach. Finally, the effect of surface roughness and residual stresses on fatigue life of Ti6Al4V alloy is evaluated. The conclusions drawn from the current research work are given below.

8.1 Conclusions

J-C Parameters

- High regression coefficients obtained from the response surface analysis indicates that the developed second order model can adequately predict the cutting force, feed force and chip thickness.
- For the same range of cutting conditions, prediction of flow stress is accurate with J-C constants obtained at 7º rake angle for Ti6Al4V alloy.

- At lower temperatures, strain hardening effect is more in case of J-C parameters obtained at positive rake angle when compared to J-C parameters obtained at negative rake angle. Similarly, considerable difference in flow stress is observed when rake angle changes from negative to positive.

- The flow stress error calculated from J-C constants identified from the present approach gives smaller error when compared to J-C constants obtained from other methods.

- Present work is validated for limited range of cutting conditions. The sensitivity analysis for determined J-C constants need to be done to validate for wide range of cutting conditions.

Ultrasonic Vibration Assisted Turning process

- Analytically, it is found that frequency, amplitude and cutting speed are three important parameters controlling TWCR in UVAT process. TWCR decreases with increase in frequency and amplitude whereas it increases with increase in cutting speed.

- Experimentally, it is found that the performance of UVAT process is improved with lower values of TWCR.

- In UVAT process, the reduction in cutting force, cutting temperature and surface roughness are observed with increase in percentage intensity of ultrasonic power.

- At lower cutting conditions, cutting forces are increased initially and then decreased with increase in cutting speed. Whereas at medium and higher cutting conditions, cutting forces are decreased and then increased with increase in cutting speed.

- The cutting temperature is increased and surface roughness is decreased with increase in cutting speed for both UVAT and CT process.

- Both mechanical and thermal loading are influencing the machining performance in UVAT process. However, at lower values of machining conditions the influence of mechanical loading is dominant and at higher values of machining conditions the thermal loading is dominant, this is because of combined effect of TWCR, adiabatic heat and aero dynamic lubrication.

- The reduction in cutting force is 10-40%, cutting temperature is 10-30% and surface roughness is 20-50% in UVAT compared to CT.

- BUE formation is observed in UVAT of Ti6Al4V alloy when vibration is applied in tangential direction. The rate of BUE formation is increased and then converted to smooth wear with prolonged machining time in UVAT process. However, worn out of cutting edge is observed in CT with prolonged machining time due to diffusion wear mechanism.

- The average and maximum flank wear of the tool are decreased with increase in ultrasonic power due to less contact time at higher ultrasonic power in UVAT process compared to CT. The tool life is doubled when ultrasonic power increased from 80 to 90%.

- Both average and maximum flank wear of the tool increased with increase in cutting velocity due to increase in cutting temperature in both CT and UVAT process. However, the rate of increase in UVAT is low at all cutting speeds. At 300 μm average flank wear, the tool life in CT is 4.75 min whereas in UVAT, it is 12.5 min. At higher cutting speeds, chatter suppression due to ultrasonic vibrations affect the tool wear in UVAT process.

- The variation of cutting force with flank wear is increased rapidly after 0.2 mm average flank wear with cutting speed for both 120 m/min and 150 m/min. Similarly, the reduction in variation of cutting force is observed after 0.1 mm average flank wear with increase in ultrasonic power.

- The tensile and compressive layer thickness of CRS and ARS are depends on contact time between tool and workpiece at all stages of UVAT cycle.

- The increased ultrasonic power intensity changes the surface CRS from tensile to compressive and the surface ARS from lower to higher compressive state. It is also found that the tensile layer thickness is decreased and compressive layer thickness is increased for CRS and ARS with increase in ultrasonic power.

- Increased thermal load with increase in cutting speed from 30 to 110 m/min, decreases the compressive layer thickness and increases the level of surface CRS and ARS.

- Increased feed rate increases the compressive layer thickness and decreases the level of CRS and ARS due to dominance of mechanical load over thermal load. Similarly, compressive layer thickness and level of CRS and ARS are decreased with increase in depth of cut due to thermal dominance over mechanical load.

- The surface properties have significant influence on the high cycle fatigue strength of Ti6Al4V alloy.

- The compressive surface residual stresses generated in UVAT process increases the time required to initiate the crack in HCF test.
- The number of cycles required for the failure of test samples are high in UVAT compared to CT.
- Fatigue strength of Ti6Al4V alloy is improved with UVAT compared to CT.

8.2 Recommendations for future work

During the course of the present study, many challenges were treated successfully, yet there are some research points that can be achieved to expand the current study. Thus, some further research is recommended for both experimentation and finite element simulation.

- Analytically, it is found that frequency is also an important parameter affects the performance of UVAT process. Thus, it is important to conduct experiments for UVAT at different frequencies to observe its performance variation.
- In order to increase the productivity, experiments has to be done at higher cutting speeds. However, the advantage obtained from, UVAT process is reduced with increase in cutting speed. Hence, it is important to recommend optimum cutting speed which improves both productivity as well as advantage from UVAT process.
- The shear bands in chip formation indicates the generation of high cutting forces in machining process which indicates the formation of adiabatic temperature zone. The effect of ultrasonic vibrations on chip morphology can be studied for further understanding of heat generation in UVAT process.
- The superimposition of ultrasonic vibrations on the cutting tool causes reversal of chip direction on the rake face of the cutting tool per each cycle of vibration. This indicates the possibility of crater wear on the tool at high cutting speeds. Hence, the impact of crater wear in UVAT process can be studied.
- The effect of thermo-mechanical loading on residual stresses is studied in this current work. However, change in microstructure due to thermo-mechanical loading in generation of residual stresses can be studied further.
- The crack propagation in HCF test for UVAT machined samples is not studied in the current work. Hence, it is important to evaluate the effect of ultrasonic vibrations on crack propagation in HCF testing.

References

[1]   C. Leyens and M. Peters, "Titanium and Titanium Alloys:Fundamentals and Applications", *WILEY-VCH GmbH & Co., Weinheim*, 2003.

[2]   A. Roy and V. V. Silberschmidt, "Ultrasonically Assisted Machining of Titanium Alloys", *IN: Paulo Davim, J. (ed). Machining of Titanium Alloys . Heidelberg : Springer Verlag*, 131-147, 2014.

[3]   E. O. Ezugwu, J. Bonney, and Y. Yamane, "An overview of the machinability of aeroengine alloys," *Journal of Materials Processing Technology,* 134(2):233–253, 2003.

[4]   A. Shokrani, V. Dhokia, and S. T. Newman, "Environmentally conscious machining of difficult-to-machine materials with regard to cutting fluids," *International Journal of Machine Tools and Manufacture*, 57: 83–101, 2012.

[5]   F. Klocke, G. Eisenblätter, and T. Krieg, "Machining: Wear of Tools", *In Encyclopedia of Materials: Science and Technology; Elsevier Ltd.: New York, NY, USA*, 4708–4711, 2001.

[6]   N. N. Ahmed, A. V. Mitrofanov, V. I. Babitsky, and V. V. Silberschmidt, "Analysis of forces in ultrasonically assisted turning," *Journal of Sound and Vibration.* 308(3–5): 845–854, 2007.

[7]   V. I. Babitsky, A. N. Kalashnikov, A. Meadows, and A. A. H. P. Wijesundara, "Ultrasonically assisted turning of aviation materials," *Journal of Materials Processing Technology*,132(1–3):157–167, 2003.

[8]   A. V. Mitrofanov, V. I. Babitsky, and V. V. Silberschmidt, "Finite element analysis of ultrasonically assisted turning of Inconel 718," *Journal of Materials Processing Technology*,153–154(1–3):233–239, 2004..

[9]   N. Ahmed, A. V. Mitrofanov, V. I. Babitsky, and V. V. Silberschmidt, "Analysis of material response to ultrasonic vibration loading in turning Inconel 718", *Materials Science and Engineering A* ,424(1-2):318-325, 2006.

[10]   A. V. Mitrofanov, V. I. Babitsky, and V. V. Silberschmidt, "Finite element simulations of ultrasonically assisted turning", *Computational materials science,* 28 (3-4): 645-653, 2003.

[11]   K. H. W. Seah, Y. S. Wong, and L. C. Lee, "Design of tool holders for ultrasonic machining using FEM", *Journal of Materials Processing Technology*, 37(1–4): 801–

816, 1993.

[12] M. Roopa Rani and R. Rudramoorthy, "Computational modeling and experimental studies of the dynamic performance of ultrasonic horn profiles used in plastic welding," *Ultrasonics*, 53(3):763–772, 2013.

[13] D. E. Brehl and T. A. Dow, "Review of vibration-assisted machining," *Precision Engineering*,32(3):153–172, 2008.

[14] R. C. Skelton, "Effect of ultrasonic vibration on the turning process," *International Journal of Machine Tool Design and Research,* 9(4):363–374, 1969.

[15] C. Ma, E. Shamoto, T. Moriwaki, and L. Wang, "Study of machining accuracy in ultrasonic elliptical vibration cutting," *International Journal of Machine Tools and Manufacture*, 44(12-13):1305–1310, 2004.

[16] Y. Karpat, "Temperature dependent flow softening of titanium alloy Ti6Al4V: An investigation using finite element simulation of machining," *Journal of Materials Processing Technology*, 211(4):737–749, 2011.

[17] T. Kitagawa, A. Kubo, and K. Maekawa, "Temperature and wear of cutting tools in high-speed machining of Inconel 718 and Ti-6Al-6V-2Sn," *Wear*, 202(2):142–148, 1997.

[18] M. B. Ponce, J. M. Vazquez-Martinez, J. P. Davim, and J. S. Gomez, "Analysis of secondary adhesion wear mechanism on hard machining of titanium aerospace alloy," *Materials*,12(12), 2019.

[19] J. C. Outeiro, J. C. Pina, R. M'Saoubi, F. Pusavec, and I. S. Jawahir, "Analysis of residual stresses induced by dry turning of difficult-to-machine materials," *CIRP Annals - Manufacturing Technology*, 57(1):77–80, 2008.

[20] A. Javidi, U. Rieger, and W. Eichlseder, "The effect of machining on the surface integrity and fatigue life," *International Journal of Fatigue*, 30(10–11):2050–2055, 2008.

[21] D. Novovic, R. C. Dewes, D. K. Aspinwall, W. Voice, and P. Bowen, "The effect of machined topography and integrity on fatigue life," *International Journal of Machine Tools and Manufacture*,44(2–3):125–134, 2004.

[22] C. Krempner, H. Reinke, and H. Oehme, "Synthesis of Transient Silenes by a Modified Peterson Reaction," *Chemische Berichte*, 128(2):143–149, 1995.

[23] D. Umbrello and G. Rotella, "Fatigue life of machined Ti6Al4V alloy under different cooling conditions," *CIRP Annals*, 67(1):99–102, 2018.

[24] H. Sasahara, "The effect on fatigue life of residual stress and surface hardness resulting from different cutting conditions of 0.45%C steel," *International Journal of Machine Tools and Manufacture*, 45(2):131–136, 2005.

[25] G.R. Johnson and W.H.Cook, "A constitutive model and data for materials subjected to large strains, high strain rates, and high temperatures.," *Proceedings 7th International Symposium on Ballistics,* The Hague, 19-21 April 1983, 541-547.

[26] R. Stevenson, "Study on the correlation of workpiece mechanical properties from compression and cutting tests," *Machning Science and Technology,*l(1): 67–79, 1997.

[27] Y. B. Guo, "An integral method to determine the mechanical behavior of materials in metal cutting," *Journal of Materials Processing Technology*,142(1):72–81, 2003.

[28] W. K. Rule, "A numerical scheme for extracting strength model coefficients from Taylor test data," *International Journal of Impact Engineering*, 19(9–10):797–810, 2002.

[29] M.Rahman, Y.S.Wong and A.R.Zareena, " Machinability of Titabium alloys," *JSME International Journal Series C*, 46(1):107-115,2003 .

[30] E.O.Ezugwu , "High Speed Machining of Aero-Engine Alloys," *Journal of the Brazilian Society of Mechanical Sciences and Engineering,* 26(1),2004.

[31] J. Barry, G. Byrne, and D. Lennon, "Observations on chip formation and acoustic emission in machining Ti – 6Al – 4V alloy," *International Journal of Machine Tools and Manufacture*,41(7):1055–1070, 2001.

[32] E. O. Ezugwu and Z. M. Wang, "Titanium alloys and their machinability," *Journal of Materials Processing Technology* , 68(3): 262–274, 1997 .

[33] C. H. Che-Haron, "Tool life and surface integrity in turning titanium alloy," *Journal of Materials Processing Technology*, 118(1–3):231–237, 2001.

[34] A. Jawaid, C. H. Che-haron, and A. Abdullah, "Tool wear characteristics in turning of titanium alloy Ti-6246," *Journal of Materials Processing Technology,*92-93: 329–334, 1999.

[35] Y. Altintas and I. Yellowley, "In-Process Detection of Tool Failure in Milling Using Cutting Force Models," *Journal of Manufacturing Science and Engineering ,* 111(2):149-157,1989.

[36] Y. B. Guo and Y. K. Chou, "The determination of ploughing force and its influence on material properties in metal cutting," *Journal of Materials Processing Technology,* 148(3):368–375, 2004.

[37] R. Komanduri and Z. B. Hou, "A review of the experimental techniques for the measurement of heat and temperatures generated in some manufacturing processes and tribology," *Tribology International*, 34(10):653–682, 2001.

[38] C. Dinc, I. Lazoglu, and A. Serpenguzel, "Analysis of thermal fields in orthogonal machining," *Journal of Materials Processing Technology* ,198(1):147–154, 2007.

[39] P. C. Wanigarathne, A. D. Kardekar, O. W. Dillon, G. Poulachon, and I. S. Jawahir, "Progressive tool-wear in machining with coated grooved tools and its correlation with cutting temperature," *Wear,*259(7):1215–1224, 2005.

[40] I. Lazoglu and Y. Altintas, "Prediction of tool and chip temperature in continuous and interrupted machining," *International Journal of Machine Tools and Manufacture*,42(9):1011–1022, 2002.

[41] C. Dinc, I. Lazoglu, and A. Serpenguzel, "High Precision Infrared Thermal Measurements in Orthogonal Machining," *Conference on Design and Production of Machines and Dies/Molds,*Cesme,Turkey, 2007.

[42] R. C. Skelton, "Turning with an Oscillating Tool," *International Journal of Machine Tool Design and Research,* 8(4):239–259, 1968.

[43] H. Weber, J. Herberger, and R. Pilz, "Turning of Machinable Glass Ceramics with an Ultrasonically Vibrated Tool," *CIRP Annals - Manufacturing Technology*,33(1):85–87, 1984.

[44] J. Kumabe and M. Hachisuka, "Super-precision cylindrical machining," *Precision Engineering,* 6(2):67–72, 1984.

[45] J. Kumabe, T. Soutome, and Y. Nishimoto, "Ultrasonic Super-position Vibration Cutting of Ceramics," *Journal of the Japan Society for Precision Engineering,* 52(11):1851–1857, 1986.

[46] T. Moriwaki and E. Shamoto, "Ultraprecision Diamond Turning of Stainless Steel by Applying Ultrasonic Vibration," *CIRP Annals - Manufacturing Technology*, 40(1):559–562, 1991.

[47] J. Du Kim and E. S. Lee, "A study of ultrasonic vibration cutting of carbon fibre reinforced plastics," *International Journal of Advanced Manufacturing,*12(2):78–86, 1996.

[48] E. Shamoto and T. Moriwaki, "Study on Elliptical Vibration Cutting," *CIRP Annals - Manufacturing Technology*, 43(1):35–38, 1994.

[49] T. Moriwaki and E. Shamoto, "Ultrasonic Elliptical Vibration Cutting," *CIRP Annals -*

Manufacturing Technology,44(1): 31–34, 1995.

[50] J. Du Kim and I. H. Choi, "Micro surface phenomenon of ductile cutting in the ultrasonic vibration cutting of optical plastics," *Journal of Materials Processing Technology*, 68(1): 89–98, 1997.

[51] E. Shamoto and T. Moriwaki, "Ultraprecision diamond cutting of hardened steel by applying elliptical vibration cutting," *CIRP Annals - Manufacturing Technology*,48(1):441–444, 1999.

[52] C. S. Liu, B. Zhao, G. F. Gao, and F. Jiao, "Research on the characteristics of the cutting force in the vibration cutting of a particle-reinforced metal matrix composites SiCp/Al," *Journal of Materials Processing Technology*, 129(1–3):196–199, 2002.

[53] M. Xiao, S. Karube, T. Soutome, and K. Sato, "Analysis of chatter suppression in vibration cutting," *International Journal of Machine Tools and Manufacture*, 42(15):1677–1685, 2002.

[54] G. F. Gao, B. Zhao, F. Jiao, and C. S. Liu, "Research on the influence of the cutting conditions on the surface microstructure of ultra-thin wall parts in ultrasonic vibration cutting," *Journal of Materials Processing Technology*, 129(1–3):66–70, 2002.

[55] N. Suzuki, S. Masuda, M. Haritani, and E. Shamoto, "Ultraprecision micromachining of brittle materials by applying ultrasonic elliptical vibration cutting," *Proceedings of the 2004 International Symposium on Micro-NanoMechatronics and Human Science, MHS2004; The Fourth Symposium 'Micro-NanoMechatronics for and Information-Based Society' The 21st Century,* 133–138, 2004.

[56] V. I. Babitsky, A. V. Mitrofanov, and V. V. Silberschmidt, "Ultrasonically assisted turning of aviation materials: Simulations and experimental study," *Ultrasonics*, 42(1–9):81–86, 2004.

[57] A. V. Mitrofanov, V. I. Babitsky, and V. V. Silberschmidt, "Thermomechanical finite element simulations of ultrasonically assisted turning," *Computational Material Science*, 32(3–4):463–471, 2005.

[58] C. Ma, E. Shamoto, T. Moriwaki, Y. Zhang, and L. Wang, "Suppression of burrs in turning with ultrasonic elliptical vibration cutting," *International Journal of Machine Tools and Manufacture*, 45(11):1295–1300, 2005.

[59] Z. W. Zhong and G. Lin, "Diamond turning of a metal matrix composite with ultrasonic vibrations," *Materials and Manufacturing Processes*, 20(4):727–735, 2005.

[60] N. Ahmed, A. V. Mitrofanov, V. I. Babitsky, and V. V. Silberschmidt, "Stresses in

ultrasonically assisted turning," *Applied Mechanics and Materials*, 5:351–358, 2006.

[61] N. Ahmed, A. V. Mitrofanov, V. I. Babitsky, and V. V. Silberschmidt, "3D finite element analysis of ultrasonically assisted turning," *Computational Material Science,*39(1):149–154, 2007.

[62] C. Nath, M. Rahman, and S. S. K. Andrew, "A study on ultrasonic vibration cutting of low alloy steel," *Journal of Materials Processing Technology*, 192–193:159–165, 2007.

[63] M. J. Nategh, H. Razavi, and A. Abdullah, "Analytical modeling and experimental investigation of ultrasonic-vibration assisted oblique turning, part I: Kinematics analysis," *International Journal of Mechanical Science*, 63(1):1–11, 2012.

[64] H. Razavi, M. J. Nategh, and A. Abdullah, "Analytical modeling and experimental investigation of ultrasonic-vibration assisted oblique turning, part III: Experimental investigation," *International Journal of Mechanical Science*, 63(1):26–36, 2012.

[65] A. V. Mitrofanov, N. Ahmed, V. I. Babitsky, and V. V. Silberschmidt, "Effect of lubrication and cutting parameters on ultrasonically assisted turning of Inconel 718," *Journal of Materials Processing Technology,*162–163:649–654, 2005.

[66] M. Xiao, Q. M. Wang, K. Sato, S. Karube, T. Soutome, and H. Xu, "The effect of tool geometry on regenerative instability in ultrasonic vibration cutting," *International Journal of Machine Tools and Manufacture,*46(5):492–499, 2006.

[67] C. Nath and M. Rahman, "Effect of machining parameters in ultrasonic vibration cutting," *International Journal of Machine Tools and Manufacture,*48(9): 965–974, 2008.

[68] R. Muhammad, N. Ahmed, A. Roy, and V. V. Silberschmidt, "Numerical modelling of vibration-assisted turning of Ti-15333," *Procedia CIRP*, 1(1):347–352, 2012.

[69] A. Maurotto, R. Muhammad, A. Roy, and V. V. Silberschmidt, "Enhanced ultrasonically assisted turning of a β-titanium alloy," *Ultrasonics*, 53(7):1242–1250, 2013.

[70] S. Patil, S. Joshi, A. Tewari, and S. S. Joshi, "Modelling and simulation of effect of ultrasonic vibrations on machining of Ti6Al4V," *Ultrasonics*, 54(2): 694–705, 2014.

[71] V. V. Silberschmidt, S. M. A. Mahdy, M. A. Gouda, A. Naseer, A. Maurotto, and A. Roy, "Surface-roughness improvement in ultrasonically assisted turning," *Procedia CIRP*, 13: 49–54, 2014.

[72] A. S. Adnan and S. Subbiah, "Experimental investigation of transverse vibration-

assisted orthogonal cutting of AL-2024," *International Journal of Machine Tools and Manufacture,*50(3):294–302, 2010.

[73] A. Celaya ,L.N. López de Lacalle ,F.J.Campa and A. Lamikiz, "Ultrasonic Assisted Turning of mild steels ," *International Journal of Materials and Product Technology,*37(1):60–70, 2010.

[74] H. Jamshidi and M. J. Nategh, "Theoretical and experimental investigation of the frictional behavior of the tool-chip interface in ultrasonic-vibration assisted turning," *International Journal of Machine Tools and Manufacture,* 65:1–7, 2013.

[75] J. Zhang and D. Wang, "Investigations of tangential ultrasonic vibration turning of Ti6Al4V using finite element method," *International Journal of Material Forming*, 12(2):257–267, 2019.

[76] M. A. Sofuoğlu, F. H. Çakır, S. Gürgen, S. Orak, and M. C. Kuşhan, "Numerical investigation of hot ultrasonic assisted turning of aviation alloys," *Journal of the Brazilian Society of Mechanical Sciences and Engineering*, 40(3):1–12, 2018..

[77] M. Lotfi and S. Amini, "FE simulation of linear and elliptical ultrasonic vibrations in turning of Inconel 718," *Proceedings of the Institution of Mechanical Engineers, Part E: Journal of Process Mechanical Engineering*, 232(4):438–448, 2018.

[78] V. K. Astashev and V. I. Babitsky, "Ultrasonic cutting as a nonlinear (vibro-impact) process," *Ultrasonics*, 36(1–5):89–96, 1998.

[79] M. Jin and M. Murakawa, "Development of a practical ultrasonic vibration cutting tool system," *Journal of Materials Processing Technology*,113(1–3): 342–347, 2001.

[80] E. Di Iorio, R. Bertolini, S. Bruschi, and A. Ghiotti, "Design and development of an Ultrasonic vibration assisted turning system for machining bioabsorbable magnesium alloys," *Procedia CIRP*,77:324–327, 2018.

[81] H.Puga, J.Grilo, and V.H.Carneiro, "Ultrasonic Assisted Turning of Al alloys: Influence of Material Processing to Improve Surface Roughness," *Surfaces*, 2(2):326–335, 2019.

[82] Y. Xu, Z. Wan, P. Zou, and Q. Zhang, "Experimental study on chip shape in ultrasonic vibration–assisted turning of 304 austenitic stainless steel," *Advances in Mechanical Engineering*, 11(8):1–17, 2019.

[83] M. Lotfi, S. Amini, and M. Aghaei, "Tool Wear Prediction and Surface Improvement in Vibration Cutting," *Tribology Transsctions,* 61(3):414–423, 2018.

[84] N. K. Maroju, K. P. Vamsi, and J. Xiaoliang, "Investigations on feasibility of low-

frequency vibration-assisted turning," *International Journal of Advanced Manufacturing Technology*,91(9–12):3775–3788, 2017.

[85]   N. K. Maroju and V. K. Pasam, "FE Modeling and Experimental Analysis of Residual Stresses in Vibration Assisted Turning of Ti6Al4V," *International Journal of Precision Engineering and Manufacturing*, 20(3):417–425, 2019.

[86]   C. R. Liu and M. M. Barash, "Variables governing patterns of mechanical residual stress in a machined surface," *Journal of Manufacturing Science and Engineering Transactions of ASME*, 104(3): 257–264, 1982.

[87]   A. B. Sadat and J. A. Bailey, "Residual stresses in turned AISI 4340 steel," *Experimental Mechanics*,27(1): 80–85, 1987.

[88]   D. Y. Jang, T. R. Watkins, K. J. Kozaczek, C. R. Hubbard, and O. B. Cavin, "Surface residual stresses in machined austenitic stainless steel," *Wear*, 194(1–2):168–173, 1996.

[89]   Y. Matsumoto, F. Hashimoto, and G. Lahoti, "Surface integrity generated by precision hard turning," *CIRP Annals - Manufacturing Technology*, 48(1): 59–62, 1999.

[90]   M. Jacobson, "Surface integrity of hard-turned M50 steel," *Proceedings of the Institution of Mechanical Engineers Part B, Journal of Engineering Manufacture*,216(1): 47–54, 2002.

[91]   J. D. Thiele and S. N. Melkote, "Effect of cutting edge geometry and workpiece hardness on surface generation in the finish hard turning of AISI 52100 steel," *Journal of Material Processing Technology"*, 94(2): 216–226, 1999.

[92]   E. Capello, "Residual stresses in turning: Part I: Influence of process parameters," *Journal of Materials Processing Technology*, 160(2):221–228, 2005.

[93]   P. J. Arrazola *et al.*, "On the machining induced residual stresses in IN718 nickel-based alloy: Experiments and predictions with finite element simulation," *Simulation Modelling Practice and Theory*, 41:87–103, 2014.

[94]   H. Xin, Y. Shi, L. Ning, and T. Zhao, "Residual Stress and Affected Layer in Disc Milling of Titanium Alloy," *Materials and Manufacturing Processes*,31(13):1645–1653, 2016.

[95]   A. Mishra and T. Prasad, "Residual stresses due to a moving heat source," *International Journal of Mechanical Sciences,* 27(9):571–581, 1985.

[96]   Z. C. Lin, Y. Y. Lin, and C. R. Liu, "Effect of thermal load and mechanical load on the residual stress of a machined workpiece," *International Journal of Mechanical*

Sciences, 33(4): 263–278, 1991.

[97] C. Wiesner, "Residual stresses after orthogonal machining of AlSl 304: numerical calculation of the thermal component and comparison with experimental results," *Metallurgical Transactions A*, 23(3):989–996, 1992.

[98] I. J. Mech, S. Vol, and A. J. Shih, "Finite Element Analysis of The Rake Angle Effects In Orthogonal Metal Cutting ," *International Journal of Mechanical Sciences* , 38(1):1-17, 1996.

[99] J. Hua ,R.Shivpuri,X.Cheng, V.Bedekar,Y.Matsumoto, F.Hashimoto, and T.R.Watkins, "Effect of feed rate, workpiece hardness and cutting edge on subsurface residual stress in the hard turning of bearing steel using chamfer + hone cutting edge geometry," *Materials Science and Engineering A*,394(1–2):238–248, 2005.

[100] C. R. Liu and Y. B. Guo, "Finite element analysis of the effect of sequential cuts and tool-chip friction on residual stresses in a machined layer," *International Journal of Mechanical Sciences*, 42(6):1069–1086, 2000.

[101] R. Singh and J. S. Khamba, "Investigation for ultrasonic machining of titanium and its alloys," *Journal of Materials Processing Technology*, 183(2–3): 363–367, 2007.

[102] A. Nestler and A. Schubert, "Surface properties in ultrasonic vibration assisted turning of particle reinforced aluminium matrix composites," *Procedia CIRP*, 13:125–130, 2014.

[103] V. Sharma and P. M. Pandey, "Optimization of machining and vibration parameters for residual stresses minimization in ultrasonic assisted turning of 4340 hardened steel," *Ultrasonics*, 70: 172–182, 2016.

[104] R.B.Da Silva , A.R.Machado ,E.O.Ezugwu and J. Bonney, "Evaluation of the Machinability Of Ti-6al-4v Alloy With (Sicw) Whisker Reinforced Alumina Ceramic Cutting Tool under vaious cooling environments," 18th International congress of Mechanical Engineering COBEM, Brazil,2005.

[105] Z. G. Wang, M. Rahman, and Y. S. Wong, "Tool wear characteristics of binderless CBN tools used in high-speed milling of titanium alloys," *Wear*, 258(5–6):752–758, 2005.

[106] S. Zhang, J. F. Li, J. X. Deng, and Y. S. Li, "Investigation on diffusion wear during high-speed machining Ti-6Al-4V alloy with straight tungsten carbide tools," *International Journal of Advanced Manufacturing Technology*, 44(1–2): 17–25, 2009.

[107] S. S. Cho and K. Komvopoulos, "Cutting force variation due to wear of multi-layer

ceramic coated tools," *Journal of Tribology*, 120(1):75–81, 1998.

[108] E. O. Ezugwu, D. A. Fadare, J. Bonney, R. B. Da Silva, and W. F. Sales, "Modelling the correlation between cutting and process parameters in high-speed machining of Inconel 718 alloy using an artificial neural network," *International Journal of Machine Tools and Manufacture*, 45(12–13):1375–1385, 2005.

[109] A. Devillez, F. Schneider, S. Dominiak, D. Dudzinski, and D. Larrouquere, "Cutting forces and wear in dry machining of Inconel 718 with coated carbide tools," *Wear*, 262(7–8): 931–942, 2007.

[110] S. K. Choudhury and K. K. Kishore, "Tool wear measurement in turning using force ratio," *International Journal of Machine Tools and Manufacture*, 40(6): 899–909, 2000.

[111] Y. Koren, T. R. Ko, A. G. Ulsoy, and K. Danai, "Flank wear estimation under varying cutting conditions," *Journal of Dynamic Systems. Measurement and Control. Transanctions of ASME*, 113(2):300–307, 1991.

[112] A. Jawaid, S. Sharif, and S. Koksal, "Evaluation of wear mechanisms of coated carbide tools when face milling titanium alloy," *Journal of Materials Processing Technology*, 99(1):266–274, 2000.

[113] D. Venkata Sivareddy, P. Vamsi Krishna, and A. Venu Gopal, "Tool-Work Contact Ratio and Parametric Influence in Ultrasonic Vibration–Assisted Turning of Ti6Al4V Alloy," *Journal of Testing and. Evaluation*, 49(5), 2021.

[114] E. O. Ezugwu, K. A. Olajire, and J. Bonney, "Modelling of tool wear based on component forces," *Tribology Letters*,11(1): 55–60, 2001.

[115] V. P. Astakhov, "The assessment of cutting tool wear," *International Journal of Machine Tools and Manufacture*, 44(6): 637–647, 2004.

[116] C. Tan, Q. Sun, L. Xiao, Y. Zhao, and J. Sun, "Cyclic deformation and microcrack initiation during stress controlled high cycle fatigue of a titanium alloy," *Materials Science and Engineering: A*, 711:212–222, 2018.

[117] A. L. Mantle and D. K. Aspinwall, "Surface integrity and fatigue life of turned gamma titanium aluminide," *Journal of Materials Processing Technology*, 72(3): 413–420, 1997.

[118] Ch.Tan, Q.Sun, L.Xiao and Y.Zhao,"Cyclic Deformation and Micro crack Initiation during stress controlled high cycle fatigue of Ti6Al4V alloy," *Materials Science and Engineering: A*,2017.

[119] T. Gao,Z.Sun, H.Xue, E.Bayraktar, Z.Qin,B.Li and H.Zhang, "Effect of turning on the surface integrity and fatigue life of a TC11 alloy in very high cycle fatigue regime," *Metals (Basel)*, 10(11):1–15, 2020.

.[120] H. Chandrasekaran, R. M'Saoubi, and H. Chazal, "Modelling of material flow stress in chip formation process from orthogonal milling and split hopkinson bar tests," *Machining Science and Technology*, 9(1):131–145, 2005.

[121] P. Sartkulvanich, F. Koppka, and T. Altan, "Determination of flow stress for metal cutting simulation - A progress report," *Journal of Materials Processing Technology*,146(1):61–71, 2004.

[122] J. Ning and S. Y. Liang, "Inverse identification of Johnson-Cook material constants based on modified chip formation model and iterative gradient search using temperature and force measurements," *International Journal of Advanced Manufacturing Technology*, 2865-2876,2019.

[123] J. Pujana, P. J. Arrazola, R. M'Saoubi, and H. Chandrasekaran, "Analysis of the inverse identification of constitutive equations applied in orthogonal cutting process," *International Journal of Machine Tools and Manufacture*,47(14):2153–2161, 2007.

[124] N. Tounsi, J. Vincenti, A. Otho, and M. A. Elbestawi, "From the basic mechanics of orthogonal metal cutting toward the identification of the constitutive equation," *International Journal of Advanced Manufacturing Technology*, 42(12):1373–1383, 2002.

.[125] J. Ning, V. Nguyen, and S. Y. Liang, "Analytical modeling of machining forces of ultra-fine-grained titanium," *International Journal of Advanced Manufacturing Technology*,101(1–4): 627–636, 2019.

[126] T. Shatla, M., Kerk, C. and Altan, "Process modeling in machining. Part I: Determination of flow stress data," *International Journal of Machine Tools and Manufacture*, 41(10):1511–1534, 2001.

[127] A. Malakizadi, S. Cedergren, I. Sadik, and L. Nyborg, "Inverse identification of flow stress in metal cutting process using Response Surface Methodology," *Simulation Modeling Practice and Theory*, 60:40–53, 2016.

[128] M. Daoud, W. Jomaa, J. F. Chatelain, and A. Bouzid, "A machining-based methodology to identify material constitutive law for finite element simulation," *International Journal of Advanced Manufacturing Technology*, 77(9–12): 2019–2033, 2015.

[129] D. I. Lalwani, N. K. Mehta, and P. K. Jain, "Extension of Oxley's predictive machining theory for Johnson and Cook flow stress model," *Journal of Materials Processing Technology*, 209(12–13): 5305–5312, 2009.

[130] J J. Ning, V. Nguyen, Y. Huang, K. T. Hartwig, and S. Y. Liang, "Inverse determination of Johnson–Cook model constants of ultra-fine-grained titanium based on chip formation model and iterative gradient search," *International Journal of Advanced Manufacturing Technology*, 99(5–8):1131–1140, 2018.

[131] Simulia, "ABAQUS / CAE User ' s Manual," , 2001.

[132] G. R. Johnson and W. H. Cook, "A Computational Constitutive Model and Data for Metals Subjected to Large Strain, High Strain Rates and High Pressures," *Proceedings 7th International Symposium on Ballistics,*541–547, 1983.

[133] G. R. Johnson and W. H. Cook, "Fracture characteristics of three metals subjected to various strains, strain rates, temperatures and pressures," *Engineering Fracture Mechanics*, 21(1): 31–48, 1985.

[134] N. K. Maroju, P. V. Krishna, and X. Jin, "Assessment of high and low frequency vibration assisted turning with material hardness," *International Journal of Machining and . Machinability of Materials*, 19(2):110–135, 2017.

[135] W. Lee and C. Lin, "Plastic deformation and fracture behaviour of Ti–6Al–4V alloy loaded with high strain rate under various temperatures," *Materials Science and Engineering: A*, 241(1-2): 48–59, 1998.

[136] J. T. Carroll and J. S. Strenkowski, "Finite element models of orthogonal cutting with application to single point diamond turning," *International Journal of Mechanical Sciences*, 30(12):899–920, 1988.

[137] Z. C. Lin and Y. Y. Lin, "A study of an oblique cutting model," *Journal of Materials Processing Technology*, 86(1–3):119–130, 1998.

[138] Z. C. Lin and Y. Y. Lin, "Three-dimensional elastic-plastic finite element analysis for orthogonal cutting with discontinuous chip of 6-4 brass," *Theoritical and applied Fracture Mechanics*, 35(2):137–153, 2001.

[139] K. Komvopoulos and S. A. Erpenbeck, "Finite element modeling of orthogonal metal cutting," *Journal of Manufacturing Science and Engineering Transactions of ASME*, 113(3):253–267, 1991.

[140] T T. Obikawa and E. Usui, "Computational machining of titanium alloy-finite element modeling and a few results," *Journal of Manufacturing Science and Engineering*

Transactions of ASME, 118(2): 208–215, 1996.

[141] T. Childs, T.Obikawa and Y.Yamane, "Metal Machining,"*Arnold publishers*, 2000.

[142] T. Özel and E. Zeren, "Finite element modeling the influence of edge roundness on the stress and temperature fields induced by high-speed machining," *International Journal of Advanced Manufacturing Technology*, 35(3–4):255–267, 2007.

[143] X. Yang and C. R. Liu, "A new stress-based model of friction behavior in machining and its significant impact on residual stresses computed by finite element method," *International Journal of Mechanical Sciences*,44(4):703–723, 2002.

[144] V. Sharma and P. M. Pandey, "Optimization of machining and vibration parameters for residual stresses minimization in ultrasonic assisted turning of 4340 hardened steel," *Ultrasonics*, 70:172–182, 2016.

[145] P. L. B. Oxley, "Mechanics of Machining: An analytical approach to assessing machinability," *John Wiley and sons N.Y*, 1989.

[146] P. L. B. Oxley and M. J. M. Welsh, "Calculating the Shear Angle in Orthogonal Metal Cutting from Fundamental Stress, Strain, Strain-rate Properties of the Work piece Material," *Proceedings of Fourth International Machine Tool Design and Research Conference*,73–86, 1963.

[147] J.Kennedy, *Particle Swarm Optimization, Encyclopedia of Machine Learning*. US,: Springer, 2010.

[148] D. C. Montgomery, *Design and Analysis of Experiments*. wiley, 2017.

[149] Woei-Shyan Lee and Chi-Feng Lin, "High-temperature deformation behaviour of Ti6Al4V alloy evaluated by high strain-rate compression tests," *Journal of Materials Processing Technology*,75:127–136, 1998.

[150] W. Hubert, J. Meyer, and D. S. Kleponis, "Modeling the high strain rate behavior of titanium undergoing ballistic impact and penetration," *International Journal of Impact Engineering*, 26: 509–521, 2001.

[151] G. Chen, C. Ren, X. Yang, X. Jin, and T. Guo, "Finite element simulation of high-speed machining of titanium alloy (Ti-6Al-4V) based on ductile failure model," *International Journal of Advanced Manufacturing Technology*,56(9–12):1027–1038, 2011.

[152] S. Nemat-Nasser, W. G. Guo, V. F. Nesterenko, S. S. Indrakanti, and Y. B. Gu, "Dynamic response of conventional and hot isostatically pressed Ti-6Al-4V alloys: Experiments and modeling," *Mechanics of Materials*, 33(8):425–439, 2001.

[153] N. K. Maroju, K. P. Vamsi, and J. Xiaoliang, "Investigations on feasibility of low-frequency vibration-assisted turning," *International Journal of Advanced Manufacturing Technology*, 91(9–12):3775–3788, 2017.

[154] P. Zou, Y. Xu, Y. He, M. Chen, and H. Wu, "Experimental investigation of ultrasonic vibration assisted turning of 304 austenitic stainless steel," *Shock and Vibration*, 2015.

[155] M. Nouari and H. Makich, "On the Physics of Machining Titanium Alloys: Interactions between Cutting Parameters, Microstructure and Tool Wear," *Metals (Basel)*,4(3): 335–358, 2014.

[156] K. A. Venugopal, S. Paul, and A. B. Chattopadhyay, "Growth of tool wear in turning of Ti-6Al-4V alloy under cryogenic cooling," *Wear*, 262(9–10):1071–1078, 2007.

[157] M. A. Sofuoğlu, F. H. Çakır, S. Gürgen, S. Orak, and M. C. Kuşhan, "Experimental investigation of machining characteristics and chatter stability for Hastelloy-X with ultrasonic and hot turning," *International Journal of Advanced Manufacturing Technology*,95(1-4):83–97, 2018.

[158] F. R. Kaschel, R.K.Vijayaragjavan, A.Shmeliov, E.K.McKarthy, M.Canavan, P.J.McNally, D.P.Dowling, V.NIcolosi, and M.Celikin., "Mechanism of stress relaxation and phase transformation in additively manufactured Ti-6Al-4V via in situ high temperature XRD and TEM analyses," *Acta Material*,188: 720–732, 2020.

[159] N. W. Paschoalinoto, E. C. Bordinassi, R. Bortolussi, F. Leonardi, and S. Delijaicov, "The effect of process parameters and cutting tool shape on residual stress of SAE 52100 hard turned steel by high speed machining," *Proceedings of the Institution of Mechanical Engineers Part B, Journal of Engineering Manufacture*, 235(1-2): 290–300, 2021..

[160] M. H. Miguélez, R. Zaera, A. Molinari, R. Cheriguene, and A. Rusinek, "Residual stresses in orthogonal cutting of metals: The effect of thermomechanical coupling parameters and of friction," *Journal of Thermal Stresses*, 32(3): 269–289, 2009.

[161] M. Lotfi and S. Amini, "Effect of ultrasonic vibration on frictional behavior of tool–chip interface: Finite element analysis and experimental study," *Proceedings of the Institution of Mechanical Engineers Part B, Journal of Engineering Manufacture*, 232(7):1212–1220, 2018.

[162] "Standard Practice for Statistical Analysis of Linear or Linearized Stress-Life (S-N) and Strain-Life (ε -N) Fatigue Data" *Annu. B. ASTM Stand.*, i: 1–7, 2012.

List of Publications

1. D Venkata Sivareddy, P Vamsi Krishna , A Venu Gopal ," Effect of Thermo-Mechanical Loading on Machining Induced Residual Stresses in Ultrasonic Vibration Assisted Turning of Ti6Al4V Alloy", Proceedings of the Institution for Mechanical Engineers, Part B: Journal of Engineering Manufacture.(Review completed)(SCIE/SCOPUS).

2. D Venkata Sivareddy, P Vamsi Krishna , A Venu Gopal ," Experimental Investigation on Flank Wear of the Tool in Ultrasonic Vibration Assisted Turning of Ti6Al4V Alloy", Smart and sustainable manufacturing systems, Vol:5, 2021, 101-112. Published)(ESCI/Scopus)

3. D Venkata Sivareddy, P Vamsi Krishna , A Venu Gopal ," Tool-work contact ratio and parametric influence in ultrasonic vibration assisted turning of Ti6Al4V alloy", Journal of Testing and Evaluation, Vol:48,2020. (Published)(SCI).

4. D Venkata Sivareddy, P Vamsi Krishna , A Venu Gopal ," Determination of Constitutive Material Model Constants for Ti6Al4V alloy at near orthogonal machining conditions", Material processing and Characterization, Vol:9, 2020,531-548..(Published (ESCI/SCOPUS).

5. D Venkata Sivareddy, P Vamsi Krishna, A Venu Gopal, Parameter optimization in Vibration Assisted Turning of Ti6Al4V alloy using ANOVA and Grey relational Analysis, International Journal of Automotive and Mechanical Engineering, Vol:15 No: 3, 2018, 5400-5420.(Published)(ESCI/SCOPUS).

6. D Venkata Sivareddy, P Vamsi Krishna , A Venu Gopal ,"Optimization of Machining Parameters for Vibration Assisted Turning of Ti6Al4V Alloy Using Analysis of Variance",ICAMER-2019, NIT Warangal. (Published in LNME Springer series)(SCOPUS).

7. D Venkata Sivareddy, A Venu Gopal, P Vamsi Krishna , M Naresh Kumar, Effect of Johnson cook material constants on the prediction of stresses and forces in Vibration Assisted Turning of Ti6Al4V Alloy,ICMTS-2017, July 7-8-, 2017, IIT Madras.

8. D Venkata Sivareddy, P Vamsi Krishna, A Venu Gopal, Influence of Tool Geometry on Residual Stresses in Vibration Assisted Turning of Ti6Al4V Alloy,COPEN-2017, December 7-9-, 2017, IIT Madras.